

**Parental smoking behavior – cellular
and molecular consequences for
murine offspring**

Dissertation

zur Erlangung des Doktorgrades
der Mathematisch-Naturwissenschaftlichen Fakultät
der Christian-Albrechts-Universität zu Kiel

vorgelegt von

Barbara Hammer

Borstel, 2020

Erster Gutachter: Prof. Dr. Holger Heine

Zweiter Gutachter: Prof. Dr. Thomas Roeder

Tag der mündlichen Prüfung: 18.03.2020

1 ABSTRACT

Despite epidemiological data exist on adverse effects of maternal smoking during pregnancy, it remains a risk factor for increased susceptibility of pulmonary diseases like childhood asthma and chronic obstructive pulmonary disease (COPD). Infants prenatally exposed to cigarette smoke have decreased birth weights and postnatal lung function deficits. Smoking during pregnancy is frequently underreported in human studies, wherefore mild maternal smoking might be inadequately recorded. Children from mildly smoking mothers are likely to escape epidemiological assessments without showing lower birth weights and lung function declines. This study hypothesizes that mild maternal smoking during pregnancy could affect the immune system of the progeny in absence of growth retardation and lung function deficits.

Furthermore, until recently, paternal influences on offspring's disease risks have been deemed to be restricted via genetic transmission, but recent multicenter epidemiological studies have postulated that environmental factors like smoking during adolescence of fathers increase the risk of obesity and asthma in future children. At present, the underlying mechanism is unexplored. This study aims to establish a murine model of preconceptional smoking during puberty to investigate paternal and offspring's phenotype as putative mechanisms of ancestral transmission.

After intrauterine mild cigarette smoke exposure, altered T cell populations were observed in lungs and spleen throughout the life course of murine offspring. At postnatal day (PND) 21, pulmonary and splenic CD4⁺ T cells were increased, whereas CD8⁺ T cells were decreased in both organs. In addition, thymic CD4 single-positive (SP) T cells were elevated at PND21. Next-generation sequencing (NGS) data of thymic CD8⁺SP T cells from 21-day-old offspring revealed 92 up- and 36 downregulated genes. Genes of most interest – involved in immune-regulatory pathways – were *interleukin 4 receptor alpha (Il4ra)*, *runt-related transcription factor 3 (Runx3)*, *forkhead box protein P1 (Foxp1)*, *interleukin 10 receptor beta (Il10rb)* and *phosphoinositide-3-kinase (PI3K)*. *Eomesodermin (Eomes)* expression was supported by quantitative real-time polymerase chain reaction.

Adolescent smoking of fathers increased body weights in male offspring, whereas female offspring remained normal. Offspring of pubertal smoking mothers were lighter in both

sexes. Frequency of spermatozoa from the epididymis and spermatogonia in testes of smoking fathers were comparable to the non-smoker's control. NGS of spermatozoal microRNAs (miRNAs) revealed 13 upregulated and 32 downregulated miRNAs of smoking fathers. After *in silico* analysis, miR-340-5p, miR-204-5p and miR-96-5p were of most interest.

In conclusion, this murine study of mild maternal smoking during pregnancy identified altered pulmonary and thymic T cell populations in offspring at PND21. The development of 'innate memory' CD8 T (T_{IM}) cells in the thymus is IL-4-dependent and together with the expression of *Runx3* and *Eomes* in CD8SP thymocytes, this study postulates that T_{IM} cells could be affected by mild prenatal cigarette smoke exposure in offspring. These cells differentiate into a memory-like phenotype in the thymus and are suggested to provide support of the immune system against pathogens in young children, as their memory of peripheral adaptive immunity is insufficiently established.

Parental smoking during adolescence affected the body weight of offspring in a sex-specific manner and was parent-of-origin-dependent. In this study, the hypothesis was supported that sperm-borne miRNAs can carry ancestral memory and influence early gene translation in the early zygote. Putative targets and pathways of miRNA-340-5p, miR-204-5p and miR-96-5p make these miRNAs highly interesting candidates to further investigate their possible role on the altered body weight in murine offspring, and their influence on early embryogenesis and development in zygotes.

This study highlights that maternal as well as paternal smoking behavior can influence the offspring.

2 ZUSAMMENFASSUNG

Obwohl epidemiologische Daten die negativen Auswirkungen des Rauchens während der Schwangerschaft aufzeigen, bleibt es ein Risikofaktor für eine erhöhte Anfälligkeit für Lungenerkrankungen wie Asthma bei Kindern und chronisch obstruktiver Lungenerkrankung (COPD). Säuglinge, die pränatal Zigarettenrauch ausgesetzt wurden, haben ein verringertes Geburtsgewicht und zeigen Lungenfunktionsdefizite. Rauchen während der Schwangerschaft wird in humanen Studien häufig unterschätzt, weshalb das milde mütterliche Rauchen möglicherweise unzureichend erfasst wird. Kinder von mild rauchenden Müttern entgehen möglicherweise epidemiologischen Untersuchungen, da sie durch die schwache pränatale Exposition kein geringes Geburtsgewicht und eine Verschlechterung der Lungenfunktion aufweisen. In dieser Studie soll untersucht werden ob mildes Rauchen der Mutter während der Schwangerschaft das Immunsystem der Nachkommenschaft beeinflusst, obwohl Geburtsgewicht und Lungenfunktion unauffällig sind.

Zudem galt bis vor kurzem der Einfluss des Vaters auf das Krankheitsrisiko der Nachkommen rein über genetische Übertragung. Neue multizentrische epidemiologische Studien postulieren, dass Umweltfaktoren wie das Rauchen von Vätern in der Pubertät das Risiko für Fettleibigkeit und Asthma bei zukünftigen Kindern erhöhen könnte. Der zugrundeliegende Mechanismus ist derzeit noch unerforscht. In dieser Studie soll ein Mausmodell etabliert werden, das präkonzeptionelles väterliches Rauchen während der Pubertät auf den Phänotyp der Väter und der Nachkommen untersucht, um mutmaßliche Mechanismen zu identifizieren, die als Übertragungsmedium dienen könnten.

Nachkommen von Mäusen, die im Mutterlaib mit einer milden Dosis an Zigarettenrauch exponierte wurden, zeigten veränderte T-Zellenpopulationen in der Lunge und der Milz im Verlauf des Alters. 21 Tage alte Mäuse hatten erhöhte CD4⁺ T-Zellen in der Lunge und der Milz, während verminderte CD8⁺ T-Zellen in beiden Organen beobachtet wurden. Im Thymus waren CD4 single-positiven (SP) T-Zellen in denselben Nachkommen erhöht. Daten aus Next-Generation-Sequencing (NGS) zeigten 92 hoch- und 36 herunterregulierte Gene in CD8^{SP} Thymozyten von 21 Tage alten Mäusen. Gene, die an immunregulatorischen Pathways beteiligt sind, waren von größtem Interesse, wie

interleukin 4 receptor alpha (Il4ra), *runt-related transcription factor 3 (Runx3)*, *forkhead box protein P1 (Foxp1)*, *interleukin 10 receptor beta (Il10rb)* und *phosphoinositide-3-kinase (PI3K)*. Die Expression von *Eomesodermin (Eomes)* wurde von einer Analyse mittels quantitativer Echtzeit-Polymerase-Kettenreaktion (qRT-PCR) unterstützt.

Jugendliches Rauchen von Vätern führte zu einem erhöhten Körpergewicht der männlichen Nachkommen, während weibliche Nachkommen normal blieben. Nachkommen beider Geschlechter von Muttermäusen, die während der Pubertät geraucht hatten, wiesen ein leichteres Körpergewicht auf. Die Anzahl von Spermatozoen aus dem Nebenhoden und Spermatogonien in den Hoden von rauchenden Vätern waren nicht verändert im Vergleich zur Nichtraucherkontrolle. NGS Daten aus Spermien von pubertär rauchenden männlichen Mäusen zeigten 13 hochregulierte und 32 herunterregulierte microRNAs (miRNAs). Die miRNAs miR-340-5p, miR-204-5p und miR-96-5p erwiesen sich nach anschließender *in silico* Analyse als besonders interessant.

Zusammenfassend hat diese Studie in Mäusen über mildes mütterliches Rauchen während der Schwangerschaft veränderte T-Zellenpopulationen in der Lunge und im Thymus von 21 Tage alten Nachkommen nachgewiesen. Diese Studie postuliert, dass die Entwicklung von T-Zellen mit Eigenschaften von Gedächtniszellen-T-Zellen (T_{IM}) im Thymus durch eine milde pränatale Zigarettenrauchexposition in den Nachkommen beeinflusst werden könnten. Die Entwicklung von T_{IM} -Zellen ist IL-4-abhängig und durch die Expression von *Runx3* und *Eomes* in CD8SP Thymozyten charakterisiert. Diese Zellen erhalten ihren Gedächtniszellen-Phänotyp im Thymus und es wird angenommen, dass sie das Immunsystem gegen Krankheitserreger bei Kleinkindern unterstützen, da deren Gedächtnis-T-Zellen von der peripheren adaptiven Immunität noch unzureichend etabliert sind.

Das elterliche Rauchen während der Pubertät wirkte sich geschlechtsspezifisch auf das Körpergewicht der Nachkommen aus und war abhängig davon welcher Elternteil geraucht hatte. In dieser Studie wurde die Hypothese unterstützt, dass miRNAs in Spermien frühe Gentranslationen in der Zygote beeinflussen könnten. Mutmaßliche Angriffsstellen und Pathways von miRNA-340-5p, miR-204-5p und miR-96-5p machen diese miRNAs zu hochinteressanten Kandidaten, um ihre mögliche Rolle auf das veränderte Körpergewicht bei murinen Nachkommen und ihren Einfluss auf die frühe Embryogenese und

Entwicklung der Zygote weiter zu untersuchen. Diese Studie zeigt auf, dass sowohl mütterliches als auch väterliches Rauchverhalten die Nachkommenschaft beeinflussen kann.

3 TABLE OF CONTENTS

1 ABSTRACT	I
2 ZUSAMMENFASSUNG	III
3 TABLE OF CONTENTS.....	VI
4 INTRODUCTION.....	1
4.1 The prevalence of cigarette smoking in Europe	1
4.2 Asthma	3
4.2.1 Asthma epidemiology and pathophysiology.....	3
4.2.2 The relationship of parental smoking and offspring’s asthma risk	4
4.3 Prenatal smoking on offspring’s immune development	6
4.3.1 Thymus and T cell development.....	7
4.4 Preconceptional adolescent smoking and how it can affect the male germ line	8
4.4.1 Puberty.....	9
4.4.1.1 Spermatogenesis	10
4.4.1.2 Small non-coding RNAs in sperm cells	11
4.4.1.3 miRNA biogenesis	12
4.5 Rationale.....	14
5 AIMS AND OBJECTIVES	15
6 MATERIALS AND METHODS.....	16
6.1 Materials.....	16
6.1.1 Mouse strain.....	16
6.1.2 Chemicals and reagents	16
6.1.3 Buffers and solutions	18
6.1.4 Antibodies	19
6.1.5 Oligonucleotides	19
6.1.6 Commercial kits	20
6.1.7 Equipment and devices.....	21

6.1.8	Software and websites.....	23
6.1.9	Consumables	24
6.2	Methods	25
6.2.1	Mouse models	25
6.2.1.1	Animals.....	25
6.2.1.2	Cigarette smoke exposure protocols	26
6.2.1.2.1	Dose finding CS exposure	26
6.2.1.2.2	Prenatal CS exposure.....	26
6.2.1.2.3	Preconceptional CS exposure	27
6.2.1.3	Quantification of CS exposure	28
6.2.1.4	Mating.....	28
6.2.1.5	Body weight.....	28
6.2.1.6	Lung function assessment	28
6.2.1.7	Bronchoalveolar lavage.....	29
6.2.1.8	Serum.....	29
6.2.1.9	Spermatozoa isolation	29
6.2.2	Flow cytometry.....	30
6.2.2.1	Single cell preparation	30
6.2.2.2	Fluorescence activated cell sorting.....	30
6.2.3	RNA expression analysis.....	32
6.2.3.1	Tissue processing for RNA isolation.....	32
6.2.3.2	RNA Isolation	32
6.2.3.3	RNA quality control	32
6.2.3.3.1	RNA gel electrophoresis	32
6.2.3.3.2	Capillary electrophoresis	32
6.2.3.4	RNA reverse transcription	33
6.2.3.5	qRT-PCR.....	33
6.2.3.6	Amplicon validation	34
6.2.3.6.1	DNA gel electrophoresis	34
6.2.3.6.2	PCR Clean-Up	34
6.2.3.6.3	Eurofins Genomics sequencing.....	34
6.2.3.7	Library preparation and Next Generation Sequencing	35
6.2.3.7.1	mRNA sequencing	35

TABLE OF CONTENTS

6.2.3.7.2 miRNA sequencing35

6.2.4 Histology..... 35

6.2.4.1 Stainings36

6.2.4.1.1 Hematoxylin and Eosin (H&E)36

6.2.4.1.2 Diff-Quik Staining36

6.2.4.1.3 Immunohistochemistry.....36

6.2.4.2 Histology analyses37

6.2.4.2.1 Thymus histology37

6.2.4.2.2 Testes histology37

6.2.5 Statistical analyses 37

6.2.5.1 Statistics with Prism37

6.2.5.2 Statistics: mRNA NGS analysis38

6.2.5.3 Statistics: miRNA NGS analysis.....38

6.2.5.4 Statistics: offspring’s body weight analysis after adolescent parental smoking .39

7 RESULTS 40

7.1 CS dose finding for prenatal and preconceptional murine exposure models 40

7.1.1 Characterization of CS exposure of mild and heavy smoking..... 40

7.1.2 Macrophages and neutrophils are increased in BALF after CS exposure 42

7.2 Mild maternal smoking affects the frequency and transcriptome of thymic T cells in murine offspring 43

7.2.1 Characteristics of dams and offspring following mild maternal smoking 43

7.2.1.1 Maternal phenotype and pregnancy outcome43

7.2.1.2 Offspring’s phenotype after mild prenatal CS exposure44

7.2.2 T cell populations are affected by prenatal CS exposure in lung, spleen and thymus in offspring 44

7.2.2.1 T cells in lungs and spleen44

7.2.2.2 Thymocytes.....46

7.2.3 Changes in transcriptome of CD8SP thymocytes after prenatal CS exposure 47

7.2.3.1 Canonical pathway analysis of CD8SP thymic T cells48

7.2.3.2 *In silico* network analysis of CD8SP thymocytes48

7.2.3.3 Confirmation of gene regulation in the NGS dataset via qRT-PCR50

7.3 Paternal preconceptional smoking in puberty affects miRNAs in spermatozoa and increases body weight in male but not in female offspring 52

TABLE OF CONTENTS

7.3.1	Adolescent smoking characteristics of future fathers and mothers	52
7.3.1.1	Parental body weight development during CS exposure	52
7.3.1.2	Inflammatory cell counts in BALF of CS-exposed future fathers	52
7.3.2	Frequency and morphology of spermatogonia and spermatozoa were normal after adolescent CS exposure	53
7.3.3	Preconceptional CS exposure affects body weight development in offspring	55
7.3.3.1	Parent-of-origin and sex-dependent body weight progression until PND3	55
7.3.3.2	PND21 - the body weight follow-up	56
7.3.4	Spermatozoal miRNAs were altered in developmental pathways	58
7.3.5	PND21 offspring of CS-exposed fathers do not suggest metabolic changes in the liver	62
8	DISCUSSION	64
8.1	Mild maternal smoking during pregnancy	64
8.1.1	<i>In utero</i> exposure to CS can decrease the thymus size	64
8.1.2	Nicotine affects thymocytes	65
8.1.3	Origin of prenatal CS-induced changes in lymphocytes	65
8.1.4	Innate memory-like CD8SP thymocytes	66
8.1.5	Limitations I	67
8.1.6	Conclusion I	68
8.2	Paternal adolescent smoking	69
8.2.1	Parental smoking and effects of nicotine during puberty	69
8.2.2	Environmental exposures of fathers can alter disease risk in offspring	70
8.2.3	Sperm-borne miRNAs and paramutations in offspring	70
8.2.4	Limitations II	73
8.2.5	Conclusion II	73
8.3	Future perspectives	75
8.3.1	Prenatal mild maternal smoking	75
8.3.2	Preconceptional adolescent smoking	75
8.3.3	Asthma models	76
9	BIBLIOGRAPHY	77

10 EIDESSTATTLICHE VERSICHERUNG.....	91
11 APPENDIX.....	92
11.1 Supplemental results	92
11.2 Abbreviations	99
11.3 List of figures	104
11.4 List of tables.....	106
11.5 Curriculum vitae	107
11.6 Acknowledgments	109

4 INTRODUCTION

4.1 The prevalence of cigarette smoking in Europe

Despite declining rates in some countries, the overall prevalence of smoking in Europe remains high with 29% of Europeans over the age of 15 using not only cigarettes but also other tobacco products (1). The implementation of smoking bans has been stepwise effectuated in several European countries, such that smoking is prohibited in public places, playgrounds and in cars in the presence of children. In Italy, smoking in vehicles is further not allowed in the presence of a pregnant woman. Diminishing exposures to second-hand smoke is important but does not eliminate the negative consequences of prenatal smoking on the health of future children (1). Active smoking during pregnancy remains a public health issue with 15% to 27% of pregnant women continuing to smoke (2,3). Of note, smoking behavior is mostly assessed through self-report in epidemiological studies (4–8). Therefore, underreporting of smoking during pregnancy has shown to be an issue in human studies (9–12). In consequence, mild smoking behaviors might be concealed and could escape epidemiological assessments thus preventing to systematically investigate the effect of mild maternal smoking on offspring's health.

But not only smoking during pregnancy remain an health issue, also smoking among teenagers. Although the age at which minors start to smoke has been progressively decreasing over the years, the prevalence of smoking has been steadily increasing with age in 11 to 15-year-old boys and girls (**Figure 1A-B**) (1). Worldwide, the World Health Organization (WHO) reported on 7% of children actively smoking at the age of 13 to 15. This 7% of smoking minors translates to 24 million children worldwide with highest prevalence in Europe and America, where girls tend to smoke equally as much as boys (**Figure 1C**) as well as in high-income counties (**Figure 1D**) (13).

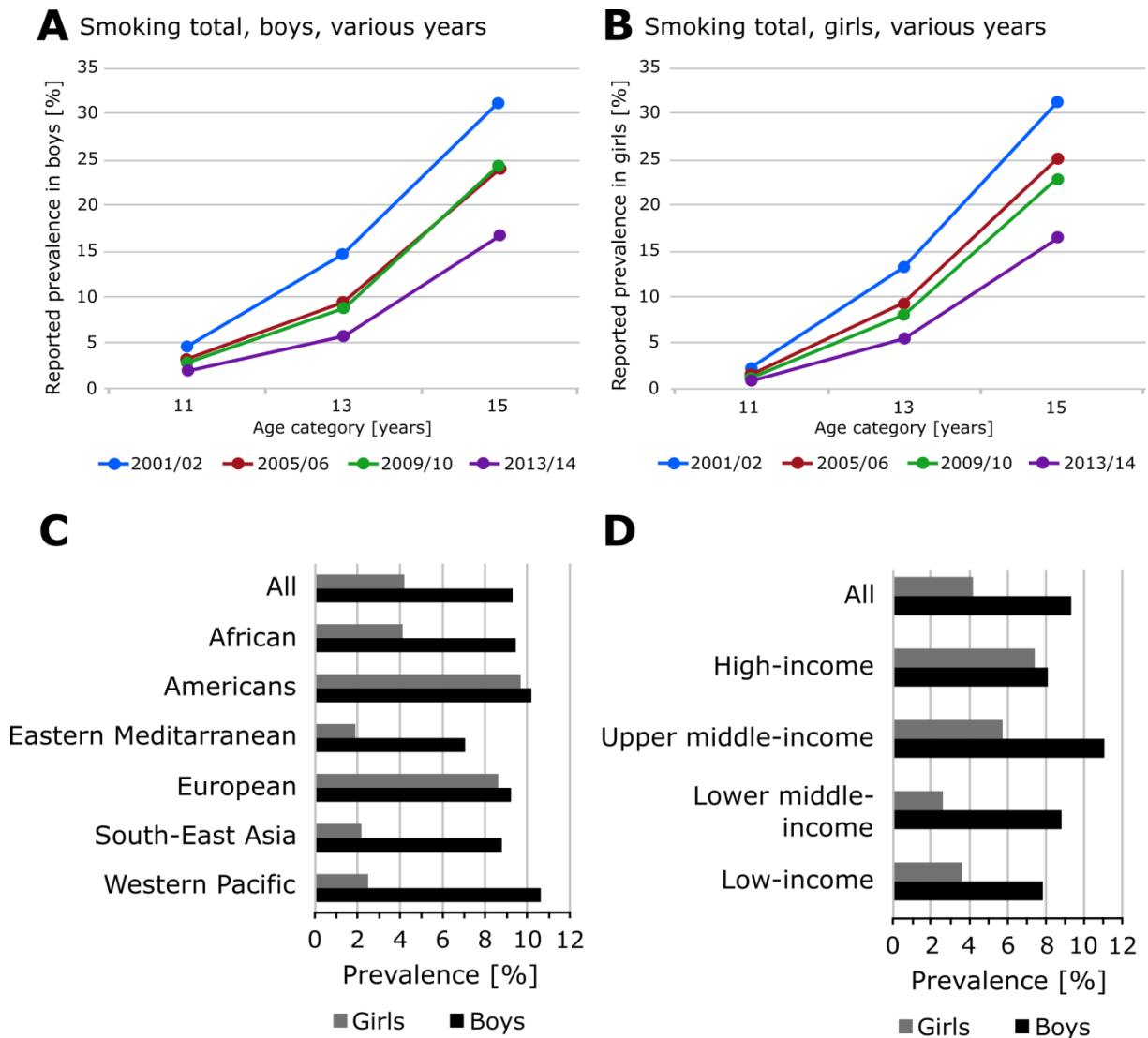


Figure 1 The prevalence of tobacco smoking in boys and girls in Europe and worldwide. 11-15-year-old smoking in A, boys and B, girls in Europe. The smoking behavior of children was assessed in the Health Behaviors in School-aged Children survey 2001-2014. Data are reflecting the following age categories in years: 2001/2 (●), 2005/6 (●), 2009/10 (●) and 2013/14 (●) (1). C, Smoking prevalence in children from age 13 to 15 worldwide; Girls (■), Boys (■). D, Smoking prevalence worldwide in 13-15-year-old children categorized on income; Girls (■), Boys (■) (13). The figure has been adapted from (1,13).

The rising smoking prevalence in adolescence bears the question of smoking harming the germ cells, thereby affecting the health of future generations. In smoking mothers, not only the fetus is affected by cigarette smoke (CS) *in utero*, also the germ cells of the fetus. Thus, prenatal cigarette smoke exposure leads to potential harms in grandchildren (14–18).

4.2 Asthma

4.2.1 Asthma epidemiology and pathophysiology

In Europe, the number of people suffering from asthma is estimated to be 10 million (19). The disease is clinically characterized by breathlessness, chest tightness, and coughing as main symptoms caused by narrowing of the airways and mucus obstruction. This is accompanied by histological changes including goblet cell hyperplasia, airway inflammation and airway smooth muscle thickening (**Figure 2**). Most frequently, asthma starts in childhood affecting 17.6% of children in Europe (20) leading to irreversible airway remodeling and pulmonary dysfunction. Of note, asthma is the most frequent chronic disease in childhood and can persist into adulthood. This explains – apart from severe asthma cases – the high economic burden caused by the disease. Although asthma is well treatable in the majority of cases, it is not curable. Moreover, it is not preventable apart from avoiding parental smoking. In fact, parental tobacco smoking has been described as a leading environmental risk factor of childhood asthma (20).

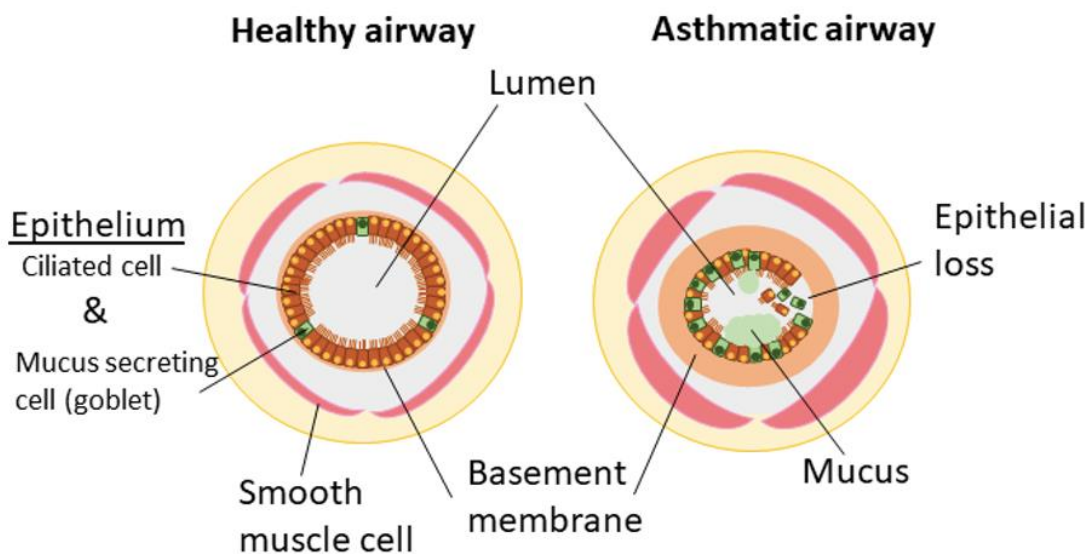


Figure 2 Simplified illustration of the pathophysiology of asthma. In asthmatic airways, the smooth muscle cell layer (red) and the basement membrane (brown) have thickened. The healthy airway epithelium consists of ciliated epithelial cells (orange), and goblet cells (green) that secrete mucus (light green). In asthmatic patients, goblet cells increase in numbers in the airway epithelium (goblet cell hyperplasia), accompanied by a higher mucus production. Hence, the epithelium gets damaged and suffers from epithelial loss. The processes of airway remodeling lead to a narrowing of the lumen. The figure has been published in (21).

4.2.2 The relationship of parental smoking and offspring's asthma risk

Multiple epidemiological studies have correlated maternal smoking and increased asthma susceptibility in offspring after prenatal cigarette smoke exposure (5,22,23). Moreover, recent evidence suggests that also a father smoking in his own puberty could contribute to the asthma risk of children born many years later (8,24). In humans, prenatal cigarette smoking has been associated with decreased birth weights (4,25,26), lung function deficits (23) and a higher susceptibility for asthma and wheeze in children (7,27). Furthermore, it has been shown that asthma developed in childhood can persist into adulthood (8,24). *In utero* exposures to cigarette smoke have further been correlated with immune-related disorders (reviewed in (28)).

To identify the mechanisms how the asthma risk is shaped by maternal smoking behavior in particular, different animal models have been used. An advantage of simpler model organisms like the fruit fly (*Drosophila melanogaster*) and zebrafish (*Danio rerio*) are their fast reproduction by generating a high number of offspring and fast maturation into adulthood (reviewed in (29)). In addition, these animal models have established their use for asthma research (30,31) and respiratory research (32). In zebrafish, exposure to cigarette smoke is limited to water soluble components (33–35). The fruit fly and zebrafish serve as primary screening tools for evolutionary conserved pathways influenced by smoking.

The lung of the mouse is more comparable to the human lung (**Figure 3A-D**) than the trachea of the fruit fly (**Figure 3E-F**) or the gills and swim bladder of zebrafish (**Figure 3G-H**) (reviewed in (29)), and mice offer a variety of models to study asthma.

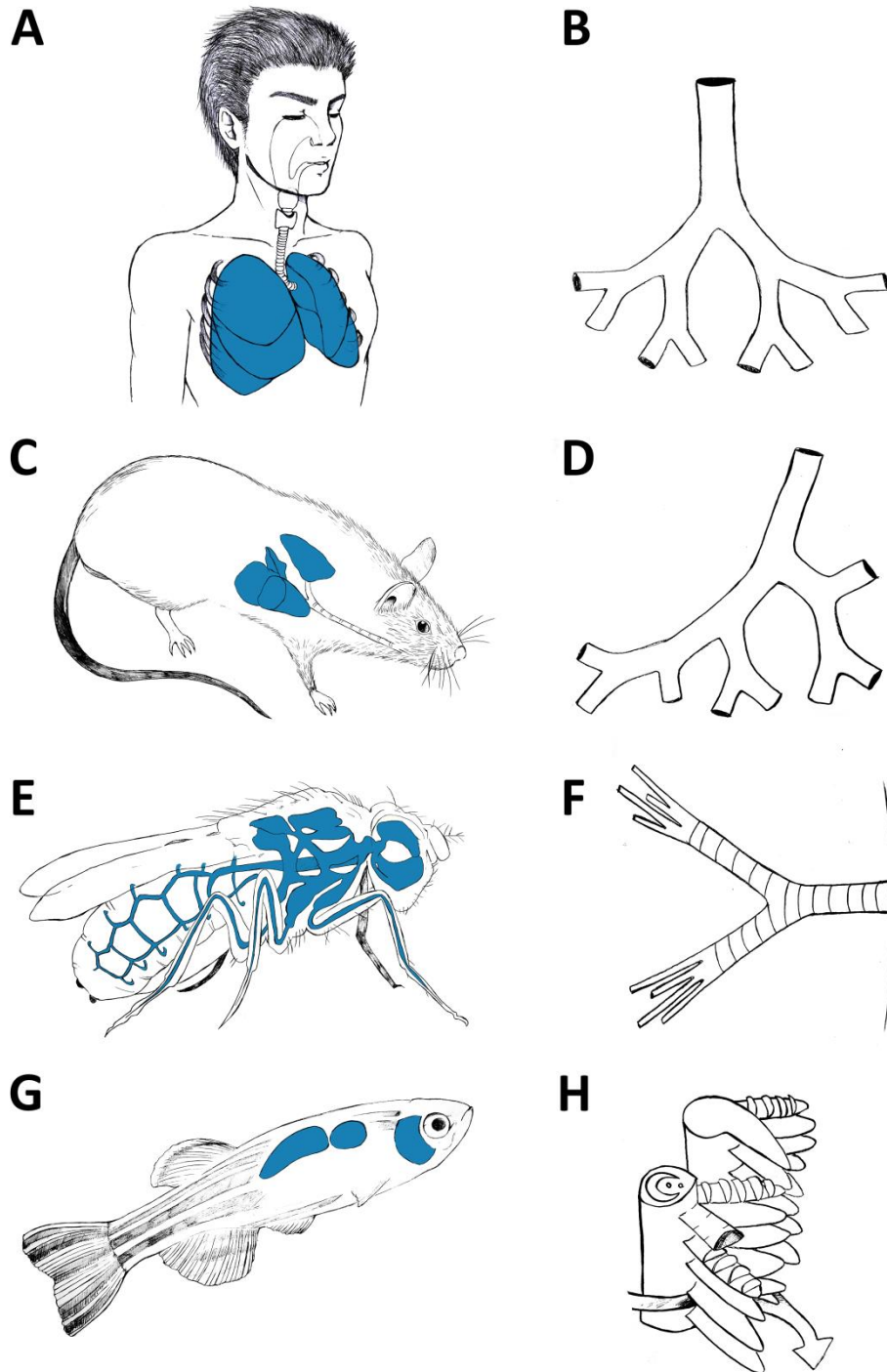


Figure 3 Comparison of the 4 different respiratory systems of human, mouse, fruit fly and zebrafish. A, The human lungs (right lung: 3 lobes; left lung: 2 lobes) are enclosed by the rib cage in the thorax and B, airway branching is arranged dichotomously. C, Murine lungs (right lung: 4 lobes; left lung: 1 lobe) are protected by the rib cage and D, have a monopodial airway branching. E, The fruit fly has a highly branched tubular network with air sacs and breathing openings (spiracles), serving for gas exchange and transport. F, The tracheoles (terminal endings) facilitate gas exchange directly into the tissue via haemolymph (open blood system). G, The swim bladder of zebrafish is filled with air from the esophagus and H, gas exchange occurs through the gills filaments where the lamina is in contact with water. The figure has been published in (29).

In mice, smoking during pregnancy on asthma risk in offspring has been investigated using several heavy or moderate smoking models. Similar to humans, lung function deficits and increased airway resistance together with a decreased body weight in offspring from CS-exposed dams could be reproduced in mice (36). As parental smoking predisposes children to become smokers themselves (37), a murine study investigated adolescent smoking additional to *in utero* CS exposure and observed even stronger lung function deficits, a more pronounced decrease in body weight and structural changes by increased collagen deposition around the main bronchi (38). Furthermore, elevated mucus production correlating with stronger goblet cell hyperplasia and increased stiffness of airways by collagen deposition was observed in offspring from smoking mothers challenged postnatally with the allergens of house dust mite (HDM) (39). In other murine studies, lung function measurements after challenging the airways with the bronchoconstrictor methacholine (MCh), revealed enhanced airway hyperresponsiveness (AHR) in the offspring after prenatal CS exposure (40,41).

The above-mentioned studies therefore demonstrate that the mouse is a suitable model organism, to study mechanisms how increased asthma risk is established after prenatal smoke exposure.

4.3 Prenatal smoking on offspring's immune development

Evidence is sparse that smoking during pregnancy affects the immune system of future generations. In allergic asthma, T cells are important players of the pathophysiology of the disease (42–44) but the mechanisms how prenatal cigarette smoke exposure influences immune cells are unknown. Epidemiological studies on *in utero* exposure of cigarette smoke have observed lower numbers of regulatory T cells in cord blood (45,46) going in hand with an increased expression of the microRNA (miRNA or miR) miR-223 (46). Furthermore, leucocytes isolated from cord blood of children from prenatally smoking mothers had lower levels of insulin-like growth factor 1 (IGF-1) (47). In addition, an IL-13 production after allergen stimulation was observed in cord blood leucocytes, which was absent in donors of non-smoking mothers (48). Moreover, isolated cord blood leucocytes from prenatally cigarette smoke exposed children had higher oxidative stress (49).

4.3.1 Thymus and T cell development

The thymus is a primary lymphatic organ, which holds the T cell development. The organ consists of two lobes, which are segmented into two main areas: the outer cortex and the inner medulla. The cortex is densely populated with T cells and cortical thymic epithelial cells (cTECs). The medulla on the other hand is less cellular and contains macrophages, dendritic cells and medullary thymic epithelial cells (mTECs) besides T lymphocytes.

Thymocyte progenitors develop in the bone marrow, enter the thymus and migrate to the cortex as double-negative (DN) T cells. Double-negative thymocytes do not express the cell surface markers CD4 and CD8. DN thymocytes are further distinguished by sequential upregulation of the markers CD25 and CD44 (**Figure 4**). In the next stage, thymic T cells express CD4 and CD8, so-called double-positive (DP) T cells and undergo positive selection. During the positive selection, $\alpha\beta$ T cell receptors (TCR) bind to class I and class II major histocompatibility complexes (MHC) of cTECs that present peptides of self-antigens. Thymocytes are promoted to survive if the binding of the two receptors have low affinities. Apoptosis is induced in T cells that do not recognize self-MHC-molecules (death by neglect). During negative selection, thymocytes which TCRs bind with high avidity to self-peptides presented on MHC molecules either go into apoptosis or differentiate into natural regulatory T cells (nTreg). During the selections processes, T cells start to express CD3, the co-receptor of TCR. Committing to either CD4 or CD8, single-positive (SP) thymocytes migrated into the medulla, where the T cells bind to MHCs of macrophages, dendritic cells and mTECs. The negative selection is not only occurring to DP thymocytes in the cortex but also to SP thymocytes in the medulla. Mature naïve SP T cells then leave the thymus to circulate the periphery (reviewed in (50)).

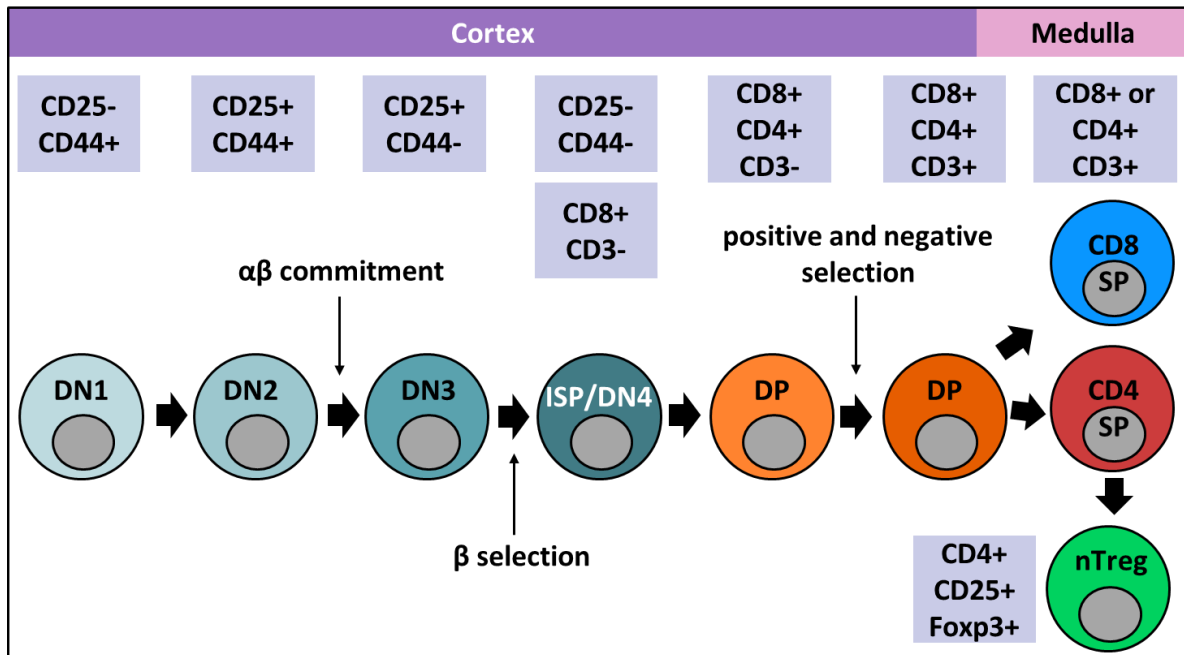


Figure 4 Stages of thymic T cell development. Progenitor T cells migrate from bone marrow (not shown) into the thymus. First, T cells are double negative (DN), lacking CD8 and CD4 expression. DN stages 1-4 are distinguished by the markers CD25 and CD44. After the T cell receptor (TCR) completes $\alpha\beta$ commitment, cells express CD8 and CD4 (double positive, DP). During positive and negative selection, T cells are tested and selected. DP thymocytes differentiate into single-positive (SP) CD8 or CD4. CD4SP T cells can further differentiate into natural regulatory T cells (expression of the transcription factor forkhead box protein P3 (Foxp3)) in the thymus. The figure has been adapted from (51).

4.4 Preconceptional adolescent smoking and how it can affect the male germ line

Until recently, the paternal contribution to an offspring's disease risk has been deemed purely via genetics. Latest studies in human and mice however identified environmental conditions of the father like mental stress (52,53), obesity (54–56) and pubertal smoking (57,58) as potential risk factors for disease susceptibilities in future children. Recent multicenter epidemiological studies investigated smoking during paternal adolescence on obesity (57) and asthma risk (58) in offspring. Svanes and colleagues (2017) observed an increased risk of early-onset non-allergic asthma, particularly when fathers smoked before the age of 15 (58). Men transmit their genetic information via sperm to the next generation. Potential effects of smoking on sperm quality have been suggested as alterations in DNA methylation (59,60), histone-to-protamine transition (61) and influencing small non-coding RNA (sncRNA) contents in sperm cells (62). Thus, murine

models for smoking during puberty are needed to identify the processes of the underlying mechanisms in more detail.

4.4.1 Puberty

Puberty describes the phase of sexual maturation for reproduction and ends into adulthood. The onset of puberty in most mammals is initiated by the release of gonadotropin releasing hormone (GnRH) from the hypothalamus (63–66). The subsequent increase of three gonadal steroids (estradiol, progesterone and testosterone) induces changes of the body and in the brain of boys and girls. In boys, the main gonadal steroid is testosterone (67), while estradiol and progesterone dominate in girls (68). In mice, the onset of adolescence is initiated during their fourth week of life (**Figure 5**). Female rodents start puberty with the vaginal opening (69,70), followed by the first estrus several days later, which reaches regular cyclicity within days (71). In male rodents, the beginning of adolescence is not as easily observable as in females. It is characterized as the separation of the prepuce from the glans penis, defined as the preputial separation (72). Mice complete puberty at the age of seven weeks and reach adulthood with eight weeks of age (**Figure 5**). (reviewed in (73))

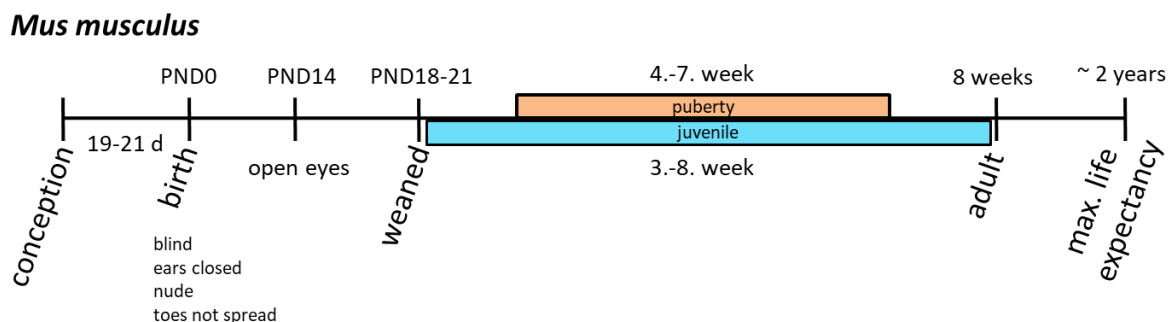


Figure 5 Murine development. In mice, gestation occurs to 19-21 days (d) after conception. Pups are born with closed ears, non-spread toes, underdeveloped eyes and without fur (PND0). At PND14, they open their eyes and mice are fully developed although small. They get weaned from the mother at PND18-21. During their 4th week of age, mice enter puberty, which is completed in the 7th week. From week 3 until week 8 mice are considered as juvenile and enter adulthood in their 8th week of age. The maximum life expectancy for laboratory stains is estimated to 2 years. The figure has been published in (29).

4.4.1.1 Spermatogenesis

Spermatogenesis is the production of haploid sperm cells in males. In mammals, this process is restricted to the testes, located in the tubular system of seminiferous tubules. The tubules consist of different layers of particular cell types. The development starts with the spermatogonia at the basal membrane and ends with the release of spermatozoa into the lumen (**Figure 6**). Sertoli cells are the epithelial cells of seminiferous tubules and provide nutrition, connection and protection to the different cell stages of sperm development (74,75). Sertoli cells are connected by tight junctions that form the blood-testis barrier and separate the germinal epithelium into a basal (BC) and adluminal compartment (AC) (75). Type A spermatogonia (SpG_A) are stem cells located at the basal membrane. They develop into intermediate spermatogonia (SpG_i) and further into type B spermatogonia (SpG_B) by mitosis (74). Type B spermatogonia pass the blood-testis barrier entering the adluminal compartment (75) and undergo the last mitosis into primary spermatocytes (SpC I). Through meiosis, the secondary spermatocytes (SpC II) derive, which undergo a second meiosis to generate 4 haploid spermatids. At this stage, the early spermatids (eSpt) are still connected via cytoplasmic bridges that make them functionally diploid. Located at the boarder of the lumen, the late spermatids (lSpt) lose their cytoplasmic connections and release redundant cytoplasm (residual bodies (R)) (**Figure 6**) (74,75). Spermatids differentiate into spermatozoa by the formation of the acrosome from the Golgi apparatus, the condensation of the nucleus and the formation of the acrosomal cap. Thus, the nucleus rotates towards the basal membrane and the flagellum develops extending into the lumen. In the nucleus, histones are replaced by protamines. Protamines facilitate an inhibition of transcription in the nucleus. The sperm cells get released into the lumen (now called spermatozoa) by the Sertoli cells that phagocyte the residual bodies (74). The immotile spermatozoa are transported into the *rete testis* by the contraction of the myofibroblasts (My) surrounding the seminiferous tubules (75). The overall duration of spermatogenesis is estimated to 65 days in humans and 34.5 days in mice (74).

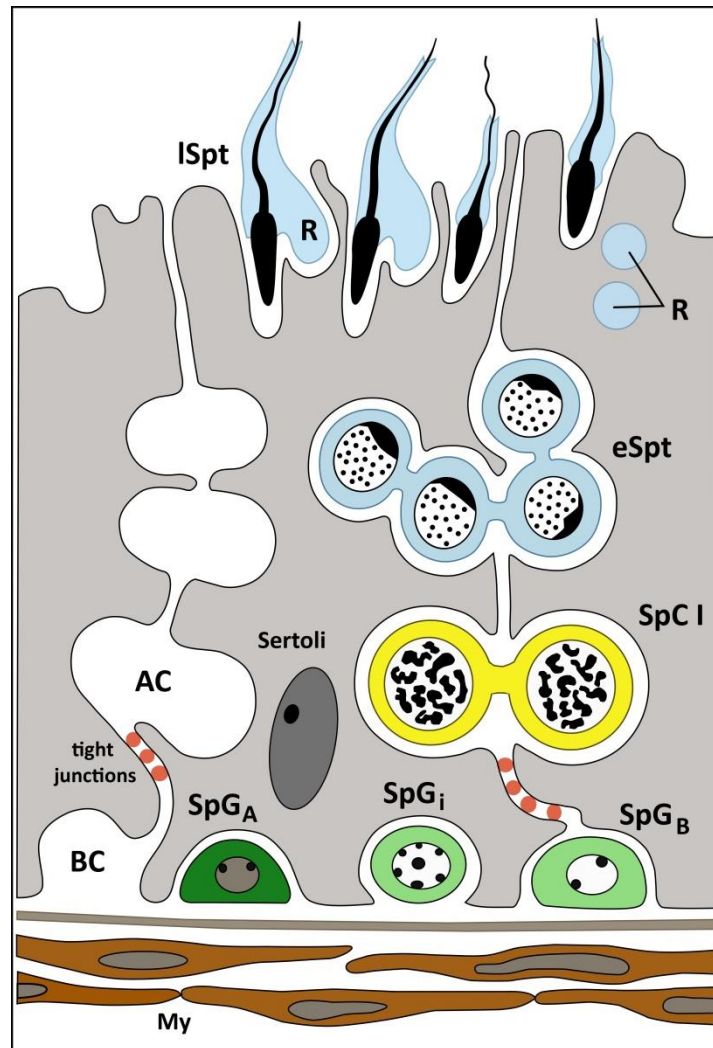


Figure 6 Schema of the germinal epithelium in testis. Sertoli cells (grey) are connected via tight junctions and form the blood-testis barrier. Thus, the germinal epithelium is segmented in the basal (BC) and adluminal compartment (AC). Spermatogonia are located at the basal membrane. Type A spermatogonia (SpG_A) proliferate, hence characterized as intermediate spermatogonia (SpG_i). After their second proliferation, they are characterized as type B spermatogonia (SpG_B), which yield primary spermatocytes ($SpC I$). Through 2 steps of meiosis, early spermatids (eSpt) arise. Late spermatids (ISpt) are located at the border of the lumen. Residual bodies (R) contain spare cytoplasm. Myofibroblasts (My). The figure has been adapted from (75).

4.4.1.2 Small non-coding RNAs in sperm cells

Small non-coding RNAs (sncRNAs) are short RNA fragments derived from messenger (mRNAs), transfer RNAs (tRNAs), introns or encoded in the DNA, that are functionally active by enhancing or silencing mRNA translation. It has been shown that sperm contain a variety of sncRNAs including miRNAs, transfer-RNA-derived small RNAs (tsRNAs or tRNA-derived RNA fragments (tRFs)) and PIWI-interacting RNAs (piRNAs). During spermatogenesis in testis, sperm cells are enriched with miRNAs, tsRNAs and piRNAs throughout their developmental stages. In the epididymis, the content of sncRNAs is

dominated by miRNAs and tsRNAs while spermatozoa undergo maturation (**Figure 7**) (reviewed in (76)).

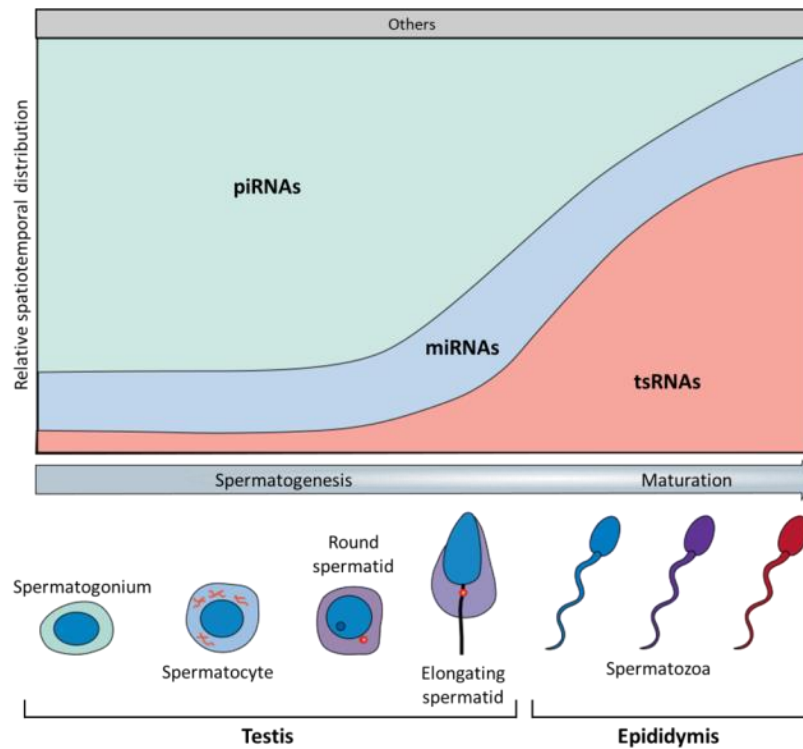


Figure 7 Spatiotemporal distribution of snRNAs. During spermatogenesis in the testis, piRNAs and miRNAs are prominent in spermatogonia (green cell), spermatocytes (blue cell) and round/elongated spermatids (violet). During spermatozoa maturation in the epididymis, sperm cells contain tsRNAs and miRNAs for the greater part, while the frequency of miRNAs is more stable throughout the spatiotemporal distribution. PIWI-interacting RNA (piRNA), microRNA (miRNA), transfer-RNA-derived small RNA (tsRNA). The figure has been adapted from (76).

4.4.1.3 miRNA biogenesis

The first miRNA was discovered in *Caenorhabditis elegans* in 1993 (77). miRNAs are transcribed by RNA polymerase II/III in the nucleus directly from encoding loci of the DNA or derive from introns or degraded mRNA. The generated RNA sequence is defined as primary miRNA (pri-miRNA), forming a hairpin structure (**Figure 8**) (78,79). Drosha, a RNase III endonuclease, shortens both ends of the pri-miRNA by cleavage and generates the precursor miRNA (pre-miRNA) (78). Exportin 5 transports the pre-miRNA through a nuclear pore out of the nucleus into the cytoplasm (80,81), where the pre-miRNA is recognized and processed by the RNase III endonuclease Dicer (82). Dicer cleaves at both strands of the hairpin structure to remove the loop, which generates the miRNA:miRNA* duplex (guide:passenger strand). Argonaute 2 (AGO2) associates with Dicer and bind the

miRNA:miRNA* duplex. The strands get unwind and the passenger strand gets released from the complex. The biological active strand (mostly the guiding strand, ~22 nt long) remains bound to AGO2 and they form the RNA-induced silencing complex (RISC). Most commonly, RISC targets the 3' untranslated region (UTR) of the mRNA where the miRNA binds to the complementary mRNA outside the open reading frame. The complex induces mRNA degradation or translational repression by prevention of ribosomal binding. (reviewed in (83,84))

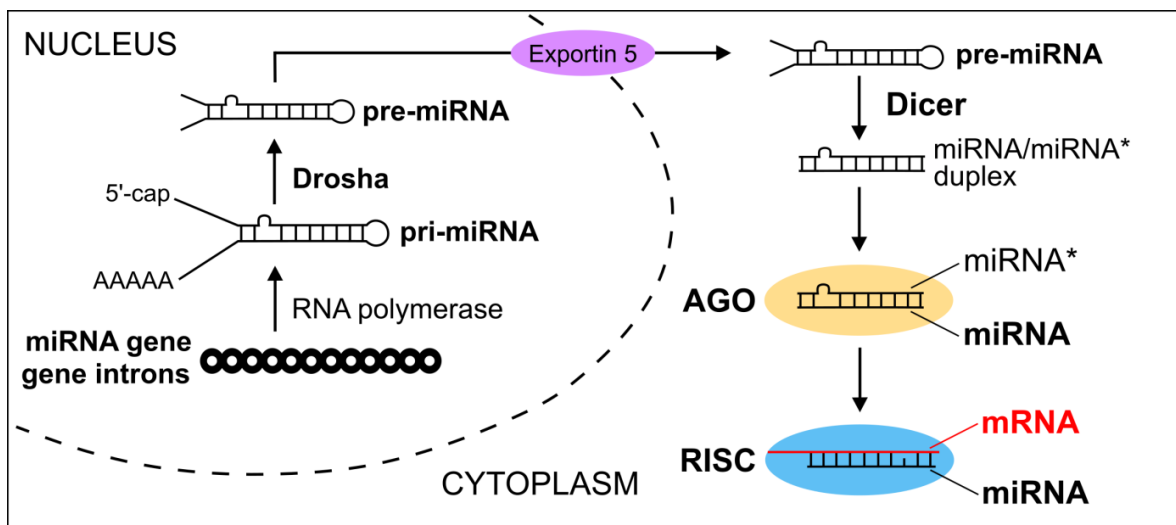


Figure 8 Simplified schema of miRNA biogenesis. miRNAs can be encoded directly from genes or derive from introns by RNA polymerase II or III. The primary miRNA (pri-miRNA) has a poly-adenine tail (AAAAA) and a 5-prime cap (5'-cap). The pri-miRNA is cleaved by the endonuclease Drosha and generates the precursor miRNA (pre-miRNA). The transporter protein Exportin 5 transports the pre-miRNA from the nucleus into the cytoplasm, where the hairpin loop is removed by the endonuclease Dicer. Argonaute (AGO) binds the miRNA duplex and the passenger strand (miRNA*) gets released. RNA-induced silencing complex (RISC) binds to the messenger RNA (mRNA) at the complementary sequence of the miRNA. The figure has been adapted from (85).

4.5 Rationale

As stated above, smoking during pregnancy is a well-known risk factor for impaired respiratory health in offspring but mild maternal smoking during pregnancy is underreported and therefore might escape epidemiological assessments. Therefore, it is unknown at present how prenatal mild smoking affects the offspring health. This knowledge is, however, required to decide if public resources for smoking cessation programs could primarily be spent on heavily smoking mothers or not. This knowledge gap can only be addressed in cigarette smoke exposure-controlled mouse models.

In a second aspect, paternal smoking during adolescence gains more and more relevance for the respiratory health of future offspring but the underlying inheritable mechanisms in mature spermatozoa remain elusive.

5 AIMS AND OBJECTIVES

The aims of the present work were to obtain insight into the mechanisms how

- I. Mild maternal smoking during pregnancy affects immunity in offspring
- II. Paternal smoking in adolescence affects epigenetic signatures in sperm cells

Therefore, the main objectives for aim I were to:

1. Develop a mouse model for mild maternal smoking in pregnancy
2. Identify a dose of cigarette smoke corresponding to mild maternal smoking in pregnancy
3. Investigate if mild maternal smoking during pregnancy, even in absence of growth retardation and lung function deficits, changes proportions of peripheral T cells in offspring
4. If so, are these changes tissue specific or have a common origin in the thymus
5. If the putative changes of T cells are similar in male and female offspring

The main objectives for aim II were to:

1. Develop a mouse model for parental smoking in adolescence
2. Investigate if parental smoking in adolescence affects the phenotype of offspring
3. If so, are these effects a) sex- specific and/or b) differ if a father or a mother had smoked during their own puberty
4. Clarify if smoking in adolescence affects numbers and/or the morphology of sperm cells
5. Investigate if numbers of spermatogonia are affected by smoking
6. Elucidate if paternal smoking in adolescence influences the pattern of sncRNAs as potential vectors of epigenetic information in spermatozoa

6 MATERIALS AND METHODS

6.1 Materials

6.1.1 Mouse strain

Strain	Vendor	Country
C57BL/6J	Charles River	Sulzfeld, GER

Table 1 Mouse strain used for animal experiments.

6.1.2 Chemicals and reagents

Substances	Manufacturer	Country
Acetic acid	Merck	Darmstadt, GER
Acetyl- β -methylcholine chloride	Sigma-Aldrich	St. Louis, Missouri, USA
Agar-Agar, Bioscience, granulated	Carl Roth	Karlsruhe, GER
Aluminum sulfate hydrate	Sigma-Aldrich	St. Louis, Missouri, USA
Ammonium chloride	Carl Roth	Karlsruhe, GER
Aqua	B Braun	Melsungen, GER
Bench Top 1kb DNAladder	Promega	Madison, Wisconsin, USA
Bovine Serum Albumin	PAN-Biotech	Aidenbach, GER
Calcium chloride	Carl Roth	Karlsruhe, GER
Calcium chloride	Merck	Darmstadt, GER
Chloroform	AppliChem Panreac	Darmstadt, GER
Collagenase from Clostridium histolyticum	Sigma-Aldrich	St. Louis, Missouri, USA
D(+)-Glucose	Carl Roth	Karlsruhe, GER
DAPI	Invitrogen™ Thermo Fisher	Carlsbad, California, USA
Disodium phosphate	Carl Roth	Karlsruhe, GER
Entellan® new	Merck	Darmstadt, GER
Eosin Y disodium salt	Sigma-Aldrich	St. Louis, Missouri, USA
Ethanol \geq 99.8 %	Carl Roth	Karlsruhe, GER
Ethylene glycol	Sigma-Aldrich	St. Louis, Missouri, USA
Ethylenediaminetetraacetic acid Disodium Salt 2-hydrate	AppliChem Panreac	Darmstadt, GER
Foetal Calf Serum	PAN-Biotech	Aidenbach, GER

Formamide, deionized	Sigma-Aldrich	St. Louis, Missouri, USA
Gel Loading Dye, Purple (6x), no SDS	New England BioLabs	Ipswich, Massachusetts, USA
Hematoxylin	Sigma-Aldrich	St. Louis, Missouri, USA
Ketamidol®	WDT	Garbsen, GER
Liquid nitrogen	Westfalen AG	Münster, GER
Magnesium dichloride	Merck	Darmstadt, GER
Monosodium phosphate	Carl Roth	Karlsruhe, GER
Mounting medium	Dako North America	Carpinteria , California, USA
Narcoren®	Merial GmbH	Hallerbergmoos, GER
Paraformaldehyde	Sigma-Aldrich	St. Louis, Missouri, USA
Paraplast Plus	Carl Roth	Karlsruhe, GER
Potassium bicarbonate	Carl Roth	Karlsruhe, GER
Potassium chloride	Carl Roth	Karlsruhe, GER
Potassium dihydrogen orthophosphate	Carl Roth	Karlsruhe, GER
QIAzol Lysis Reagent	Qiagen	Hilden, NLD
RNAlater®	Sigma-Aldrich	St. Louis, Missouri, USA
Roti®-Histofix 4%	Carl Roth	Karlsruhe, GER
Rotiphorese 10xTBE buffer	Carl Roth	Karlsruhe, GER
Sodium acide	Sigma-Aldrich	St. Louis, Missouri, USA
Sodium azide	Sigma-Aldrich	St. Louis, Missouri, USA
Sodium chloride	Sigma-Aldrich	St. Louis, Missouri, USA
Sodium dihydrogen phosphate monohydrate	Merck	Darmstadt, GER
Sodium iodate	Sigma-Aldrich	St. Louis, Missouri, USA
Sodium Pyruvate	PAN-Biotech	Aidenbach, GER
SYBR Green II	Lonza	Basel, CHE
Trypan Blue	Sigma-Aldrich	St. Louis, Missouri, USA
UltraPure™ Agarose	Invitrogen™ Thermo Fisher	Carlsbad, California, USA
Xylavet®	cp-pharma	Burgdorf, GER
50 bp DNALadder	New England BioLabs	Ipswich, Massachusetts, USA

Table 2 Chemicals and reagents.

6.1.3 Buffers and solutions

Name	Substances	Concentration	Weight/volume
10x PBS 1 l, pH 6.6	KCl	27 mM	2 g
	KH ₂ PO ₄	17.6 mM	2.4 g
	NaCl	1.37 M	80 g
	Na ₂ HPO ₄	53.7 mM	14.4 g
Gey'sche Lysis buffer 1 l, pH 7.2	KHCO ₃	10 mM	1.0012 g
	NH ₄ Cl	155 mM	8.29095 g
	EDTA	10 µM	37.224 mg
	Aqua dest.		dissolve
4% Paraformaldehyde 1 l	PBS-Azid		960 ml
	Paraformaldehyde	4%	40 ml
FACS wash buffer 250 ml	1x PBS		225 ml
	FCS	1%	25 ml
	Sodiumazide	0,1%	2.5 g
Dulbecco's PBS + Ca ²⁺ and Mg ²⁺ 1 l, pH 7.2	NaCl		8 g
	KCl		0.2 g
	NaH ₂ PO ₄ x 2H ₂ O		1.44 g
	KH ₂ PO ₄		0.2 g
	CaCl ₂ x 2 H ₂ O		0.132 g
	MgCl ₂ x 6 H ₂ O		0.1 g
MACS buffer 1 l, pH 7.2	1x PBS		
	BSA	0.5%	
	EDTA	2 mM	
Sperm isolation medium 100 ml, pH 7.2	1x Dulbecco's PBS + Mg, Ca		93 ml
	D-Glucose	5.6 mM	1 ml
	Sodium Pyruvate	1 mM	1 ml
	BSA	10%	5 ml
RNA loading buffer per sample	Formamide, deionized	60%	18.0 µl
	5x TBE buffer	0,5x	3.0 µl
	SYBR Green II (1:100)	1:2000	1.5 µl
Hematoxylin Gill's formula 1 l	Hematoxylin		6 g
	Sodium iodate		0.6 g

	Aluminum sulfate hydrate		52.8 g
	Ethylene glycol		250 ml
	Acetic acid		60 ml
	H ₂ O		690 ml

Table 3 Buffers and solutions.

6.1.4 Antibodies

Antibody	Fluorochoime	Clone	Manufacturer	Country	Application
CD8b	FITC	YTS156.7.7	BioLegend	San Diego, California, USA	FC
CD3	APC	145-2C11	MACS Miltenyi Biotec	Bergisch Gladbach, GER	FC
CD4	APC-H7	GK1.5	BD Pharmingen	San Diego, California, USA	FC
CD4	BV421	RM4-5	BioLegend	San Diego, California, USA	FC
Fc Block (CD16 / CD32)	-	2.4G2	BD Pharmingen	San Diego, California, USA	FC
Ki-67 Monoclonal Antibody	-	SolA15	eBioscience™ Thermo Fisher	San Diego, California, USA	IHC
Goat anti-Rat IgG (H+L) Cross-Adsorbed Secondary Antibody	Alexa Fluor 546	polyclonal	Thermo Fisher scientific	Waltham, Massachusetts, USA	IHC
Anti-Caspase-3 antibody	-	polyclonal	abcam	Cambridge, GBR	IHC
Goat anti-rabbit IgG (H+L) Cross-Adsorbed Secondary Antibody	Alexa Fluor 488	polyclonal	Invitrogen™ Thermo Fisher	Carlsbad, California, USA	IHC

Table 4 Monoclonal and polyclonal antibodies used for flow cytometry (FC) and immunohistochemistry (IHC). CD4 clone GK1.5 was used for stainings measured on LSRII and CD4 clone RM4-5 was used for cell sorting with Arialu.

6.1.5 Oligonucleotides

Oligonucleotides were synthesized by metabion international AG (Planegg, Germany) and validated before use by efficiency testing, gel electrophoresis (see section 6.2.3.3) and amplicon sequencing (see section 6.2.3.6).

Gene	Sense (5'-3')	Anti-sense (5'-3')	Ensembl
HPRT	CAGGCCAGACTTTGTTGGAT	ACGTGATTCAAATCCCTGAAGT	ENSMUSG00000025630
Tbp	AATTGTACCGCAGCTTCAAAT	ATGATGACTGCAGCAAATCG	ENSMUSG00000014767
Cyp1a1	CGTTACCTGCCTAACTCTTC	ATGCTCAATGAGGCTGTCTG	ENSMUSG00000032315
Il4ra	GAAAACCTCACATGCATCCCG	GCCCACAGTTCCATCTGGTAT	ENSMUSG00000030748
Il10rb	TACACCTGCGTTTCTCAGCC	AGTAAGTTGTCCACGGCTCC	ENSMUSG00000022969
Foxp1	GAAAGCTTGTCACGAGGA	GAAAGGCTGGGAAGTCGTCA	ENSMUSG00000030067
Runx3	GGGCGAGGGAAGAGTTTC	AGCCACTTGGGTAGGGTTG	ENSMUSG00000070691
Eomes	TCATCACCAAACAGGGCAGG	CGAAAACATTGTAGTGGGCGG	ENSMUSG00000032446
IL-6	CTCCAACAGACCTGTCTATAC	GTGCATCATCGTTGTTTCATAC	ENSMUSG00000025746
Adipoq	TGACGACACAAAAGGGCTC	ACCTGCACAAGTTCCTTGG	ENSMUSG00000022878
Lepr	CAGACCCTGAAAGCAGTTCTAT	GACTCATCCTCACAGGTTAC	ENSMUSG00000057722
Insr	GAGGAGAGACCTTGAAATTGG	GAGTGATGGTGAGGTTGTGTT	ENSMUSG00000005534
Pparg	CCCTGGCAAAGCATTGTATG	GGTGATTTGTCCGTTGTCTTC	ENSMUSG00000000440
Pik3cg	TTGCAGGACTTCACACAGCA	CAGGGGCTTCTTCTTGAGG	ENSMUSG00000020573

Table 5 Genes and primer sequences for qRT-PCR.

6.1.6 Commercial kits

Kit	Manufacturer	Country
Mouse/rat Cotinine ELISA	Calbiotech	El Cajon, California, USA
miRNeasy Mini Kit	Qiagen	Hilden, NLD
miRNeasy Micro Kit	Qiagen	Hilden, NLD
QuantiTect Reverse Transcription Kit	Qiagen	Hilden, NLD
Wizard®SV Gel and PCR Clean-Up System	Promega	Madison, Wisconsin, USA
LightCycler® 480 SYBR® Green I Master	Roche Diagnostics GmbH	Mannheim, GER
Diff-Quik Kit	Siemens Healthineers	Erlangen, GER
Agilent RNA 6000 Pico Kit	Agilent Technologies	Santa Clara, California, USA
NEBNext Poly(A) mRNA Magnetic Isolation Module (NEB)	New England BioLabs	Ipswich, Massachusetts, USA
NEXTflex Rapid Directional qRNA-Seq Kit	Bioo Scientific	Austin, Texas, USA
High Sensitivity DNA Chip	Agilent Technologies	Santa Clara, California, USA
NEBNext Multiplex Small RNA Library Prep Set	New England BioLabs	Ipswich, Massachusetts, USA

Table 6 Commercial kits.

6.1.7 Equipment and devices

Device	Name	Manufacturer	Country
Centrifuges	CS-6KR Centrifuge	Beckman	Brea, California, USA
	Centrifuge 5415R	eppendorf	Hamburg, GER
	Mikro 200	Hettich Zentrifugen	Tuttlingen, GER
	Heraeus Fresco 21 Centrifuge	Thermo Fisher scientific	Waltham, Massachusetts, USA
	Rotina 420R	Hettich Zentrifugen	Tuttlingen, GER
	2-6E	Sigma	Kawasaki, JPN
Cytofuges	Cytofuce 2	Thermo Shandon GmbH	Frankfurth am Main, GER
	Cytofuce 3	Thermo Shandon GmbH	Frankfurth am Main, GER
Vortexers	IKA Vortex-Schüttler VF2	IKA	Staufen, GER
	IKA MS3 basic	IKA	Staufen, GER
Cigarette smoke machine	inExpose exposure system	SCIREQ	Montreal, CAN
Lung function device	Flexivent	SCIREQ	Montreal, CAN
Manometer	Manometer	SCIREQ	Montreal, CAN
Heating mat	ThermoLux	Witte + Sutor GmbH	Murrhardt, GER
Balance scales	precision scales	Kern	Balingen, GER
	R160 P	Sartorius	Göttingen, GER
	Entris Precision Balance	Sartorius	Göttingen, GER
Microscopes	Zeiss microscope	Zeiss	Oberkochen, GER
	Primostar	Zeiss	Oberkochen, GER
	BX51	Olympus	Waltham, Massachusetts, USA
+ camera	Olympus DP25	Olympus	Waltham, Massachusetts, USA
	BX41	Olympus	Waltham, Massachusetts, USA
+ camera	DS-Ri1	Nikon	Tokio, JPN
	Axio Observer.Z1	Zeiss	Oberkochen, GER
+ camera	Axiocam MR	Zeiss	Oberkochen, GER

MATERIALS AND METHODS

Tissue-Lyser	Tissue-Lyser II	Qiagen	Hilden, NLD
Thermocycler	Tprofessional TRIO Thermocycler	Biometra	Göttingen, GER
Thermomixer	Thermomixer F1.5	eppendorf	Hamburg, GER
Spectrophotometer	Denovix DS-11	biolab products	Bebensee, GER
Electrophoresis power supply	Powerpac Basic	Biorad	Hercules, California, USA
Gel chamber	peqLab, comb 1.5 mm 24 well	Biotechnologie GmbH	Erlangen, GER
Lightcycler	Lightcycler 480 II	Roche	Basel, CHE
Imaging system	Chemidoc Touch imaging system	Biorad	Hercules, California, USA
Tissue processor	Microm STP120	Thermo Fisher scientific	Waltham, Massachusetts, USA
Embedding station	Histostar	Thermo Fisher scientific	Waltham, Massachusetts, USA
Mikrotom	Microm HM 340 E	Thermo Fisher scientific	Waltham, Massachusetts, USA
Heating plate	Slimlive digital hotplate	Thermo Fisher scientific	Waltham, Massachusetts, USA
Cooling plate	CP-4	Kunz instruments	Nynashamn, SWE
Bioanalyzer	Bioanalyzer Agilent 2100	Agilent Technologies	Santa Clara, California, USA
Sequencer	NextSeq500	Illumina	San Diego, California, USA
	HiSeq2500	Illumina	San Diego, California, USA
Plate reader	sunrise	TECAN	Männedorf, CHE
Incubator	CO ₂ -Auto-Zero	Heraeus instruments	Hanau, GER
Hemocytometer	Neubauer counting chamber	Marienfeld Superior	Lauda-Königshofen, GER
Counter	Counter AC-8	assistent	Sondheim vor der Rhön, GER
Gooseneck lamp	Visilight LED5	VWR	Radnor, Pennsylvania, USA
Magnetic heating stirrer	IKA RET basic	IKA	Staufen, GER
	IKA type RCT	IKA	Staufen, GER
Waterbath	Haake W13	Thermo Fisher scientific	Waltham, Massachusetts, USA
pH-Meter	pH-Meter 766	Calimatic Knick	Berlin, GER

Microwave	MW 7873	Severin	Sundern, GER
Laminar hoods	Scanlaf Mars Safety Class 2	Labogene	Lillerød, DNK
	Scanlaf Mars	Labogene	Lillerød, DNK
Fridges/freezers	4°C / -20°C (privileg de luxe)	Privileg	Stuttgart, GER
	4°C / -20°C (privileg)	Privileg	Stuttgart, GER
	4°C / -20°C (öko Energiesparer)	Privileg	Stuttgart, GER
	-20°C (öko Energiesparer)	Privileg	Stuttgart, GER
	-20°C	Siemens	München, GER
	-80°C (Revco Value Plus)	Thermo Fisher scientific	Waltham, Massachusetts, USA
	-80°C (VWR 60086V)	VWR	Radnor, Pennsylvania, USA
Animal cages	Sealsafe PLUS, Green Line	Tecniplast	Italy

Table 7 Equipment and devices.

6.1.8 Software and websites

Software and websites	Source
BD FACSDiva™ Software v8.0.1	BD Bioscience-US, San Jose, USA
FlowJo software v10	FlowJo, LLC Software, Ashland, USA
GraphPad Prism v6.0	GraphPad Prism Software, San Diego, USA
LightCycler® 480 software v1.5.1	Roche, Mannheim, GER
ImageLab™ software v2.0.1	Biorad Laboratoriens, Hercules, USA
Ingenuity® Pathway Analysis	Qiagen Silicon Valley, Redwood City, USA
FlexiWare Software v6.1, (inExpose)	SCIREQ, Montreal, CAN
FlexiWare Software v7.2, (FlexiVent)	SCIREQ, Montreal, CAN
ImageJ	LOCI, University of Wisconsin, USA
Adobe Photoshop® CC 2015	Adobe, San José, USA
Inkscape v0.92.4	Free Software Foundation, Inc., USA
cell^A v3.4	Olympus Soft Imaging Solution GmbH, Münster, GER
NIS-Elements D v3.1	Nikon, Tokyo, JPN
AxioVision software v4.8	Zeiss, Oberkochen, GER
2100 expert	Agilent Technologies, Santa Clara, California, USA
RNA-seq aligner STAR v2.5	GPLv3 license; http://code.google.com/p/rna-star/

DSeq2 v1.18.1	Bioconductor, Roswell Park Cancer Institute, New York (USA)
FastQC v0.10.1	Babraham Bioinformatics, Babraham, UK
Bowtie	Johns Hopkins University, Maryland, USA
Stata 12	StataCorp LLC, Texas, USA
Stata 15	StataCorp LLC, Texas, USA
Primer-BLAST	https://www.ncbi.nlm.nih.gov/tools/primer-blast/
Standard Nucleotide BLAST	https://blast.ncbi.nlm.nih.gov/Blast.cgi?PAGE_TYPE=BlastSearch
Align Sequences Nucleotide BLAST	https://blast.ncbi.nlm.nih.gov/Blast.cgi?PAGE_TYPE=BlastSearch&BLAST_SPEC=blast2seq&LINK_LOC=align2seq
Reverse complement	http://reverse-complement.com/
miRBase	http://www.mirbase.org/
mirPath v3	http://www.microrna.gr/miRPathv3
RNAcentral	https://rnacentral.org/
Btrim	http://graphics.med.yale.edu/trim/

Table 8 Software and websites.

6.1.9 Consumables

Consumables	Manufacturer	Country
Research Cigarettes 3R4F	University of Kentucky	Lexington, Kentucky, USA
Extraction thimble	membranPure GmbH	Hermingsdorf, GER
1,5ml reaction tube	Eppendorf	Hamburg, GER
2 ml safe-cap tube	Sarstedt	Nümbrecht, GER
Tube 15ml, 120 x 17mm, PP	Sarstedt	Nümbrecht, GER
Tube 50ml, 114 x 28mm, PP	Sarstedt	Nümbrecht, GER
70 µm cell strainer	Corning	Wiesbaden, GER
1 ml syringe	BD	Heidelberg, GER
2 ml syringe	BD	Heidelberg, GER
5 ml syringe	BD	Heidelberg, GER
10 ml syringe	BD	Heidelberg, GER
50 ml syringe	BD	Heidelberg, GER
cannula 26G x 3/8"; 0.45 x 10mm	BD	Heidelberg, GER
cannula 20G x 1 1/2"; 0.9 x 40mm	BD	Heidelberg, GER

cannula 27G x 3/4"; 0.4 x 19mm	BD	Heidelberg, GER
TC Plate 6 Well	Sarstedt	Nümbrecht, GER
96 Well Cell Culture Plate	Corning	Wiesbaden, GER
Tube 5ml, 75 x 12mm	Sarstedt	Nümbrecht, GER
5ml Polystyrene Round-Bottom Tube with Cap	Sarstedt	Nümbrecht, GER
5ml Polystyrene Round-Bottom Tube with Cell-Strainer Cap	VWR	Hannover, GER
Petri dish 35x10mm with cams	Greiner Bio-One	Solingen, GER
Petri dish 92x16mm w/o cams	Sarstedt	Nümbrecht, GER
Filterpur S 0.2	Sarstedt	Nümbrecht, GER
Stericup and Steritop 0.22µm	millipore	Burlington, Massachusetts, USA
Surgical Disposable Scalpels	B Braun	Melsungen, GER
Parafilm "M", PM-996	Sigma-Aldrich	St. Louis, Missouri, USA
Transfer pipette 3.5ml	Sarstedt	Nümbrecht, GER
Slide	Langenbrinck	Emmendingen, GER
Superfrost slide	Langenbrinck	Emmendingen, GER
Leja Slide 8	Leja	Nieuw-Vennep, NLD
Swingsette biopsy embedding cassettes	Carl Roth	Karlsruhe, GER
Tissue embedding sponge	Kartell S.p.A.	Milano, ITA
Cytofuge filter	Thermo Fisher	Runcorn, GEB
PCR plate	Roche Diagnostics GmbH	Mannheim, GER
Seal film for PCR plates	Roche Diagnostics GmbH	Mannheim, GER
Sealing Tape	costar	Washington, D.C, USA
RNA Pico Chips	Agilent Technologies	Santa Clara, California, USA

Table 9 Consumables.

6.2 Methods

6.2.1 Mouse models

6.2.1.1 Animals

The study was conducted according to the guidelines for the use and care of laboratory animals according to the Federal Act on the Protection of Animals (Germany) and was approved by the Government of the District of Schleswig-Holstein (V244 – 230780/2015 (105-8/15)). Eight-week-old C57BL/6J wild type (WT) mice were obtained from Charles

River (Sulzfeld, Germany). Animals were housed in individually ventilated cages (IVC) (Sealsafe PLUS, Green Line, Tecniplast, Italy) in a specific pathogen-free facility with a 12 h light-dark cycle at constant temperature and humidity, provided with rodent chow and water *ad libitum*.

6.2.1.2 Cigarette smoke exposure protocols

Mainstream cigarette smoke (CS) served as a surrogate for active smoking and was generated using the inExpose exposure system (SCIREQ, Montreal, Canada) with 3R4F Research Cigarettes (Tobacco Research Institute, University of Kentucky, Lexington, Kentucky). Mice were exposed to room air (RA) or CS in a whole body chamber.

6.2.1.2.1 Dose finding CS exposure

Six to eight-week-old adult females were exposed to RA or CS (1 puff/min) the first three days of exposure treatment and continued from d4 with RA, 1 puff/min or 4 puffs/min of CS once per day for 60 min for 21 consecutive days. Analysis was performed on d25; 24 h after the last CS exposure (**Figure 9**).

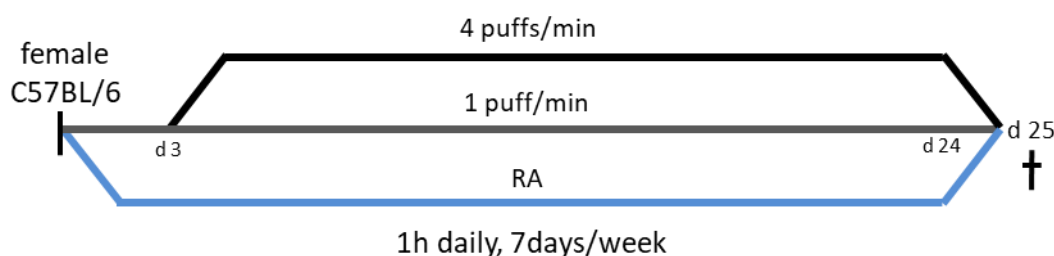


Figure 9 Schema of exposure to RA or CS for dose finding experiments. Female virgins were exposed to RA or 1 puff/min CS until d3. From d4 CS exposure was increased in one smoking group to 4 puffs/min. Exposure treatment was performed 1 h daily for 7 days/week. Mice were sacrificed on d25 (†).

6.2.1.2.2 Prenatal CS exposure

For *in utero* experiments, adult virgin female mice were handled once daily for 7 consecutive days to adjust mice to the experimenter, the weighting procedure and the new surrounding of the exposure chamber. Thereafter, females were exposed to RA or CS (1 puff/min) for 4 consecutive days for 60 min daily. The following day, female mice were mated (see section 6.2.1.4). After mating on embryonic day (ED) 2.5, exposure was continued until delivery as described above (**Figure 10**).

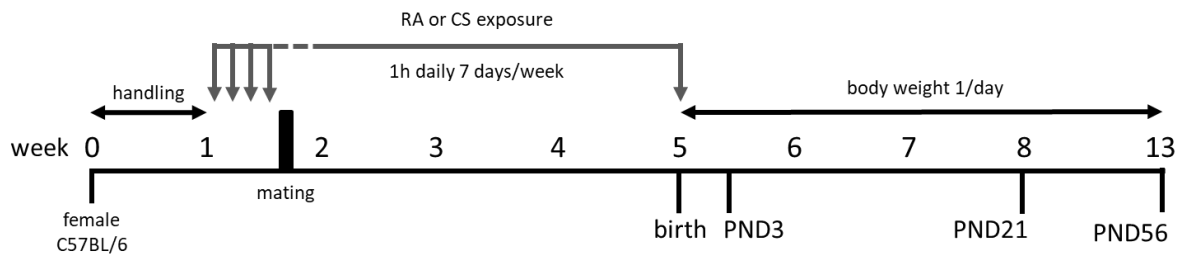


Figure 10 Schematic protocol of prenatal CS exposure (1 puff/min). Virgin females were handled once per day for 7 consecutive days to reduce stress of handling procedures. 4 days prior mating, mice were RA or CS-exposed (1h daily). Mating was performed for 48 h. From embryonic day (ED) 2.5 exposures were continued once per day, 7 days/week for 1 h until dams gave birth. Body weight of offspring was recorded once per day until analysis (PND3, PND21 or PND56). Room air (RA), cigarette smoke (CS), postnatal day (PND).

6.2.1.2.3 *Preconceptional CS exposure*

Three-week-old males and females were exposed to RA or CS (2 weeks to 1 puff/min (total particulate matter (TPM): 2,18 g/ml ± 0,25 and four weeks to 4 puffs/min (TPM: 7,83 g/ml ± 0,73)) for 1 h, 5 days/week. RA-control females were not placed into the inExpose exposure chamber. After exposure treatment, CS-exposed mice were mated with the corresponding sex of the RA control group (see section 6.2.1.4). After mating, males were analyzed. Body weight of offspring (filial generation 1 (F1)) was recorded once per day from postnatal day (PND)0 to PND21 (see section 6.2.1.5). Offspring were analyzed on PND3 and PND21. As pups were weaned on PND21, mothers were analyzed at the same time point (**Figure 11**).

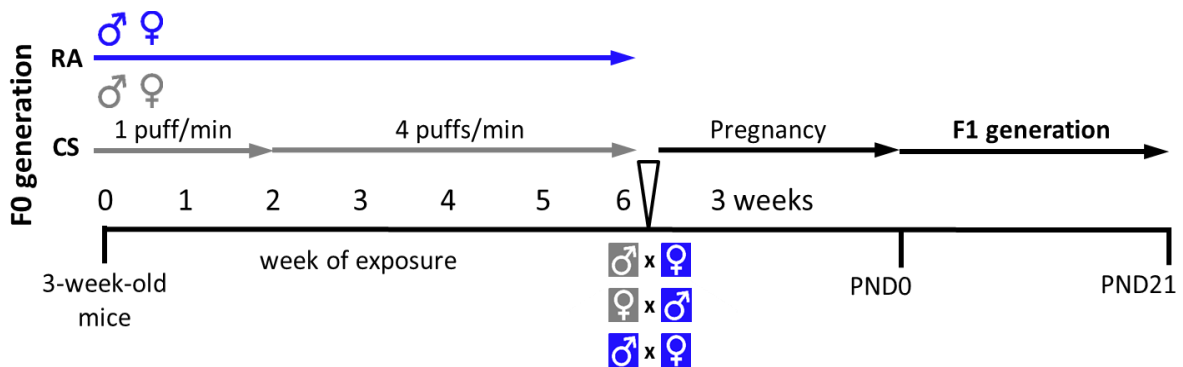


Figure 11 Schema of preconceptional RA or CS exposure of mice and experimental setup. 3-week-old male and female mice were exposed to RA (blue) or CS (grey) (2 weeks 1 puff/min, 4 weeks 4 puffs/min). Mating was performed for 48 h. PND0 is day of birth. Room air (RA), cigarette smoke (CS), postnatal day (PND).

6.2.1.3 Quantification of CS exposure

Once per week, TPM concentrations were recorded by real-time detection of CS particles by photometric measurements using the Microdust Pro (Casella, United Kingdom). Cotinine levels were quantified by ELISA (Mouse/Rat Cotinine ELISA, Calbiotech, Canada) in urine and sera from mice.

6.2.1.4 Mating

For *in utero* models, females were bred with a WT male 2:1. For smoking during adolescence, mating was approached after exposure treatment by 1:1 (female:male) with RA control females and CS-exposed males. CS-exposed and RA-exposed females were mated separately 2:1 with RA control males. Mating of female and male non-smoking mice (2:1) served as an additional control. All mating approaches were set for 48 h.

6.2.1.5 Body weight

Body weight was recorded using Entris Analytical Balance (± 0.01 g, Sartorius, Germany) for adult mice as for pups. Body weight of exposure treated mice was assessed before each exposure and body weight of pups was recorded once per day from day 0 (birth) until experimental endpoint (PND3, PND21, PND56).

6.2.1.6 Lung function assessment

After intraperitoneal (i.p.) anesthesia (Narcoren, 90 mg/kg, 16 g/100 ml pentobarbital sodium, Merial, Germany), mice were tracheostomized, intubated (cone: total length: 2.4 mm, outer diameter: 0.9 mm, estimated inner diameter: 0.7 mm) and connected to the FlexiVent ventilator (FlexiVent, SCIREQ, Montreal, Canada) equipped with FlexiWare software (v7.2). For baseline lung function measurement mice were ventilated with a tidal volume of 10 ml/kg at a frequency of 150 breaths/minute and a positive end-expiratory pressure of 2 cm H₂O by a computer-controlled ventilator. The lung volume history was standardized by one maximum expansion of the lung. All perturbations (Single frequency forced oscillation (SnapShot-150), broadband frequency forced oscillation (Prime-8) and recruitment maneuver (Deep Inflation)) were performed one-by-one until three acceptable measurements (coefficient of determination >0.95) were recorded in each individual subject. To assess airway hyperresponsiveness, methacholine

(Sigma-Aldrich, Germany) was nebulized with a tidal volume of 30 ml/kg at a frequency of 60 breaths/minute and administered at increasing concentrations (0, 6.25, 12.5, 25, 50, 100 mg/ml) for 10 sec (Aeroneb Pro nebulizer, 3.1 µm MMAD; Aerogen Ltd, Ireland) and measurements were performed until a maximum was reached.

6.2.1.7 Bronchoalveolar lavage

Lungs were rinsed once with ice-cold 1x phosphate buffered saline (PBS) of 400 µl (PND21) and 1 ml (PND56), respectively. The obtained fluid was centrifuged (1.200 rpm, 4°C, 10 min) to separate the cells from the supernatant. With a hemocytometer, total cell count was determined before performing the cytopins (900 rpm, RT, 8 min) (Cytospin 2, Thermo Shandon GmbH, Germany). After staining (Diff-Quik Staining Set; Siemens Healthineers, protocol see section 6.2.4.1.2), alveolar macrophages, neutrophils, eosinophils and leucocytes were identified by morphology and counted. A minimum of 200 cells were evaluated per slide using (Olympus BX51; Olympus DP 25, USA). In bronchoalveolar lavage (BALF), total cell numbers were calculated multiplying the percentages obtained in cytopsin analysis with total cell counts from the count via a hemocytometer (Neubauer, Germany) (see section 6.2.2.1).

6.2.1.8 Serum

Blood was collected from the Vena cava and kept on room temperature for >1 h. The blood clot was removed before centrifugation (10.000 rpm, RT, 10 min).

6.2.1.9 Spermatozoa isolation

Cauda epididymis and Ductus deferens were collected and reduced to smaller pieces in sperm isolation medium (Dulbecco's PBS with Ca, Mg, 5.6 mM D-glucose, 1 mM pyruvate and 5 mg/ml BSA (low endotox), pH 7.2) at 37°C. Spermatozoa were allowed to swim out for 10 min at 37°C and filtered subsequently. Spermatozoa were counted using a hemocytometer and Zeiss microscope. For microscopy, Leja slides (SD-20-01-08-B, Nieuw-Vennep, the Netherlands) were used and pictures were taken at 20x (Olympus BX41, USA; DS-Ri1, Nikon, Japan). Spermatozoas were centrifuged (600 x g, RT, 5 min) and transferred into QIAzol Lysis Reagent (Qiagen, Venlo, Netherlands) for RNA isolation.

6.2.2 Flow cytometry

6.2.2.1 Single cell preparation

Lung: The whole lung parenchyma (PND3) or the left lung lobe (PND21, PND56) were minced with a scalpel and processed in digestion buffer of 1 mg/ml collagenase (Sigma-Aldrich, USA) in 1xPBS for 45 min at 37 °C (water bath). After digestion, lungs were homogenized using a 10 ml syringe with a 20G needle (Braun, Germany) and filtered through a 70 µm cell strainer (Corning, USA).

Spleen: Spleens were pushed gently through a 70 µm cell strainer with the plunger of a 2 ml syringe (Braun, Germany) and rinsed with 1xPBS.

Thymus: In a 6-well plate, thymi were minced in 2 ml 1xPBS with a scalpel and carefully grinded between two slides to obtain single cell suspensions. The slides were rinsed with 1xPBS and cells were filtered through a 70 µm cell strainer.

Erythrocytes in single cell suspensions from lung and spleen were lysed by Gey'sche lysis buffer (10 mM KHCO₃ (Merck, Germany), 155 mM NH₄Cl (Merck, Germany), 100 µM EDTA (Sigma-Aldrich, USA)). All single cell suspensions were counted via a hemocytometer (dead cell exclusion via trypan blue (0,05% in NaCl solution)) and adjusted to 2x10⁷ cells/ml. The total cell number was calculated with the following formula: total cell number = counted cells / (counted squares * dilution factor * volume [ml] * 10.000).

6.2.2.2 Fluorescence activated cell sorting

Flow cytometric analysis was conducted using a LSRII and sorting was performed using an Ariallu instrument (BD Bioscience, USA), equipped with 405 nm, 488 nm and 633 nm lasers. Both instruments are equipped with BD FACSDiva software (v8.0.1). Single cell suspensions of lung, thymus and spleen were incubated with Fc Block (CD16/CD32) to prevent non-specific binding of antibodies. Then, cells were stained with fluorochrome-conjugated antibodies against surface markers and intracellular markers (**Table 4**). Cells were fixed with 4% paraformaldehyde before measurements.

Analyses were performed using FlowJo software version 10 (FlowJo, LCC Software, USA). Leukocytes were analyzed after doublet exclusion using the forward-scatter-area/forward-scatter-height profile. Gating strategies of lung, spleen and thymus are visualized within **Figure 12**.

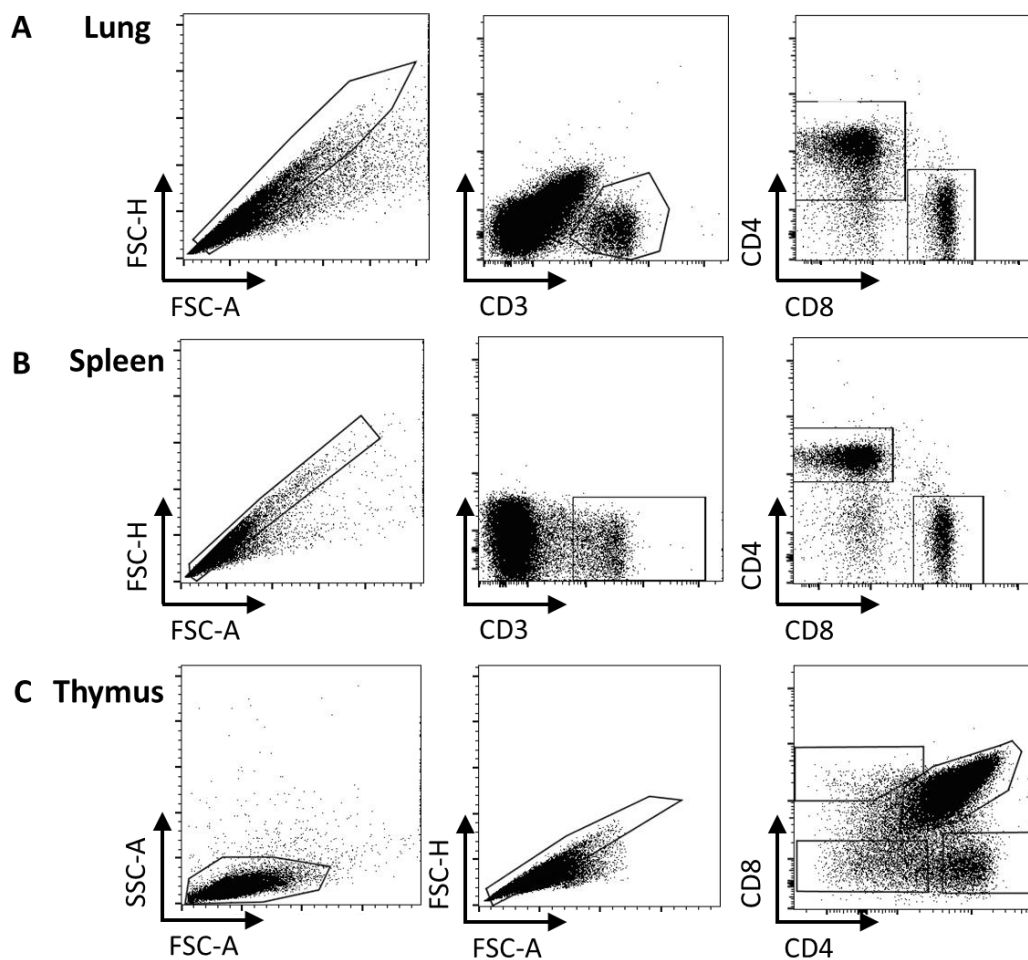


Figure 12 Gating strategies for flow cytometry. A-B, Gating strategy for the identification of CD3⁺ T cells in lungs and spleen, and the subpopulations of CD4 and CD8. C, Thymocytes were specified with the markers CD4 and CD8 to gate DN (CD4⁻CD8⁻), DP (CD4⁺CD8⁺), CD4SP (CD4⁺CD8⁻) and CD8SP (CD4⁻CD8⁺) thymic T cells. Forward scatter height (FSC-H), Forward scatter area (FSC-A), Sideward scatter area (SSC-A).

Using Ariallu, sorted thymic populations included double-negative (DN, CD4⁻CD8⁻), double-positive (DP, CD4⁺CD8⁺), single-positive CD4 (CD4SP, CD4⁺CD8⁻) and CD8 (CD8SP, CD4⁻CD8⁺) cell populations. Thymic single cell suspensions were treated before surface antibody staining with Fc Block (CD16/CD32) and then stained with CD4-BV421 and CD8-FITC (**Table 4**). Stained thymocytes were resolved in MACS buffer for cell sorting.

For dead cell exclusion, propidium iodide (eBioscience, USA) was administered shortly before single-cell sorting. Sorted populations were reanalyzed to ensure purity, afterwards centrifuged and stored at -80°C in QIAzol Lysis Reagent (Qiagen, The Netherlands) for further analysis.

6.2.3 RNA expression analysis

6.2.3.1 Tissue processing for RNA isolation

Lung tissue was processed with a bead-based tissue homogenization method for 2 min at 30 Hz (TissueLyser II, Qiagen, The Netherlands). For snap-frozen liver tissue, a mortar was cooled with liquid nitrogen and used to grind the tissue into powder. 40-50 mg of liver powder was used for RNA isolation.

6.2.3.2 RNA Isolation

Total RNA including small RNAs was isolated using the miRNeasy Mini Kit for lung and liver tissue, and the miRNeasy Micro Kit (Qiagen, The Netherlands) for sorted thymocyte populations and spermatozoa following manufacturer's instructions. RNA of the aqueous phase was bound on a membrane and washed once with RWT buffer and twice with RPE buffer solutions provided by the kit. Centrifugation was performed at 10.000 x g for washing. Before eluting the RNA from the membrane using nuclease-free H₂O, the membrane was dried by centrifugation with an open lid at 14.000 x g for 1 min. The RNA was eluted in a volume of 20 µl when Mini kit was used and 14 µl after the use of the Micro kit.

6.2.3.3 RNA quality control

6.2.3.3.1 RNA gel electrophoresis

RNA quality and quantity were controlled via spectrometry (DeNovix DS-11, DeNovix Inc., USA) and standard gel electrophoresis. 1 µg RNA was added to RNA loading buffer (60 % deionized Formamide, 0.5x of Tris-borate-EDTA (TBE) buffer, SYBR green (1:2000)) and denaturated for 15 min at 65 °C. Immediately after denaturation, samples were put on ice for 3 min. Afterwards, samples were separated in a 1.2% agarose gel in 0.5x TBE buffer at 60 V for 120 min. Utilizing the Chemidoc Touch Imaging System (Biorad) and UV light, the gel was analyzed for the detection of the 28S and 18S bands of intact RNA. Only samples with satisfactory RNA quality were used for further analysis.

6.2.3.3.2 Capillary electrophoresis

For sorted thymocyte populations the RNA quality and integrity was analyzed by capillary electrophoresis (Bioanalyzer Agilent 2100, Agilent Technologies, USA) following

manufacturer's protocol (Agilent RNA 6000 Pico Kit, Agilent Technologies, USA). Only high-quality RNA samples (260/280 ratio > 1.66, no degradation as detected by capillary electrophoresis) were used for further analyses.

6.2.3.4 RNA reverse transcription

RNA was converted to complementary DNA (cDNA) with the QuantiTect Reverse Transcription Kit, (Qiagen, the Netherlands) according to the manufacturer's protocol. For the transcription, 500 ng RNA was adjusted to 12 µl in nuclease-free water. Residual genomic DNA was removed using gDNA Wipeout Buffer and incubated for 2 min at 42 °C. Thereafter, the master mix for the reverse transcription (Quantiscript Reverse Transcriptase, Quantiscript RT Buffer and RT Primer Mix) was put into the thermocycler (Tprofessional TRIO, Biometra, Germany) for 30 min at 42 °C and 3 min at 95 °C. The cDNA was diluted 1:10 for the use in qRT-PCR.

6.2.3.5 qRT-PCR

Quantitative real-time polymerase chain reaction (qRT-PCR) was performed on a LightCycler 480 system (Roche Diagnostics, Germany) under the protocol shown in **Table 10**. 2.6 µl of cDNA (1:10) was mixed with 7.4 µl of Light Cycler 480 SYBR Green I Master Mix and the primer of the gene of interest. The master mix included 10 pmol/µl of the sense and anti-sense primer.

Step	Time [min]	Temperature
Denaturation	10:00	95 °C
Amplification for 45 cycles	00:10	95 °C
	00:15	60 °C
	00:10	72 °C
	00:01	78 °C
	00:05	95 °C
Melting Curve	01:00	60 °C
	0.11°C/sec	continuous
		99 °C
Cool down	00:10	40 °C

Table 10 Light cycler protocol for qRT-PCR.

For normalization, dose finding data were normalized with the housekeeping genes *hypoxanthine guanine phosphoribosyltransferase (HPRT)* and *TATA binding protein (Tbp)*. Prenatal and preconceptional smoking data were normalized with *HPRT*. The $2^{-\Delta\Delta C_t}$ value was used to indicate the fold change (FC) in mRNA expression relative to RA controls. Primer gene sequences are provided in **Table 5** (metabiom, Germany).

6.2.3.6 Amplicon validation

6.2.3.6.1 DNA gel electrophoresis

To confirm the correct amplification of the primer product, amplicons from qRT-PCR were analyzed by DNA gel electrophoresis using a 1 % agarose gel (see section 6.2.3.3.1). The PCR reaction and corresponding No-Template-Control (NTC) of gene (10 μ l) were mixed with 2 μ l of loading dye (6x Gel Loading Dye, SYBR Green (1:10)) and individually loaded onto the agarose gel. The samples were separated using 0.5x TBE running buffer at 60 V for 180 min. Bands were visualized with ChemiDoc using UV light. Amplicon size was compared to Bench Top ladder (1kb, Promega, USA).

6.2.3.6.2 PCR Clean-Up

Additionally, qRT-PCR amplicons were processed with Wizard[®]SV Gel and PCR Clean-Up System (Promega, USA). Membrane binding solution was added to PCR reaction samples taken directly from qRT-PCR plate and transferred into a SV Minicolumn. After an incubation of 1 min at RT, columns were spinned at 16.000 x g for 1 min. The membrane was washed with 700 μ l Membrane Wash Solution (16.000 x g, 1 min) and 500 μ l Membrane Wash Solution (16.000 x g, 5 min). To allow evaporation of residual ethanol, the column was spinned with an open lid for 1 min. DNA was eluted from the membrane with 20 μ l nuclease-free water, incubated for 1 min and centrifuged at 16.000 x g for 1 min.

6.2.3.6.3 Eurofins Genomics sequencing

For DNA sequencing of amplicons, 2 ng/ μ l purified amplicon DNA was diluted in 15 μ l. 10 pmol/ μ l of the primer used for the qRT-PCR was added to gain a final volume of 17 μ l. Prepaid barcodes from Eurofins Genomics were adjusted to the tube. The samples were

sent on room temperature (RT) for sequencing to the company. The received nucleotide sequences from Eurofins Genomics were analyzed with Standard Nucleotide BLAST and Align Sequence Nucleotide BLAST to identify the gene encoded by the sequence of the amplicon. Only primers producing the correct amplicon were used in qRT-PCRs.

6.2.3.7 Library preparation and Next Generation Sequencing

6.2.3.7.1 mRNA sequencing

Prior to sequencing, RNA quality was determined on a Bioanalyzer RNA Pico Chip (Agilent Technologies, USA). Total RNA was used for mRNA extraction with the NEBNext Poly(A) mRNA Magnetic Isolation Module (NEB) (New England BioLabs, USA). Sequencing libraries were then prepared using the NEXTflex Rapid Directional qRNA-Seq Kit (Bioo Scientific, USA) as recommended according to the manufacturer's protocol. On a Bioanalyzer High Sensitivity DNA Chip (Agilent Technologies, USA), size and quality of the libraries were visualized. Diluted libraries (2 nM) were multiplex-sequenced on the Illumina NextSeq500 instrument (Illumina, USA). For each sample between 14 and 20 million single reads of length 75bp were generated.

6.2.3.7.2 miRNA sequencing

Sperm RNA from RA- and CS-exposed adult male mice was characterized by unbiased small RNA sequencing (RNA-seq), starting with 100 ng of total RNA. Sequencing libraries were prepared as previously reported in Reithmair et al (2017) (86), using the NEBNext Multiplex Small RNA Library Prep Kit for Illumina (New England BioLabs, USA). Low input of RNA was compensated with a 1:2 dilution of all adaptors and primers in nuclease-free water. PCR-amplified libraries were size-selected on a high-resolution agarose gel (4 %) prior to extracting bands of 130–150 bp in length. Libraries were subsequently quality-controlled by capillary electrophoresis (High Sensitivity DNA Kit, 2100 Bioanalyzer, Agilent Technologies, Germany) and sequenced using 50 cycles of single-end sequencing on a HiSeq2500 machine (Illumina, USA).

6.2.4 Histology

Thymi and testes were harvested and stored in Histofix for 24 h at RT. In a tissue processor, the tissues were dehydrated with increasing concentrations of ethanol (70%,

80%, 90%, 96% and 3x 100%, 1 h/concentration) and further washed 2x with xylene for 1 h. The last step included 2x incubation in paraffin for 1.5 h. Thymi and testes were cut into 2 µm thin slices on a microtome (Microm HM 340 E, Thermo scientific).

For tissue stainings, the paraffin was removed from the tissue slices by incubation in xylene (2x, 5 min) and decreasing EtOH concentrations (2x, 5 min in 100%, 2x, 5 min in 96% and 5 min in 70%). The tissue slides were rinsed with H₂O.

6.2.4.1 Stainings

6.2.4.1.1 Hematoxylin and Eosin (H&E)

After removal of paraffin as mentioned above, tissue slides were incubated in Hematoxylin solution modified according to Gill for 20 min and rinsed with H₂O. Then, slides were incubated in 1% Eosin (acidified) for 3 min and rinsed with Aqua dest. The tissue was dehydrated with increasing ethanol concentrations (3x for 1 sec in 70%, 2x 96% and 100%). A second incubation in 100% ethanol was performed for 2 min. Further, tissue slides were washed 3x with xylene for 5 min and covered with Entellan (Merck, Germany) and 24 x 60 mm coverslips. All steps were performed at RT.

6.2.4.1.2 Diff-Quik Staining

Cells obtained from BALF were spinned on a glass slide (see section 6.2.1.7) and stained with Diff-Quik Staining Set (Siemens Healthineers, Germany) 5x 1 sec in Fixative Solution, 5x 1 sec in Solution I and 5x 1 sec in Solution II. Stained slides were rinsed with H₂O and dried overnight at RT. After microscopy analysis, slides were covered with Entellan (Merck) and 24 x 60 mm coverslips.

6.2.4.1.3 Immunohistochemistry

Ki67 (Antigen KI-67 or MKI67) expression in tissues of murine testes was determined by immunofluorescence using a specific Ki67 antibody. First, tissue slides were treated with citrate buffer (pH 6,0) at 120°C for 45 min and further cooled down to RT for 15-25 min before washing the slides 3x with PBS-T. Thereafter, tissue slides were treated with 200 µl blocking buffer (4% BSA, 0,1% Triton X100, 0,05 % Tween 20, 1x PBS) per slide for 20 min. Tissue slides were stained with 100 µl per slide using a specific Ki67 antibody (Ki-67 Monoclonal Antibody (SolA15), 1:100) in blocking buffer and incubated in the dark at 4°C,

overnight. Afterwards, tissue slides were washed 3x with PBS-T. Secondary antibody (Goat anti-Rat IgG (H+L) Cross-Adsorbed Secondary Antibody, Alexa Fluor 546, 1:500) was added onto the slide (100 μ l/slide) and incubated in the dark for 1 h at RT. Slides were washed 1x with PBS-T and incubated in the dark with 1:1000 DAPI (100 μ l/slide) for 15 min at RT. Thereafter, tissue slides were washed 3x with PBS-T and covered with Mounting medium (Dako North America, USA). The slides were stored in the dark at 4°C.

6.2.4.2 Histology analyses

6.2.4.2.1 Thymus histology

The area of cortex and medulla were measured on the microscope (Olympus BX41, USA; DS-Ri1, Nikon, Japan) utilized by the NIS-Elements D v3.1 software (Nikon, Japan) and calculated as mean per section. Per thymus, the total tissue area of 6 sections (3 sections per lobe) was measured. To calculate the area of the cortical tissue, the sum was calculated from the medullary mean area per section and subtracted from the total area. A ratio for Cortex to Medulla was calculated.

6.2.4.2.2 Testes histology

Spermatogonia were identified as Ki67 high cells in the first cellular layer of seminiferous tubules by a fluorescence microscope (Axio Observer.Z1, Zeiss; AxioCam MR, Zeiss, Germany). Spermatogonia were counted per section using the “Multi-point” tool in ImageJ (LOCI, USA).

6.2.5 Statistical analyses

6.2.5.1 Statistics with Prism

Data were tested for normal distribution by Column Statistics with D’Agostino-Person omnibus normality test. Normally distributed data were analyzed by unpaired student's t test (t test) or 1way analysis of variance (ANOVA) with Tukey post-hoc test for more than two groups. Data not passing normality tests were analyzed by Mann-Whitney *U* test (MWU) or Kruskal-Wallis test with Dunn’s correction. For data being compared to two factors, 2way ANOVA with Tukey’s or Sidak’s post-hoc test was used. Results are expressed as mean \pm standard deviation (SD) and mean \pm standard error of the mean (SEM). Flow cytometry data from lungs and spleen are expressed as median \pm

interquartile range (IQR). Statistical significance was accepted with p-values <0.05. Data were analyzed using Graph Pad Prism version 6.0 (GraphPad Software, USA).

6.2.5.2 Statistics: mRNA NGS analysis

For next-generation sequencing (NGS) of thymic mRNA, sequenced reads were mapped on the mouse genome GRCm38 and simultaneously counted using Star v2.5 (87). Fold changes and false discovery rates (FDR) for each gene between conditions were estimated with DESeq2 v1.18.1 (88). Downstream Analysis was performed using Ingenuity Pathway Analysis (IPA®) (Qiagen, The Netherlands), differential expressed genes were selected by a FDR below 0.1 (FDR < 0.1) and a fold change ≥ 2 , ≤ 0.5 (Log2Foldchange ≥ 1 , ≤ -1). Raw sequencing data were deposited at European Nucleotide Archive (ENA) with the accession number PRJEB34795. This analysis was performed by Michael Spohn.

6.2.5.3 Statistics: miRNA NGS analysis

For NGS of spermatozoal miRNAs, data processing was carried out as described in the publications by Spornraft et al (2014) (89) and Buschmann et al (2018) (90). To summarize, length distribution and Phred quality scores of all sequences were assessed using FastQC (version 0.10.1) (91). Adaptor sequences were clipped using Btrim (92), and reads without sequencing adaptors were discarded. Additionally, reads shorter than 16 nt, which most likely stem from non-specific degradation of longer RNAs, were excluded before alignment (93). To reduce false-positive hits during the subsequent miRNA analysis, reads mapped to murine sequences of ribosomal RNA (rRNA), tRNA, snRNA and small nuclear RNAs (snoRNAs) (obtained from RNACentral) (94) were removed. The remaining reads were aligned to murine miRNA sequences in miRBase (v21) (95). Bowtie (96) and the “best” alignment command were used for all mapping steps, allowing one mismatch. Differentially expressed miRNAs were analyzed utilizing the Bioconductor Package DESeq2 (version 1.8.1) (88) with its built-in normalization strategy and false discovery correction (Benjamini–Hochberg method). Thresholds to identify significantly regulated miRNAs were set to a log2 fold change $\geq |1|$, an adjusted p-value of ≤ 0.05 and a mean expression of baseMean ≥ 50 . After the filtration through set criteria mentioned above, a list of 45 regulated miRNAs was generated. Trimmed sequence reads were deposited in the European Nucleotide Archive (ENA) under the accession number

PRJEB35967. This analysis was performed by Dominik Buschmann. The 45 regulated spermatozoal miRNAs were used for the following downstream analyses. miRNA gene targets were identified under the MicroT-CDS algorithm using the mirPath tool (v.3) (97). Targeted genes of miRNAs were identified by Kyoto Encyclopedia of Genes and Genomes (KEGG) pathway analysis and Gene Ontology (GO) analysis, undertaken by "a priori" and "a posteriori" analyses for either method. By "a priori" analysis, two gene lists were produced a) a list implementing the union of all targeted genes and b) a list with the intersection of genes targeted by at least 5 miRNAs. On the produced gene lists were run the KEGG pathway and ontology enrichment analyses. By "a posteriori" union analysis, an enrichment analysis is performed and calculates the significance levels (p-values) between each miRNA and every pathway. Subsequently, for each pathway, a merged p-value is calculated by combining the previously calculated significance levels (Fisher's meta-analysis method). These analyses were performed by Faisal I. Rezwan.

6.2.5.4 Statistics: offspring's body weight analysis after adolescent parental smoking

Body weight data were available for 72 murine offspring, belonging to 19 litter, from birth (day 0) and the days 1-21. In order to take advantage of the repeated body weight measurements and the clustering into litter, a multilevel mixed models with a random intercept and a random slope was built (xtmixed command, Stata 12). The three levels were time, mouse and litter. The mixed command of Stata 15 was employed to fit linear models for the body weight data. The time-independent variables included in the model were exposure to smoking (none, paternal or maternal) and gender of the pups.

Thus, the model performed as followed:

$$\text{Weight}_{it} \sim \text{days}_{it} + \text{exposure}_i + \text{sex}_i \quad || \quad \text{litter} \quad || \quad \text{pups: days}$$

where $i = 1, 2, \dots, 72$ pups and $t = 0, 1, \dots, 21$ days

To test for gender-specific differential growth, the following model for male (n= 36) and female (n=36) offspring was built separately:

$$\text{Weight}_{it} \sim \text{days}_{it} + \text{exposure}_i \quad || \quad \text{litter} \quad || \quad \text{pups: days}$$

This analysis was performed by Latha Kadalayil.

7 RESULTS

7.1 CS dose finding for prenatal and preconceptional murine exposure models

7.1.1 Characterization of CS exposure of mild and heavy smoking

Adult virgin females were exposed to RA or to either one of two different CS doses (**Figure 9**). Mild smoking was tested with 1 puff/min (TPM: $2.15 \pm 0.33 \text{ g/m}^3$), whereas heavy smoking was performed with 4 puffs/min (TPM: $7.69 \pm 0.76 \text{ g/m}^3$). In mice, the CS exposure led to an increased detection of cotinine in serum, as cotinine is a more stable metabolite of nicotine (**Figure 13A**). In addition, the gene *cytochrome P450 family 1 subfamily A member 1 (Cyp1a1)*, encoding for the hydroxylase that metabolizes polycyclic aromatic hydrocarbons (98), showed an increased expression in lung homogenates in both CS-exposed groups (**Figure 13B**) compared to RA controls.

On d24 of exposure treatment, the body weight was lower but not significantly decreased in virgin female mice exposed to 1 puff/min ($19.91 \pm 0.35 \text{ g}$) compared to RA-exposed mice ($20.40 \pm 0.30 \text{ g}$). However, the CS exposure of 4 puffs/min led to a significant decrease in body weight ($18.70 \pm 0.27 \text{ g}$) compared to RA controls ($20.40 \pm 0.30 \text{ g}$) (**Figure 13C**).

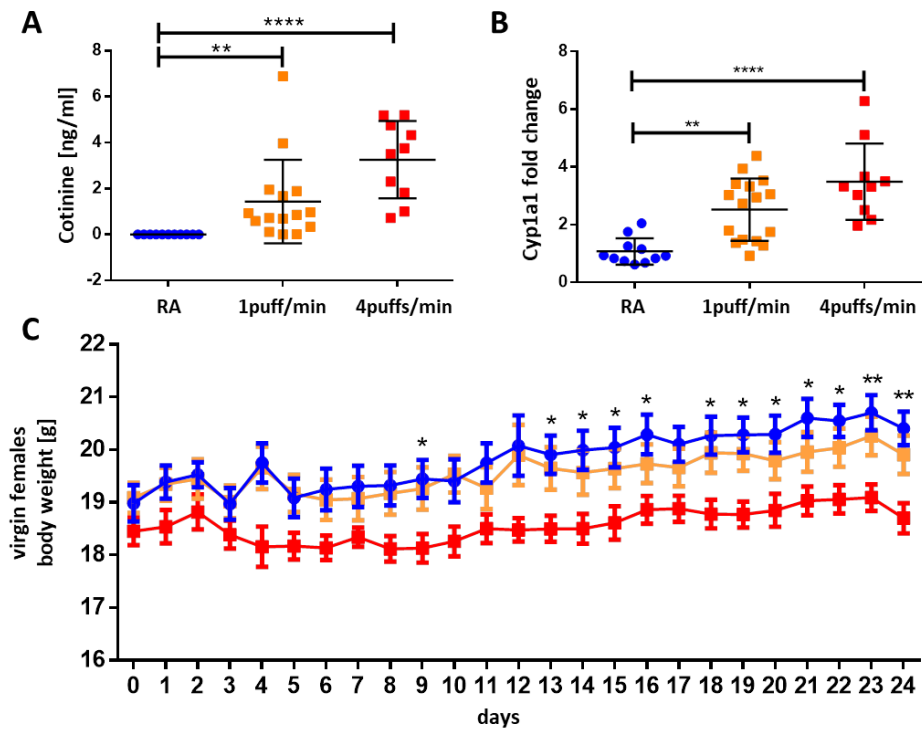


Figure 13 Validation of CS exposure in virgin females. A, Cotinine levels in serum of CS-exposed mice on d25. B, Gene expression of *Cyp1a1* in lung homogenates, normalized with *HPRT* and *Tbp*. C, The body weight progression during exposure treatment of 24 consecutive days, * RA vs 4 puffs/min. A-B, Data are expressed as mean \pm SD, each data point represents an individual animal. C, Data are expressed as mean \pm SEM. A-B, 1way ANOVA. C, 2way ANOVA. A, Dunn's multiple comparison test. B-C, Tukey's multiple comparison test. RA \bullet n= 11, 1 puff/min \blacksquare n= 15-16, 4 puffs/min \blacksquare n= 10; room air (RA), cigarette smoke (CS). * $p < 0.05$, ** $p < 0.01$, *** $p < 0.001$, **** $p < 0.0001$.

7.1.2 Macrophages and neutrophils are increased in BALF after CS exposure

In BALF, total cell counts were elevated in both CS exposure groups of adult virgin females (**Figure 14A**). In detail, increased numbers of macrophages were present in CS-exposed mice to 1 puff/min and to 4 puffs/min (**Figure 14B**), whereas a neutrophilia was only detected in mice exposed to 4 puffs/min (**Figure 14C**). Invasive lung function measurements and methacholine provocation (bronchoconstrictor) showed no effects on lung function parameters in both CS exposure groups compared to RA controls (**Figure S1**).

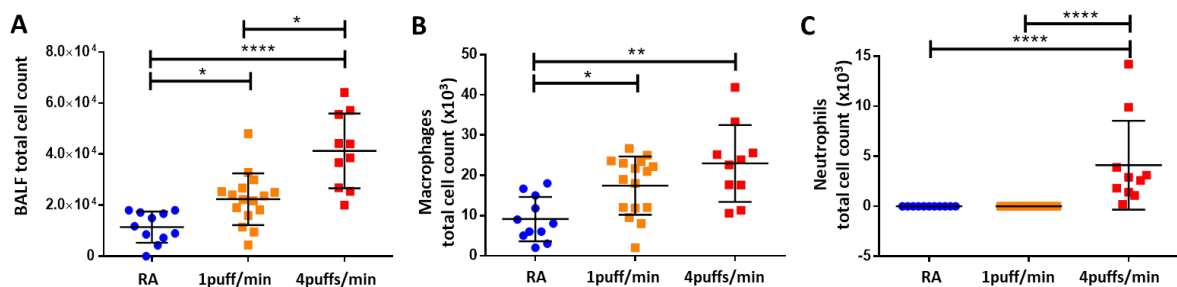


Figure 14 Inflammatory cells in BALF of virgin females. A, Total cell counts. B, Numbers of macrophages. C, Numbers of neutrophils. A-C, Data are expressed as mean \pm SD, each data point represents an individual animal. A-C, 1way ANOVA. A-B, Tukey's multiple comparison test. C, Dunn's multiple comparison test. RA \bullet n= 11, 1 puff/min \blacksquare n= 16, 4 puffs/min \blacksquare n= 10; room air (RA), bronchoalveolar lavage fluid (BALF). * p<0.05, ** p<0.01, *** p<0.001, **** p<0.0001.

To continue with the *in utero* exposure experiments, 1 puff/min was chosen as CS dose (**Figure 10**). Furthermore, 1 puff/min was selected for the exposure of three-week-old mice in the preconceptional smoking model for two weeks, increasing the CS dose to 4 puffs/min for further 4 weeks of exposure (**Figure 11**).

7.2 Mild maternal smoking affects the frequency and transcriptome of thymic T cells in murine offspring

7.2.1 Characteristics of dams and offspring following mild maternal smoking

7.2.1.1 Maternal phenotype and pregnancy outcome

CS-exposed (1 puff/min) non-pregnant mice had a comparable body weight to non-pregnant RA controls throughout the exposure treatment, similar to adult virgin females showed above. The body weight progression of CS-exposed pregnant mice was normal compared to pregnant RA control animals (**Figure S2A**). The CS exposure was validated in urine and serum of non-pregnant mice by increased cotinine levels (**Table 11**). Furthermore, the maternal body weight 1 day before delivery was normal and litter sizes were equal to RA exposed controls.

	RA (n=45)	CS (n=44)	p-value
maternal weight before conception	20.67 ±1.05 g	20.62 ±0.97 g	0.46 (t test)
number of pregnant females (pregnancy rate)	21 (47 %)	29 (66 %)	0.21 (MWU)
maternal weight 1 day before delivery	36.96 ±2.56 g	35.73 ±3.44 g	0.19 (t test)
Urine cotinine [†]	1.50 ±0.35 ng/ml	875.45 ±132.12 ng/ml	0.03 (MWU)
Serum cotinine [†]	0.00 ±0.00 ng/ml	60.72 ±7.58 ng/ml	0.03 (MWU)
∅ litter size	7.3 ±2.2	6.5 ±2.7	0.31 (t test)
weaned pups number and (%)	♂: 85 (58.6 %) ♀: 60 (41.4 %)	♂: 89 (46.4 %) ♀: 103 (53.6 %)	

Table 11 Pregnancy outcome and CS exposure characteristics of dams. Data are expressed as mean ± SD; 6 independent experiments. Groups were tested for normal distribution and compared by unpaired t test (t test), Mann-Whitney test (MWU). † analyzed in non-pregnant females. Urine collection on d11 and serum collection on d24; 1h after exposure, n= 4/group. Room air (RA), cigarette smoke (CS), day (d).

7.2.1.2 Offspring's phenotype after mild prenatal CS exposure

The birth weight (day 0) of prenatally CS-exposed offspring did not differ compared to offspring from RA control dams in absence of sex-specific effects (**Figure S2B**). The body weight follow-up until PND56 was normal, observing the characteristic sex-specific body weight development among the groups (**Figure S2C**).

Lung function parameters were comparable in offspring of CS-exposed dams compared to RA controls at PND21 and PND56. Baseline resistance, baseline compliance, inspiratory capacity and resistance of small airways as well as methacholine provocation did not differ between exposure groups at PND21 (**Figure S3**) and PND56 (**Figure S4**).

Thus, the predefined criteria proposed by the mouse model definition of mild maternal smoking were fulfilled.

7.2.2 T cell populations are affected by prenatal CS exposure in lung, spleen and thymus in offspring

7.2.2.1 T cells in lungs and spleen

T cell populations were quantified in lung homogenates to investigate if immunity is affected in offspring at different time points (PND3, PND21 and PND56) following mild maternal smoking in pregnancy (**Table S1**). Total cell counts were decreased in lungs of females at PND21 (**Figure 15A**) and in males at PND56 (**Figure 15B**) after *in utero* CS exposure. In the spleen, the total cell count was decreased in males at PND3 (**Figure 15D**).

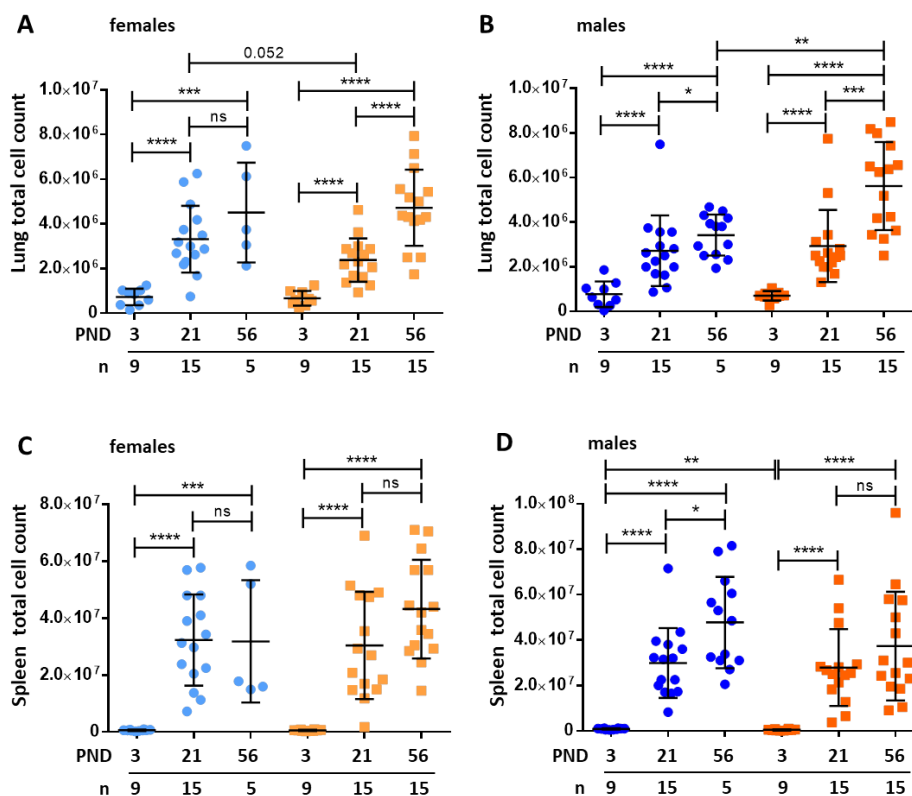


Figure 15 Total cell counts of lungs and whole spleen of prenatally exposed offspring to RA or CS at PND3, 21 and 56. Total cell count of lungs in A, female offspring (RA ●, CS ■) and B, male offspring (RA ●, CS ■). Total cell count of whole spleen in C, female offspring and D, male offspring. A-D, Each data point represents an individual animal; data are shown as mean \pm SD compared by unpaired t test or Mann-Whitney test according to equal distribution testing. Room air (RA), cigarette smoke (CS), postnatal day (PND). * $p < 0.05$, ** $p < 0.01$, *** $p < 0.001$, **** $p < 0.0001$.

Analysis by flow cytometry showed a decrease in pulmonary CD3⁺ T cells in female offspring at PND21 that remained low in males until PND56 after *in utero* CS exposure (**Figure 16A**). Relative numbers of CD4⁺ and CD8⁺ T cells were altered in both sexes. In detail, the percentage of CD4⁺ T cells in the lungs was decreased in *in utero* CS-exposed female and male offspring at PND3 and at PND56 (females only), whereas at PND21 pulmonary CD4⁺ T cells were increased in both sexes compared to their corresponding RA control (**Figure 16B**). The proportion of CD8⁺ T cells in the lungs was decreased in both sexes at PND21 compared to RA-exposed offspring (**Figure 16C**).

To identify if the effects on CD4⁺ and CD8⁺ T cells in the lungs were tissue-specific, the spleen showed similar results at PND21 using the same flow cytometric analysis (**Figure 16E-F**), whereas CD3⁺ T cells were normal in spleens of prenatally CS-exposed offspring at all three time points (**Figure 16D**).

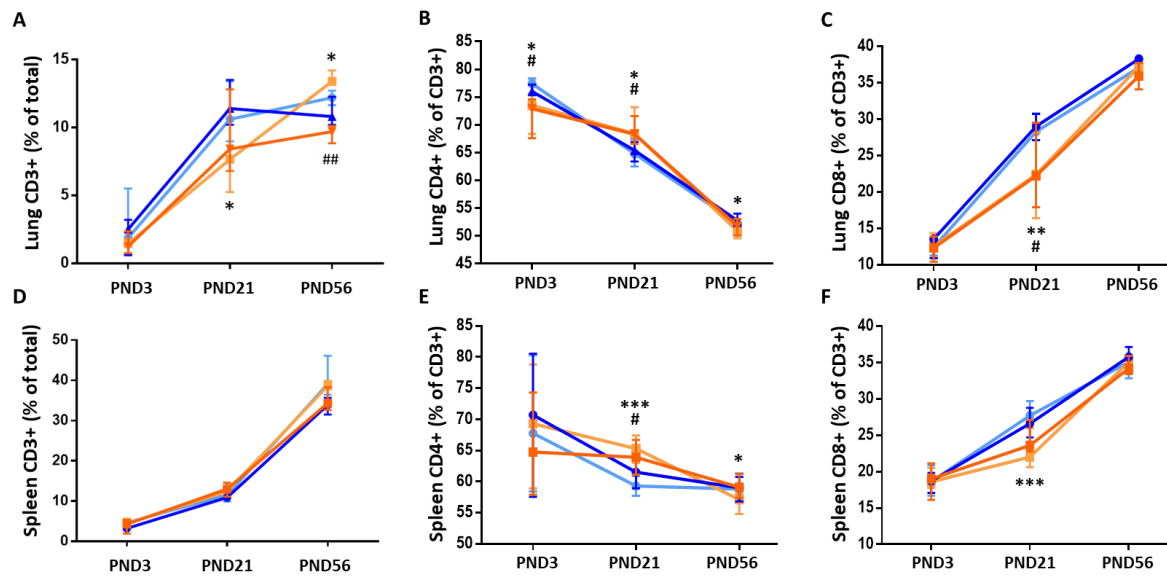


Figure 16 T cell proportions in lungs and spleen in offspring after intrauterine exposure to RA or CS. A, In lungs, CD3+ T cells were gated on total percentages of events and analyzed at PND3, 21 and 56 in female (RA ●, CS ■) and male (RA ●, CS ■) offspring. C-B, CD8+ and CD4+ T cells pre-gated on CD3+ in lungs. D-F, T cell proportions in spleen. A-F, Data are expressed as median \pm IQR compared by unpaired t test or Mann-Whitney test according to equal distribution testing. Room air (RA), cigarette smoke (CS), postnatal day (PND), interquartile range (IQR). *(female)/#(male) $p < 0.05$, ** (female)/##(male) $p < 0.01$, *** $p < 0.001$, **** $p < 0.0001$.

7.2.2.2 Thymocytes

Observing altered T cell populations in lungs and spleen, thymi from prenatally CS-exposed and RA-exposed offspring were analyzed to address the hypothesis that similar changes in two independent peripheral organs may have a joint origin during T cell development.

Total numbers of thymic T cells were very low at PND3 in offspring, as the organ size is very small at that age. At PND56, the total number of thymocytes decreased compared to the frequency at PND21, which might underlie some thymic involution. Comparing total thymic T cells at PND56, thymocytes were significantly decreased in offspring of both sexes from CS-exposed mothers compared to offspring prenatally exposed to RA (**Figure 17A-B** and **Table S1**).

Similar to the observed effects in the peripheral organs, the alterations in CD4+ T cell proportions occurred in thymus in both sexes at PND21. Thymic CD4SP (CD4+CD8-) T cells were increased in relative numbers, decreasing the DP (CD4+CD8+) thymocyte population (**Figure 17C-D**).

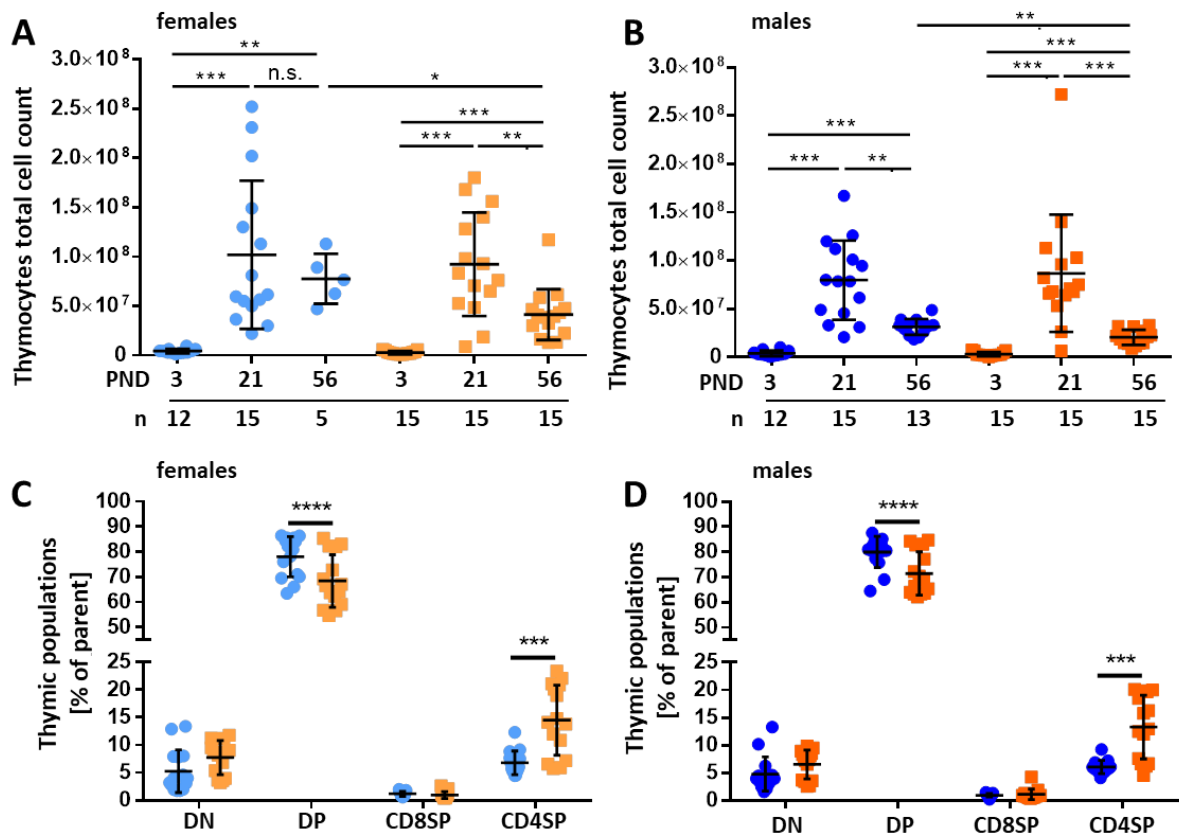


Figure 17 Thymocytes after *in utero* CS exposure in offspring. Total cell count of thymi in A, female (RA ●, CS ■) and B, male (RA ●, CS ■) prenatally RA and CS-exposed offspring. C-D, Relative numbers of DN (CD4-CD8-), DP (CD4+CD8+), CD8SP (CD4-CD8+) and CD4SP (CD4+CD8-) thymocytes at PND21 in C, female and D, male offspring (n= 15/group). A-D, Each data point represents an individual animal; data are shown as mean \pm SD. A-B, Mann-Whitney test. C-D, 2way ANOVA with Sidak's multiple comparison test. Room air (RA), cigarette smoke (CS), postnatal day (PND), n.s. (not significant). * $p < 0.05$, ** $p < 0.01$, *** $p < 0.001$, **** $p < 0.0001$.

7.2.3 Changes in transcriptome of CD8SP thymocytes after prenatal CS exposure

To identify if alterations of thymocyte proportions also involve functional changes, CD4SP and CD8SP thymocytes were sorted and analyzed at PND21 via next generation sequencing (NGS). 21-day-old offspring were chosen for this analysis as most prominent effects were observed at this time point after prenatal CS exposure. In parallel to the cellular changes, thymic organ weight, body weight to organ weight ratio and thymic cortex to medulla ratio were normal in offspring (**Figure S5**). NGS of CD8SP thymic T cells revealed 272 regulated genes in prenatally CS-exposed offspring, where the expression of 92 genes was significantly upregulated and downregulated in 36 genes (**Figure S6**). Transcriptome data of CD4SP thymocytes showed no differentially regulated gene

expression at PND21 after intrauterine CS exposure compared to RA controls. The 272 identified genes in CD8SP thymocytes were submitted to IPA® to perform canonical pathway analysis.

7.2.3.1 Canonical pathway analysis of CD8SP thymic T cells

According to IPA®, a positive z-score was calculated for the NFκB Signaling Pathways suggesting an activation of this pathway. Protein Ubiquitination, Antigen Presentation, IL-4 signaling and the CTLA4 Signaling in CTLs Pathway was further suggested by the pathway analysis (**Table 12**).

Canonical Pathways	Genes	Ratio	P-value
NFκB Signaling	5/187	0,027	1,17E-02
Protein Ubiquitination	11/265	0,042	3,81E-06
Antigen Presentation	2/38	0,053	3,08E-02
IL-4 signaling	4/94	0,043	4,68E-03
CTLA4 Signaling in CTLs	3/99	0,030	3,52E-02

Table 12 Cononical pathways suggested by IPA®. The ratio is calculated by the number of differentially expressed genes in the pathway divided by the number of genes identified in the IPA Knowledge Base. Nuclear factor 'kappa-light-chain-enhancer' of activated B-cells (NFκB), cytotoxic T-lymphocyte-associated Protein 4 (CTLA4), cytotoxic T cells (CTLs), Ingenuity Pathway Analysis (IPA).

7.2.3.2 *In silico* network analysis of CD8SP thymocytes

In IPA®, *in silico* network analysis was conducted to obtain deeper insight into disease-relevant changes of the CD8SP transcriptome. Therefore, IPA® suggested altered gene expression in 'Top Diseases and Functions' (**Table 13**).

Network	Top Diseases and Functions	Score	Focus Molecules
1	Post-Translational Modification, Cellular Assembly and Organization, DNA Replication, Recombination, and Repair	58	28
2	Cellular Assembly and Organization, Cellular Function and Maintenance, Hematological Disease	49	25
3	Cell Morphology, Hematological System Development and Function, Immunological Disease	47	24
4	Cellular Movement, Hematological System Development and Function, Immune Cell Trafficking	32	18
5	Cancer, Developmental Disorder, Hereditary Disorder	25	15
6	Lipid Metabolism, Small Molecule Biochemistry, Carbohydrate Metabolism	21	13
7	Hematological Disease, Cancer, Organismal Injury and Abnormalities	21	13
8	Cell Morphology, Nervous System Development and Function, Tissue Morphology	19	12
9	Developmental Disorder, Endocrine System Disorders, Hereditary Disorder	15	10
10	Cell-To-Cell Signaling and Interaction, Hematological System Development and Function, Hypersensitivity Response	13	9

Table 13 Top Diseases and Functions suggested by IPA®. The score provides the significant relevance based on the number of molecules in the dataset included in the network. A high significance correlates with a high score. The number of genes expressed differentially connected in a network are defined as focus molecules. Ingenuity Pathway Analysis (IPA).

Hematological system development and function, cellular movement and immune cell trafficking were 'Top Diseases and Functions' connected to network 4. Genes involved in network 4 were of most interest as they include immune-related genes like *interleukin 4 receptor alpha (Il4ra)*, *runt-related transcription factor 3 (Runx3)*, *forkhead box protein P1 (Foxp1)*, *interleukin 10 receptor beta (Il10rb)* and *phosphatidylinositol-4,5-bisphosphate 3-kinase (PI3K)*. The upregulation of *Il4ra*, *Runx3*, *Foxp1* and *Il10rb* in the NGS dataset were supported by qRT-PCR in isolated CD8SP thymic T cells with the exception of *PI3K* which was regulated in the opposite direction (**Figure 18**).

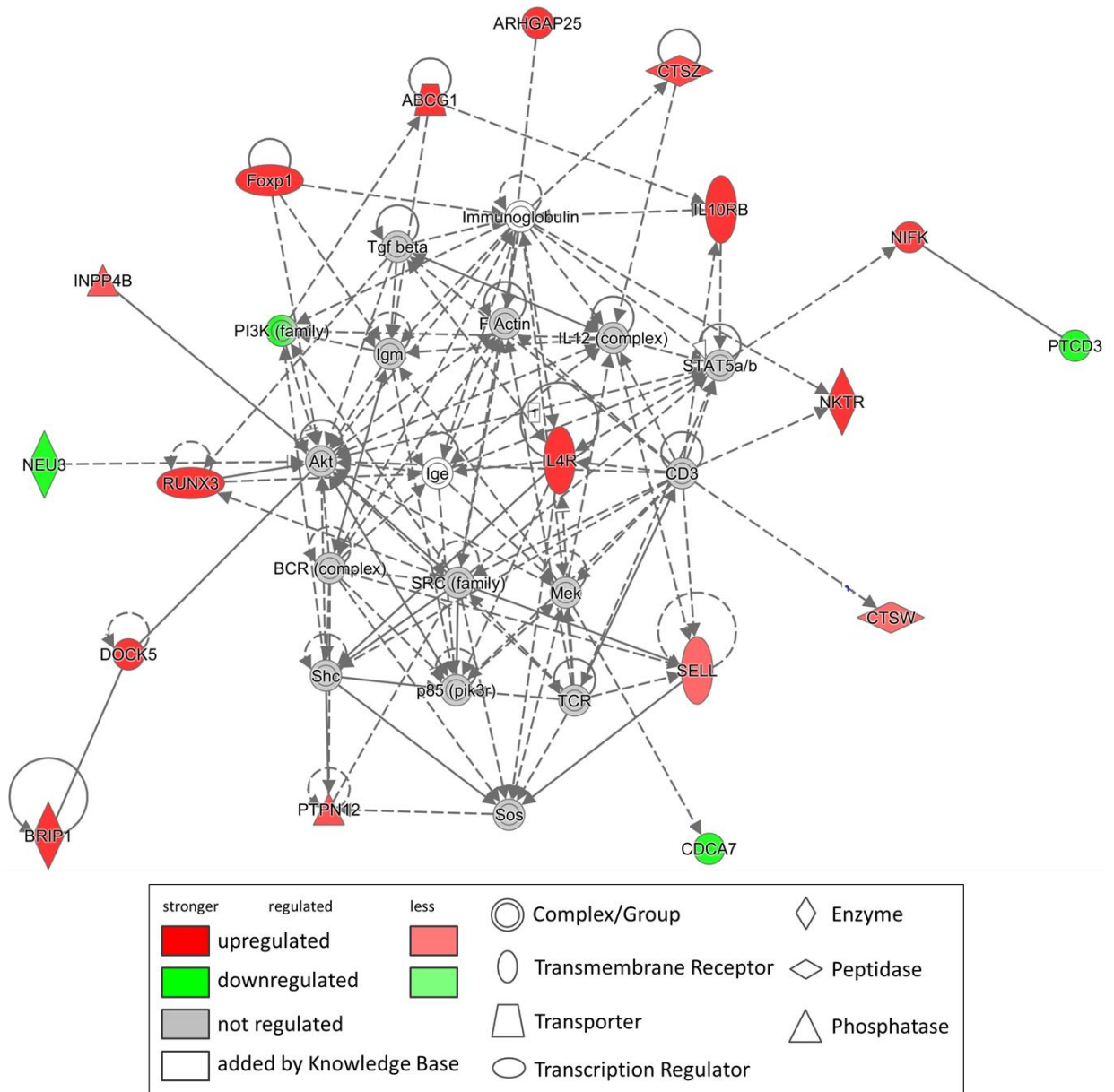


Figure 18 Regulated genes of network 4 in CD8SP thymic T cells (PND21) after *in utero* CS exposure normalized with RA-exposed offspring. Upregulated genes (red), downregulated genes (green), non-regulated genes detected in the dataset (grey), genes added by the IPA® Knowledge Base (white). Full lines indicate direct interaction between genes. Room air (RA), cigarette smoke (CS), CD8 single-positive (CD8SP), Ingenuity Pathway Analysis (IPA), postnatal day (PND).

7.2.3.3 Confirmation of gene regulation in the NGS dataset via qRT-PCR

Until adaptive immune responses are established, ‘innate memory’ CD8 T cells (T_{IM}) support early life defenses against pathogens and viruses. Characteristic features of these cells are their development in the thymus and the expression of *Ii4ra* and *Runx3* together with the T-box transcription factor *Eomesodermin* (*Eomes*). As the first two characteristic genes have been upregulated in the transcriptome data of this study, *Eomes* was included

in the qRT-PCR analyses. The upregulation of *Eomes* in CD8SP thymic T cells of intrauterine CS-exposed offspring was supported by the qRT-PCR analysis (**Figure 19**).

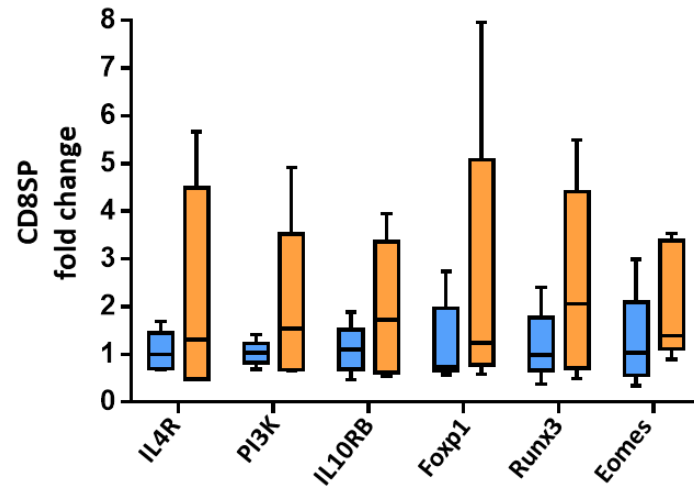


Figure 19 Validation of single genes of interest detected in CD8SP thymocytes. Data are expressed as box-whiskers blot with Min to Max and median. (RA ● n= 5, CS ■ n= 5; females only). Per gene, the expression in RA and CS exposed animals was compared with Mann-Whitney test. Room air (RA), cigarette smoke (CS), CD8 single-positive (CD8SP), *interleukin 4 receptor (IL4R)*, *phosphatidylinositol-4,5-bisphosphate 3-kinase (PI3K)*, *interleukin 10 receptor beta (IL19RB)*, *forkhead box protein P1 (Foxp1)*, *runt-related transcription factor 3 (Runx3)*, *Eomesodermin (Eomes)*. * $p < 0.05$, ** $p < 0.01$, *** $p < 0.001$, **** $p < 0.0001$.

7.3 Paternal preconceptional smoking in puberty affects miRNAs in spermatozoa and increases body weight in male but not in female offspring

7.3.1 Adolescent smoking characteristics of future fathers and mothers

7.3.1.1 Parental body weight development during CS exposure

Preconceptional smoking of future fathers induced lower weight gain (Δ body weight) compared to RA controls of the corresponding sex (**Figure 20A**), as expected by the dose finding experiments (**Figure 13C**). The same was observed in future mothers, where a decrease in weight gain was first observed to the lower CS dose (1 puff/min) during the second week of exposure (**Figure 20B**).

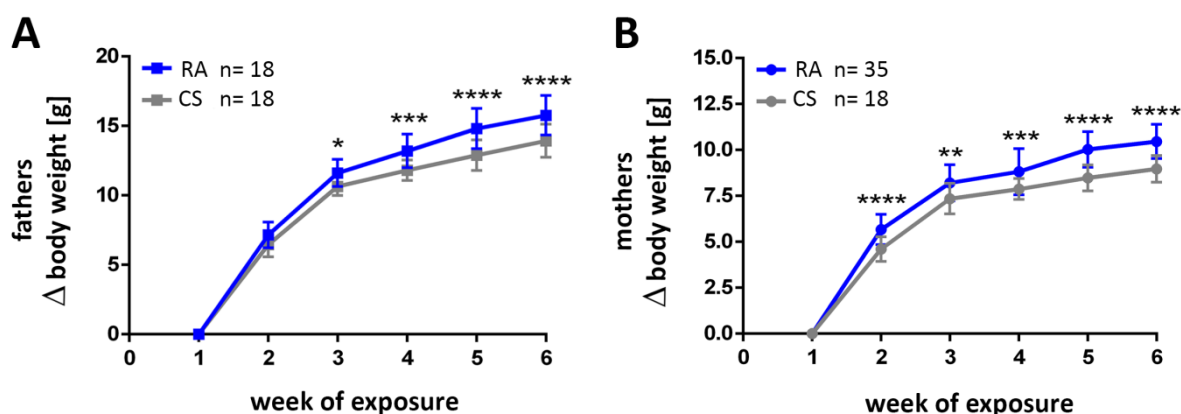


Figure 20 CS exposure during adolescence decreases weight gain in future fathers and mothers. Body weight gain (Δ body weight) of A, fathers (■) and B, mothers (●) during exposure to RA or CS. B-C, 2way ANOVA with Sidak's multiple comparisons test. Data are expressed as mean \pm SD. Room air (RA), cigarette smoke (CS). * $p < 0.05$, ** $p < 0.01$, *** $p < 0.001$, **** $p < 0.0001$.

7.3.1.2 Inflammatory cell counts in BALF of CS-exposed future fathers

In BALF obtained from fathers, cell counts were influenced by CS even 3 days after the last exposure. Detailed analysis revealed elevated levels of macrophages (**Figure 21A-B**) and neutrophilia (**Figure 21E-F**) in CS-exposed males compared to RA controls. 6 weeks after the last exposure, preconceptionally CS-exposed mothers showed an increase in numbers of macrophages (**Figure 21C-D**), whereas no neutrophils were detected (**Figure 21G-H**).

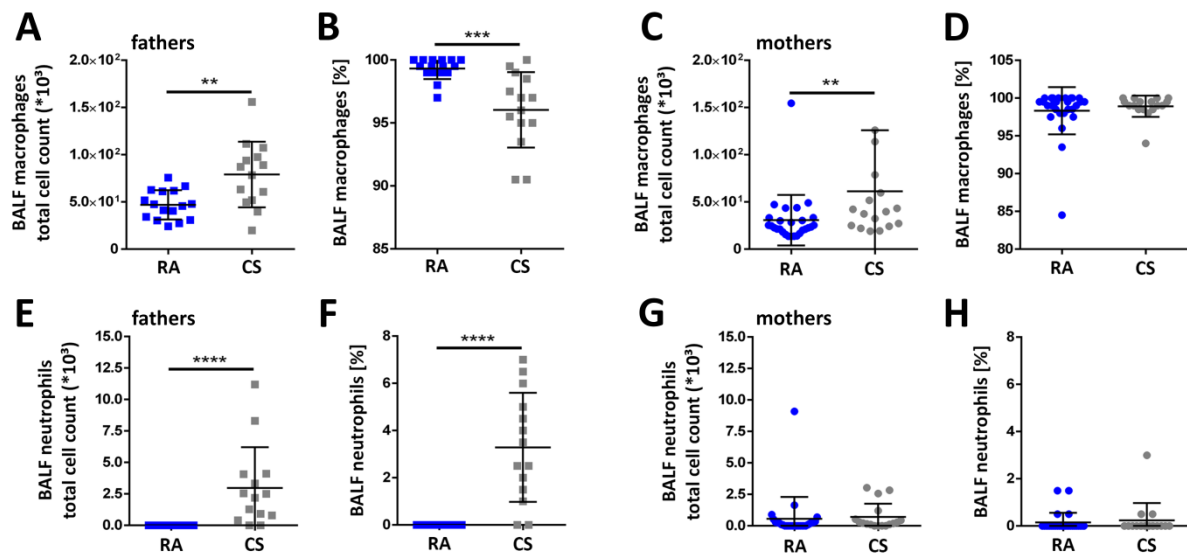


Figure 21 Analysis of inflammatory cells in BALF of lungs from RA- and CS-exposed fathers and mothers. Macrophages in A, absolute and B, relative numbers in fathers (RA ■ n= 16, CS ■ n= 14). Macrophages in C, absolute and D, relative numbers in mothers (RA ● n= 27, CS ● n= 17). Neutrophils in E, absolute and E, relative numbers in fathers. Neutrophils in G, absolute and H, relative numbers in mothers. A, Data are compared by Unpaired student's t test and B-H, Mann-Whitney test. A-H, Data are represented as mean \pm SD. Every data point represents an individual animal. Bronchoalveolar lavage fluid (BALF), room air (RA), cigarette smoke (CS). * $p < 0.05$, ** $p < 0.01$, *** $p < 0.001$, **** $p < 0.0001$.

7.3.2 Frequency and morphology of spermatogonia and spermatozoa were normal after adolescent CS exposure

To access changes in sperm development, spermatogonia in the in the seminiferous tubules of testes and spermatozoa isolated from cauda epididymis and ductus deferens were investigated. The spermatozoa count was unaltered in CS-exposed fathers compared to RA controls (**Figure 22A**). To analyze sperm morphology, spermatozoa were characterized by three different zones (head, mid-piece and tail). Despite observing defects in all three zones between exposure groups, defects were equally distributed resulting in comparable relative numbers of normal spermatozoa, indicating sustained morphological integrity (**Figure 22B**).

This was strengthened by a normal proliferation of their progenitor cells (spermatogonia) between RA and CS-exposed mice (**Figure 23A-B**).

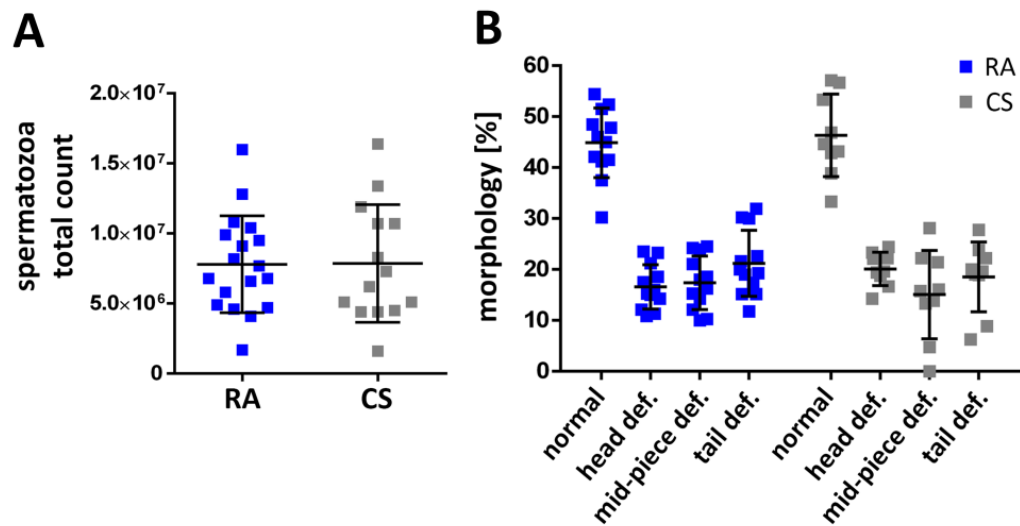


Figure 22 Total count and morphology of spermatozoa in RA- and CS-exposed fathers. A, Total sperm count (■ n= 18, ■ n= 14). B, Sperm morphology (■ n= 12, ■ n= 9) of RA and CS-exposed fathers. A, Unpaired student's t test. B, 2way ANOVA with Tukey's multiple comparisons test. A-B, Data are represented as mean \pm SD. Every data point represents an individual animal. Room air (RA), cigarette smoke (CS), defect (def.). * $p < 0.05$, ** $p < 0.01$, *** $p < 0.001$, **** $p < 0.0001$.

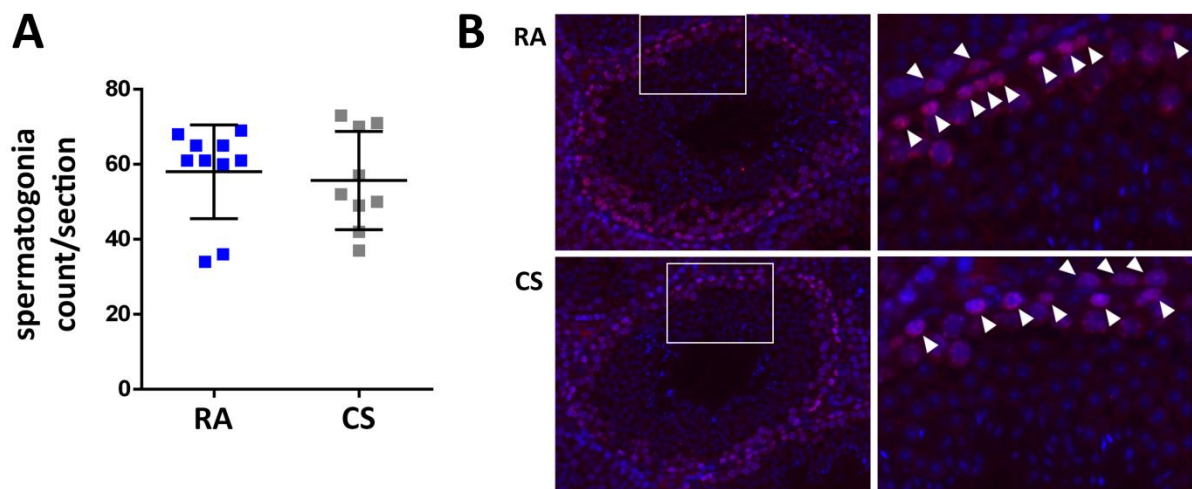


Figure 23 Analysis of spermatogonia in murine fathers. A, Immunofluorescence staining (40x; 120x, white arrows) (Ki67: red) (DAPI: blue) and quantification of spermatogonia in the testes of RA and CS-exposed fathers (■ n= 10, ■ n= 9) (D). Data are compared by Unpaired student's t test. Data are represented as mean \pm SD. Every data point represents an individual animal. Room air (RA), cigarette smoke (CS), Antigen KI-67 or MKI67 (Ki67), 4',6-diamidino-2-phenylindole (DAPI). * $p < 0.05$, ** $p < 0.01$, *** $p < 0.001$, **** $p < 0.0001$.

7.3.3 Preconceptional CS exposure affects body weight development in offspring

7.3.3.1 Parent-of-origin and sex-dependent body weight progression until PND3

Offspring's body weight was recorded from day of birth (day 0) until analysis. In the first three days of life, an altered body weight progression was observed. The body weight of male offspring from CS-exposed fathers showed a higher body weight on PND2 and PND3 compared to male offspring from non-smoking parents (**Figure 24A**). Of note, female offspring from smoking fathers had a normal body weight from PND0-3 compared to non-smoker's female offspring (**Figure 24B**). Conversely, male and female offspring from preconceptionally CS-exposed mothers showed a lower body weight (**Figure 24C-D**) with a more pronounced phenotype in the F1 females throughout the first 3 days of life (**Figure 24D**). Moreover, birth weights of female offspring from adolescent CS-exposed mothers were decreased compared to non-smoker parent's offspring. This effect could not be observed in male offspring from CS-exposed fathers.

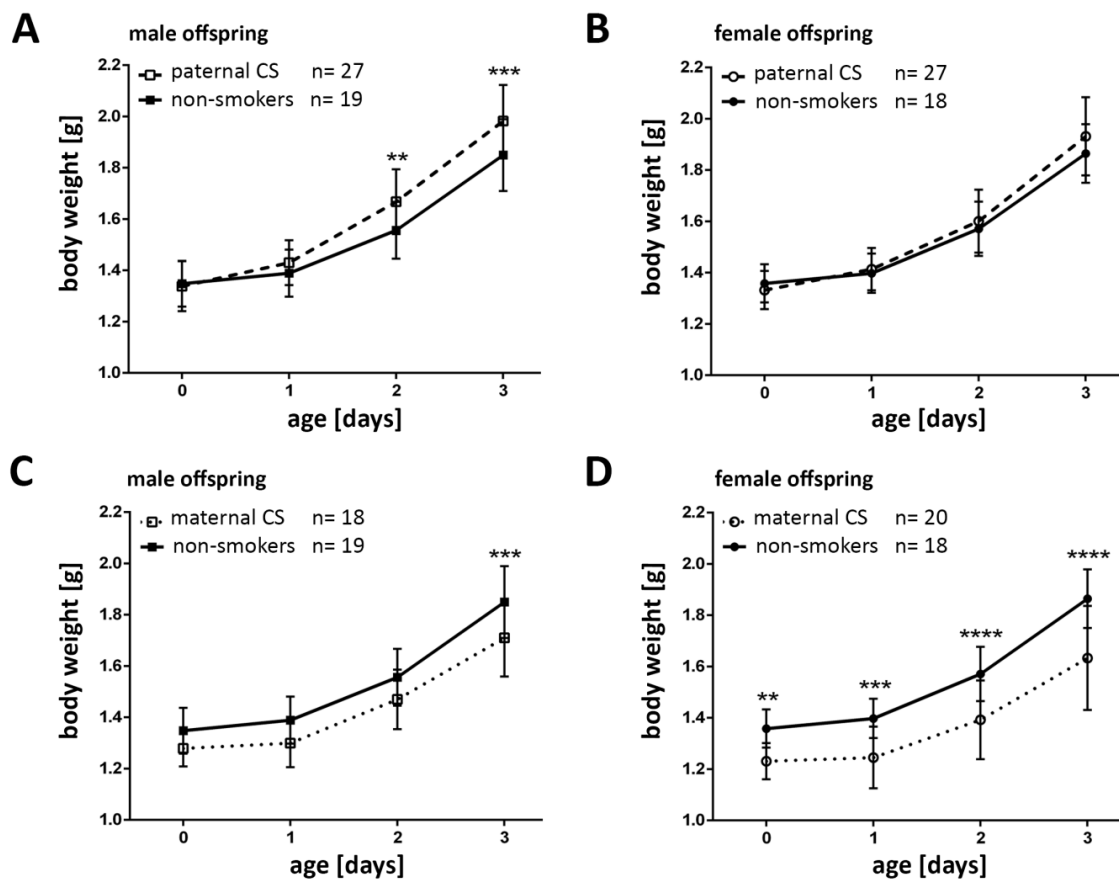


Figure 24 Influence of paternal and maternal preconceptional CS exposure on the body weight of F1 offspring until PND3. Comparison of body weights of male offspring (■) and female offspring (●) to the corresponding sex of offspring

from non-smoker parents (full lines) to A-B, paternal smoking (dashed lines) and C-D, maternal smoking groups (dotted lines) in the first 3 days of life. A-D, Two-way ANOVA with Bonferroni multiple comparisons test. Data are expressed as mean \pm SD. Room air (RA), cigarette smoke (CS), postnatal day (PND). * $p < 0.05$, ** $p < 0.01$, *** $p < 0.001$, **** $p < 0.0001$.

7.3.3.2 PND21 - the body weight follow-up

The body weight development until PND21 was analyzed using a multilevel mixed model. Not discriminating on F1 sex, offspring from smoking fathers during puberty had a trendwise increase in body weight, whereas offspring from adolescent smoking mothers were significantly lighter (**Table 14** and **Figure 25A-D**). The higher body weight in male offspring (PND2-3) after pubertal paternal smoking (**Figure 24A**) was not detected in the follow-up until PND21 using the multilevel mixed model (**Table 15** and **Figure 25A**). Male and female offspring born from mothers that smoked during adolescence had a significantly decreased body weight. On an average, F1 males (**Table 15** and **Figure 25C**) and F1 females (**Table 16** and **Figure 25D**) were lighter compared to offspring of the corresponding sex from non-smoker parents.

Body weight	n	Adjusted for	Coefficient	95% CI	p-value
Days	72	Exposure, sex	0.426	0.414 to 0.439	<0.001
Exposure	72	Time, sex			
Paternal smoker*	30		0.113	-0.006 to 0.233	0.062
Maternal smoker*	22		-0.176	-0.304 to -0.048	0.007
Sex [#]	72	Time, exposure	-0.010	-0.098 to 0.079	0.830

Table 14 Multilevel mixed analysis of body weight development (all offspring) until PND21 after paternal and maternal adolescent smoking. *The reference group is pups of non-smoker parents (n= 20). [#]The reference group is female offspring (n= 36). Number of animals (n), confidence interval (CI), postnatal day (PND). * $p < 0.05$, ** $p < 0.01$, *** $p < 0.001$, **** $p < 0.0001$.

RESULTS

Body weight	n	Adjusted for	Coefficient	95% CI	p-value
Days	36	Exposure	0.434	0.412 to 0.452	<0.001
Exposure	36 [¶]	Time			
Paternal smoker*	15		0.099	-0.045 to 0.242	0.177
Maternal smoker*	10		-0.166	-0.323 to -0.008	0.040

Table 15 Multilevel mixed analysis of body weight development (male offspring) until PND21 after paternal and maternal adolescent smoking. *The reference group is male pups of non-smoker parents (n= 11). [¶]Total number of male offspring (n=36). Number of animals (n), confidence interval (CI), postnatal day (PND). * p< 0.05, ** p< 0.01, *** p< 0.001, **** p< 0.0001.

Body weight	n	Adjusted for	Coefficient	95% CI	p-value
Days	36	Exposure	0.418	0.401 to 0.435	<0.001
Exposure	36 [¶]	Time			
Paternal smoker*	15		0.128	-0.033 to 0.289	0.120
Maternal smoker*	12		-0.193	-0.361 to -0.024	0.025

Table 16 Multilevel mixed analysis of body weight development (female offspring) until PND21 after paternal and maternal adolescent smoking. *The reference group is female pups of non-smoker parents (n= 9). [¶]Total number of female offspring (n=36). Number of animals (n), confidence interval (CI), postnatal day (PND). * p< 0.05, ** p< 0.01, *** p< 0.001, **** p< 0.0001.

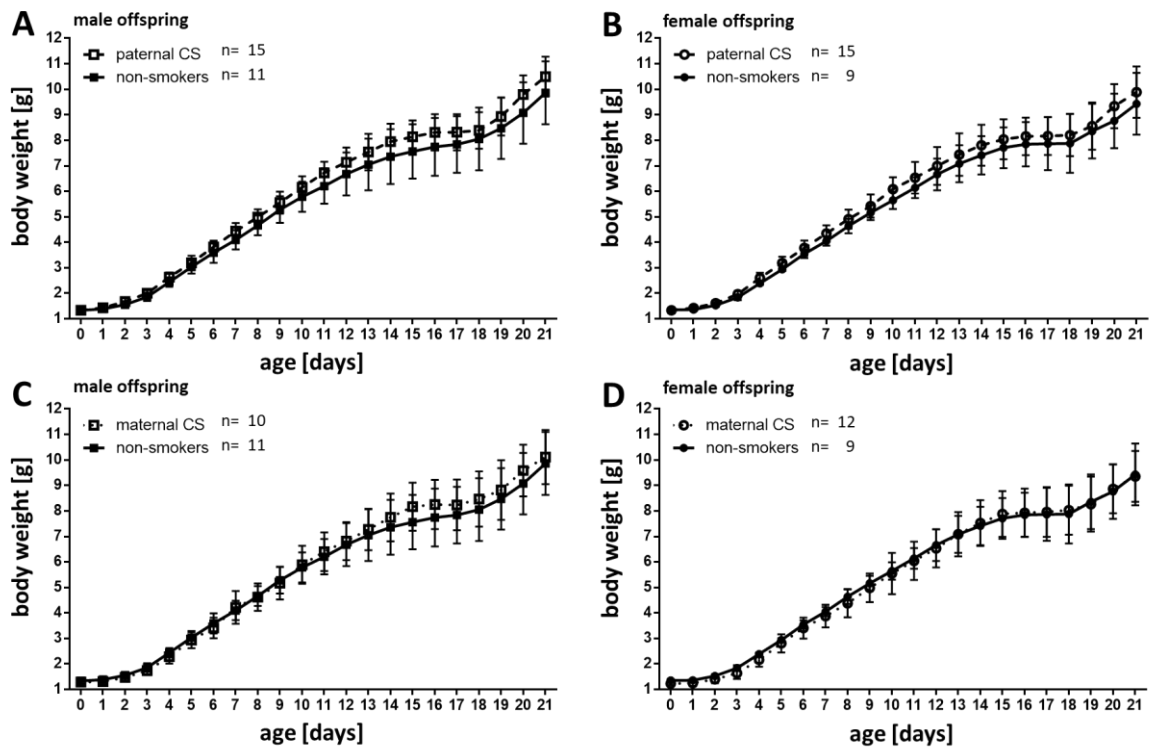


Figure 25 Influence of paternal and maternal preconceptional CS exposure on the body weight of F1 offspring until PND21. Comparison of body weights of male offspring (■) and female offspring (●) to the corresponding sex of offspring from non-smoker parents (full lines) to A-B, paternal smoking (dashed lines) and C-D, maternal smoking groups (dotted lines) until PND21. A-D, Data are expressed as mean \pm SD. Multilevel mixed analysis see Table 14-16. Room air (RA), cigarette smoke (CS), postnatal day (PND). * $p < 0.05$, ** $p < 0.01$, *** $p < 0.001$, **** $p < 0.0001$.

7.3.4 Spermatozoal miRNAs were altered in developmental pathways

Sperm are very rich in sncRNAs as miRNAs, piRNAs and tsRNAs. To identify if the observed effects on the body weight phenotype in offspring origins from the male germ line, miRNAs were analyzed in spermatozoa isolated from cauda epididymis and ductus deferens of RA- and CS-exposed fathers. The miRNA sequencing revealed 13 upregulated (Table 17) and 32 downregulated miRNAs (Table 18) in murine spermatozoa of CS-exposed fathers normalized with RA-exposed control animals. 'A priori' and 'A posteriori' analysis suggested miRNAs involved in functional and structural processes and pathways (Figure 26). 3 miRNAs were selected with particular interest as they were identified to play a role in modulating genes for tissue morphogenesis and development. Thus, miR-204-5p, miR-96-5p and miR-340-5p were chosen to be of most interest.

RESULTS

miRNA	baseMean	log2 FoldChange	lfcSE	stat	p-value	padj
mmu-miR-133a-3p	146,33	-0,88	0,3639	-2,4123	0,0159	0,0995
mmu-miR-674-3p	245,59	-0,86	0,3154	-2,7391	0,0062	0,0875
mmu-miR-204-5p	353,17	-0,76	0,2206	-3,4641	0,0005	0,0315
mmu-miR-149-5p	114,74	-0,73	0,2754	-2,6661	0,0077	0,0875
mmu-miR-125a-5p	2478,53	-0,68	0,2403	-2,8452	0,0044	0,0875
mmu-miR-574-3p	148,40	-0,65	0,2637	-2,4681	0,0136	0,0986
mmu-miR-337-5p	116,13	-0,64	0,2319	-2,7584	0,0058	0,0875
mmu-miR-99b-5p	3655,56	-0,60	0,2495	-2,4226	0,0154	0,0995
mmu-let-7d-3p	828,82	-0,57	0,2186	-2,6263	0,0086	0,0875
mmu-miR-676-3p	653,55	-0,57	0,2094	-2,7037	0,0069	0,0875
mmu-miR-744-5p	824,35	-0,56	0,2191	-2,5756	0,0100	0,0875
mmu-miR-223-5p	137,85	-0,55	0,2111	-2,6216	0,0088	0,0875
mmu-miR-205-5p	433,18	-0,55	0,2291	-2,4080	0,0160	0,0995

Table 17 13 miRNAs were upregulated in spermatozoa from preconceptionally CS-exposed fathers. *Mus musculus* (mmu), log₂-fold change standard error (lfcSE), adjusted p-value (padj).

miRNA	baseMean	log2 FoldChange	lfcSE	stat	p-value	padj
mmu-miR-30e-5p	1898,93	0,55	0,2112	2,5930	0,0095	0,0875
mmu-miR-148b-3p	2381,51	0,55	0,2131	2,6020	0,0093	0,0875
mmu-miR-140-5p	247,85	0,59	0,1897	3,1203	0,0018	0,0685
mmu-miR-101a-3p	1227,26	0,65	0,2475	2,6136	0,0090	0,0875
mmu-miR-96-5p	332,66	0,65	0,2504	2,5982	0,0094	0,0875
mmu-miR-741-3p	2342,20	0,66	0,2674	2,4823	0,0131	0,0976
mmu-miR-872-5p	1292,00	0,71	0,2598	2,7505	0,0060	0,0875
mmu-let-7a-1-3p =mmu-let-7c-2-3p	130,00	0,74	0,2504	2,9361	0,0033	0,0875
mmu-miR-9-5p	329,08	0,74	0,2718	2,7249	0,0064	0,0875
mmu-miR-743b-3p	2951,78	0,76	0,2993	2,5482	0,0108	0,0900
mmu-miR-18a-5p	70,35	0,77	0,2998	2,5815	0,0098	0,0875
mmu-miR-499-5p	74,78	0,78	0,2823	2,7722	0,0056	0,0875
mmu-miR-101b-3p	382,13	0,79	0,2730	2,8915	0,0038	0,0875
mmu-miR-34b-5p	937,66	0,81	0,3307	2,4498	0,0143	0,0995

RESULTS

mmu-miR-883a-3p	536,86	0,83	0,3225	2,5835	0,0098	0,0875
mmu-miR-3470b	63,98	0,84	0,3227	2,6073	0,0091	0,0875
mmu-miR-741-5p	73,76	0,84	0,3083	2,7366	0,0062	0,0875
mmu-miR-467d-3p	128,60	0,87	0,3584	2,4203	0,0155	0,0995
mmu-miR-34c-5p	16096,81	0,89	0,3032	2,9286	0,0034	0,0875
mmu-miR-878-3p	52,28	0,89	0,3584	2,4791	0,0132	0,0976
mmu-miR-106b-5p	65,11	0,93	0,3699	2,5190	0,0118	0,0956
mmu-miR-19a-3p	334,07	0,94	0,3596	2,6120	0,0090	0,0875
mmu-miR-881-3p	24924,42	0,96	0,2883	3,3427	0,0008	0,0404
mmu-miR-449a-5p	475,66	0,98	0,3178	3,0721	0,0021	0,0725
mmu-miR-669a-3p =mmu-miR-669o-3p	157,99	0,99	0,3536	2,8028	0,0051	0,0875
mmu-miR-878-5p	991,83	1,03	0,3148	3,2660	0,0011	0,0465
mmu-miR-340-5p	1411,07	1,06	0,3078	3,4533	0,0006	0,0315
mmu-miR-471-5p	444,80	1,07	0,2887	3,7224	0,0002	0,0168
mmu-miR-880-3p	436,15	1,27	0,3039	4,1870	0,0000	0,0096
mmu-miR-32-5p	67,31	1,39	0,3660	3,8052	0,0001	0,0161
mmu-miR-463-3p	61,15	1,43	0,3707	3,8698	0,0001	0,0161
mmu-miR-7210-5p	52,45	1,46	0,4947	2,9594	0,0031	0,0875

Table 18 32 miRNAs were downregulated in spermatozoa from preconceptionally CS-exposed fathers. *Mus musculus* (mmu), log₂-fold change standard error (lfcSE), adjusted p-value (padj).

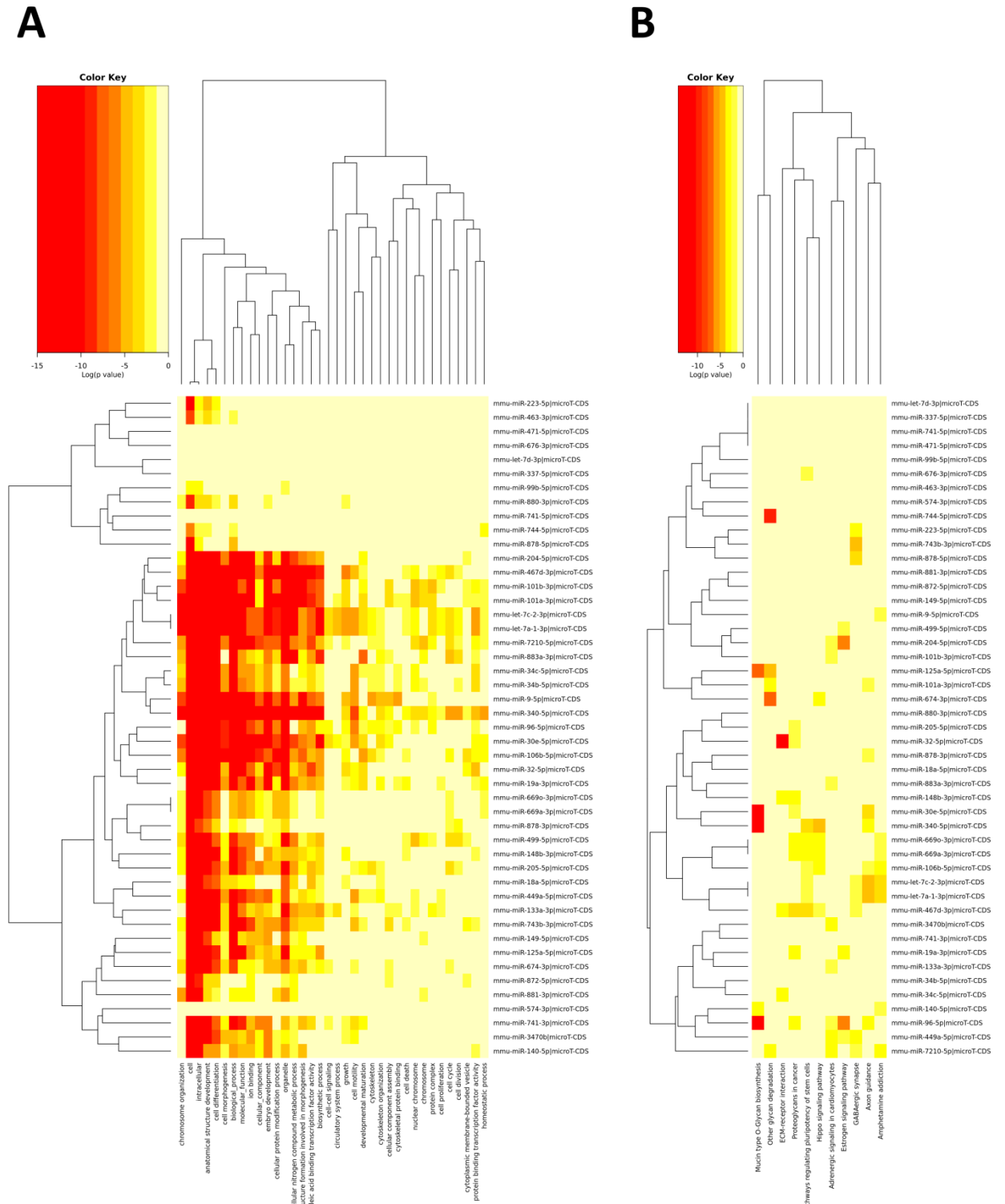


Figure 26 Heatmap of miRNAs regulated in spermatozoa from adolescent CS-exposed mice. The heatmaps represent A, gene ontology (GO) and B, Kyoto Encyclopedia of Genes and Genomes (KEGG) pathway analyses. The color key from yellow to red indicates the increasing p-value (logarithmic scale).

7.3.5 PND21 offspring of CS-exposed fathers do not suggest metabolic changes in the liver

As changes in body weight of the F1 generation and altered expression of sperm-borne miRNAs of adolescent smoking fathers were associated with metabolic pathways, livers of PND21 offspring were analyzed. The selected genes *interleukin 6 (Il6)*, *adiponectin (Adipoq)*, *leptin receptor (Lepr)*, *insulin receptor (Insr)* and *peroxisome proliferator-activated receptor gamma (Pparg)* are involved in body weight, adipogenesis and glucose metabolism in the liver. A preliminary qRT-PCR analysis was performed (experimental n= 1), detecting altered gene expression of *Il6* between F1 males and F1 females of CS-exposed fathers, whereas no effect could be observed compared to the control group of pooled male and female offspring from non-smoker parents (**Figure 27A**). A trendwise decrease of *Adipoq* was observed in males from smoking fathers compared to non-smoker's offspring (**Figure 27B**). *Lepr* and *Pparg* showed the same trend as it was elevated in F1 males compared to F1 females of CS-exposed fathers (**Figure 27C and 27E**), whereas the fold change of *Insr* was comparable among groups (**Figure 27D**).

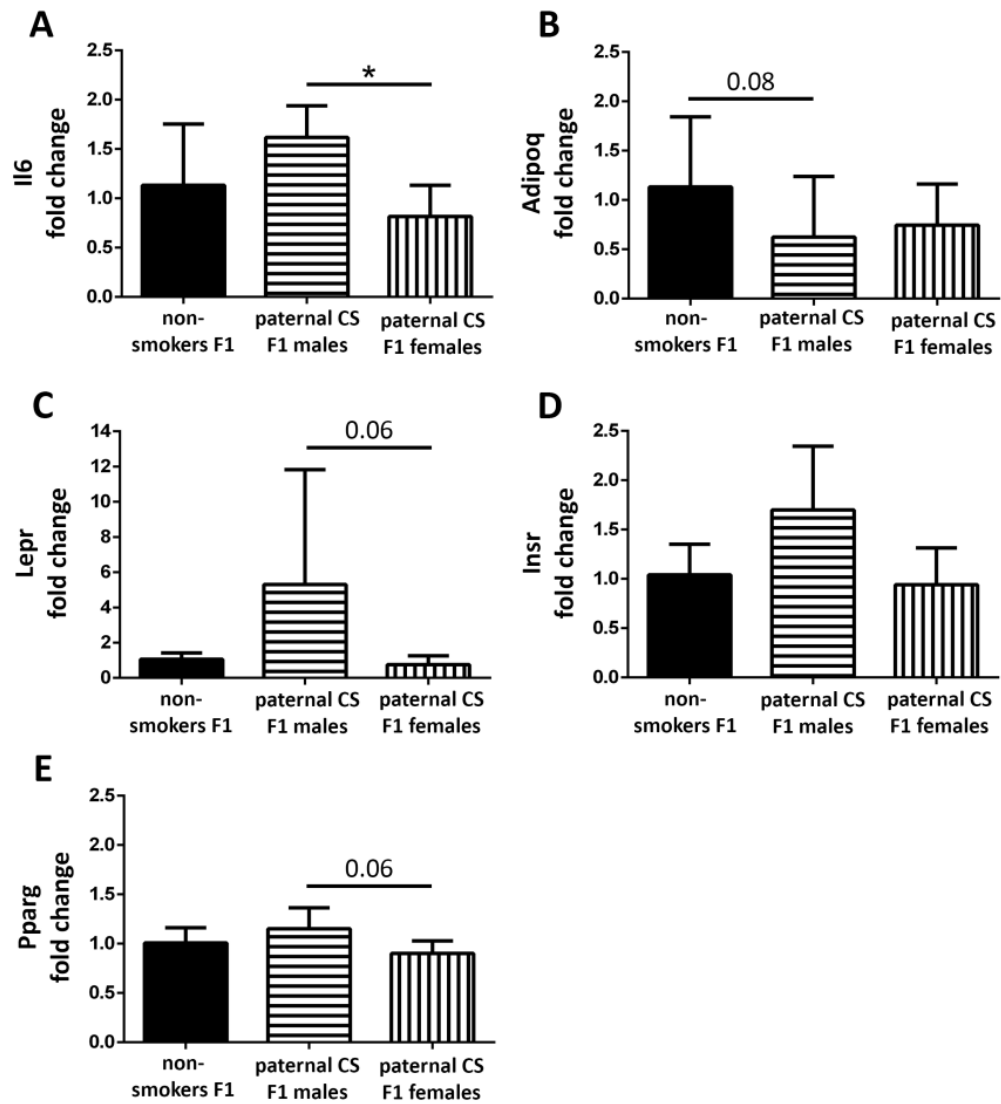


Figure 27 Regulation of selected genes in the liver of offspring at PND21 from RA and CS-exposed fathers. A, Interleukin-6 (*Il6*); B, Adiponectin (*Adipoq*); C, Leptin receptor (*Lepr*); D, Insulin receptor (*Insr*) and E, Peroxisome proliferator-activated receptor gamma (*Pparg*). Data are expressed as mean \pm SD and compared by Mann-Whitney U test. Filial generation 1 (F1), cigarette smoke (CS). * $p < 0.05$, ** $p < 0.01$, *** $p < 0.001$, **** $p < 0.0001$.

8 DISCUSSION

To this day, medical research goes in hand with the use of model organisms, as research in humans only is limited for ethical reasons and accessibility of tissues. Moreover, epidemiological studies investigating multiple generations in human depend on data collected over decades. Mouse models are well recognized tools to investigate medical questions and have proven to be a suitable model for cigarette smoke exposure experiments. As human smoking data are collected mainly by questionnaires and sparsely verified by cotinine measurements, mouse models serve controlled conditions of CS exposures to either mainstream smoke, sidestream smoke or a mixture of both.

8.1 Mild maternal smoking during pregnancy

In this study, first evidence of altered T cell subsets in lungs and thymi of offspring from mildly smoking mothers was demonstrated. The transcriptome of CD8SP thymocytes was deregulated, indicating a long-lasting effect on T cell development in the F1 progeny. These effects were observed at such low doses of cigarette smoke that neither a negative influence on body weight development nor postnatal lung function deficits were present in offspring from mildly smoking dams. The above-mentioned parameters of impaired lung function and reduced growth are regularly observed in murine models of CS exposures by us and other laboratories (39,99–102). Thus, the hypothesis was postulated that changes in T cell development caused by mild smoking during pregnancy may predispose to immune-related disorders such as asthma in the offspring.

8.1.1 *In utero* exposure to CS can decrease the thymus size

Epidemiological studies have observed that prenatal CS exposures lead to a reduced thymus size in term infants (103,104), which was dependent on the intensity of the maternal smoking behavior. The reduction in thymus size was more significant when mothers had smoked more than 10 cigarettes per day during pregnancy (104). In this study, despite the changes in cellular composition in T cells of murine offspring, the thymus weight to body weight ratio was normal. Therefore, the definition of the mild maternal smoking model is supported by the unchanged organ size. However, inbred mouse strains can respond differently. Regarding thymic involution, the C57BL/6 strain

used in this study is described as having a comparatively slow thymic involution (105). Therefore, the reduced number of total thymocytes in prenatally CS-exposed animals at PND56 requires further experiments to identify an origin that might relate to an altered thymic involution.

8.1.2 Nicotine affects thymocytes

Until now, the mechanisms have not been discovered how CS influences T cell development. Among other components, cigarette smoke consists of xenobiotics that bind to the aryl hydrocarbon receptors (AhR). Transgenic mice whose AhRs are constitutively activated in T cells were characterized to have a stronger thymic involution (106). Furthermore, thymocytes express the nicotinic acetylcholine receptor (nAChR), what indicates that nicotine can act directly on T cell subsets in the thymus as a single-selected component of CS (107–110). In mice, the administration of nicotine during pregnancy led to a reduction of fetal body weight and a decreased organ weight of the thymus, which was accompanied by an increased apoptosis of thymic T cells (111). Predominantly in male offspring, prenatal exposure to nicotine negatively affected the organ size of thymi, persisting until late adulthood (112).

8.1.3 Origin of prenatal CS-induced changes in lymphocytes

Experimental studies on prenatal smoking characterized lymphocytes in BALF (41), spleen (113) and lung (39) but omitted to expand their investigations further to the thymus to identify a possible origin of altered T cells. Using a prenatal heavy smoking model, a study in 2008 detected elevated levels of leukocytes in the blood of teenaged and adult mice, whereas no changes in cellularity or organ weight were found in the thymus and spleen (114). In this study of mild prenatal CS exposure, changes in CD4⁺ and CD8⁺ T cells in lungs and thymus were demonstrated that extend the observations of Ng and colleagues (2008).

At present, little is known about the substances contained in cigarette smoke – besides nicotine – that can cross the placenta and thus influence the fetal T cell development (109,112). However, in mildly smoking pregnant women, metabolic changes have been observed in their amniotic fluid (10).

8.1.4 Innate memory-like CD8SP thymocytes

Although thymic CD4SP T cells were elevated in this study, no changes were detected in CD4SP thymocytes at the transcriptional level. This could correlate with a disturbed positive and/or negative selection, which is not necessarily dependent on altered gene expression in thymocytes.

On the other hand, gene expression was altered in CD8SP. As immune-related pathways were of most interest in this study, the focus concentrated on genes involved in such pathways. Taken from literature, expression of *Ii4ra* on CD8SP thymocytes has been described for T_{IM} cells (reviewed in (115)). This suggests a strong correlation to T_{IM} cells as *Ii4ra*, *Runx3* and *Eomes* are characteristic genes expressed in these cells, and were found to be elevated in the CD8SP transcriptome data. T_{IM} cells are naive $\alpha\beta$ T cells, whose development in the thymus is IL-4-dependent (116), wherefore CD8SP are in need of the IL-4 receptor for recognition of the cytokine. T_{IM} cells undergo normal maturation in the thymus, but acquire a memory-like phenotype before leaving the primary lymphatic organ.

This thymic subpopulation of CD8SP T cells is not exclusive for mice, as they have been identified in humans (117). Their role has been described as supporting early immune defenses against pathogens in infants and young children before the CD8+ T cell memory responses of peripheral adaptive immunity are established (reviewed in (118)).

The T-box transcription factor *Eomes* was identified as a specific marker of T_{IM} cells and is essential for their differentiation (119–121). Furthermore, innate memory formation is promoted by *Eomes* as this transcription factor interacts with *Runx3*-bound enhancers (121). Since these two genes were upregulated in CD8SP thymocytes of offspring from mildly smoking pregnant mice, an abnormal development of T_{IM} cells is likely. Retrospectively, thymic CD8SP were not quantitatively altered in offspring of this study. However, T_{IM} cells are described as a relatively small subpopulation of CD8SP thymocytes, especially in C57BL/6 mice (reviewed in (115)), hence they might be challenging to quantify.

Foxp1 is involved in the generation of naive T cells in the thymus. *Foxp1* expression was elevated in the thymic CD8SP population, suggesting that it could correlate with a higher quiescence. In parallel, an upregulation of *Ii10rb* was found. In the thymus, the role of *Ii10rb* of T_{IM} cells has not been sufficiently understood. The IL-10 receptor (IL-10R)

consists of an α and β subunit that phosphorylate the signal transducer and activator of transcription 3 (STAT3). This signal cascade promotes the transcription of genes involved in anti-inflammatory processes (reviewed in (122)). As discussed above, smoking during pregnancy has metabolic effects on the amniotic fluid surrounding the fetus. Therefore, it is presumed that pro-inflammatory mediators deriving from maternal smoking in the amniotic fluid could support the generation of thymic T_{IM} cells as well as the expression of *Il10rb* to prevent tissue damage (123).

The results of this study show that mild doses of prenatal CS cause developmental disorders in T cell subsets. This distortion appears to affect thymic T_{IM} cells, but this statement requires further evidence and functional investigations. Nonetheless, an imbalance in T cell immunity in early childhood could lead to an oversensitivity to allergens. Moreover, bacterial compounds like lipopolysaccharides (LPS) accompany allergens and could further contribute to the development of asthma and allergies.

8.1.5 Limitations I

Several potential limitations need to be acknowledged in this study of mild maternal smoking during pregnancy. First, the translation of the observations in mice to the human situation remains challenging as it is difficult to obtain human tissues specimens such as lung or thymus, especially from infants. That impedes the confirmation of the findings observed in this mouse model to humans. Moreover, the analysis of lymphocytes in human surrogate tissue like BALF or cord blood is not sufficiently comparable to the development and regulation of thymocytes.

Second, stress is a proven confounder in animal experiments that can significantly influence the outcome of experiments. Changes in physiological parameters can occur by simple handling procedures of dams as well as stressors such as light, noise and restraint (reviewed in (124)). It has been shown that prenatal stress leads to developmental delays and negatively affects the body weight and body length of offspring (125). In addition, in offspring of stressed dams, a worsening of lung function and asthma response has been demonstrated (126). Therefore, in this model, maternal stress was tried to be minimized as much as possible. This was achieved by accustoming the animals to simple day-to-day handling and the weighing procedure, the new environment of the exposure chamber

and by introducing the first contact of CS before the onset of pregnancy. Therefore, the experimental results are suggested to be primarily induced by prenatal CS and escaped a strong influence by stressors.

Third, for NGS only female offspring were selected due to access and time limitations. Although no differences were observed regarding flow cytometric analyses of thymocytes between sexes, differences at the transcriptional level between female and male offspring cannot be excluded.

8.1.6 Conclusion I

In conclusion, to the best of knowledge this is the first study that shows that distinct T cell populations in the lung and thymus are altered by mild maternal smoking in mice in absence of lung function deficits and intrauterine growth restriction. Furthermore, a dysregulated gene expression in CD8SP thymocytes was detected. Among the affected genes were *Ii4ra*, *Runx3* and *Eomes*, that displayed an elevated expression. It therefore suggests that a certain T cell population in the thymus, called T_{IM} cells, is affected by mild CS exposure *in utero*. However, this conclusion requires further investigation. This study wants to emphasize that offspring's immunity and health underlie potential postnatal adverse effects even when exposed prenatally to a mild dose of cigarette smoke.

8.2 Paternal adolescent smoking

This is the first study to report an association between paternal preconceptional smoking in puberty and changes in the body weights of male offspring. Compelling evidence, that has gained recognition over the last 5 years, presents sncRNAs in the sperm as essential candidates in relation to alterations of metabolic processes (54,55,127,128). As frequency and morphology of spermatogonia and spermatozoa remained normal in adolescent smoking fathers, altered sncRNA content in spermatozoa is suggested to play an important role in transmitting ancestral information as already reported in some studies (54,127,128). In this study, 3 highly regulated miRNAs were identified in spermatozoa of CS-exposed fathers during puberty which are involved in developmental pathways. Several studies have shown the influence of miRNAs on the phenotypes of early zygotes (53,129,130). Relative to this was proposed that the observed increased body weight in male but not female offspring of smoking fathers might be in association with the altered diversity of miRNA in the sperm.

8.2.1 Parental smoking and effects of nicotine during puberty

First evidence of epidemiological studies reported that environmental exposures of fathers could influence offspring's health, with some emphasis on preconceptional cigarette smoking (24,57,58). Cigarette smoke contains over 5.000 chemicals (131), and nicotine is known to play a role in the addictive smoking behavior (reviewed in (132)). Experimental studies of nicotine during adolescent have been conducted, addressing primarily neuronal development (reviewed in (133)) and drug abuse (134–136). A study in male rats observed that low nicotine administration during puberty led to a decreased fertility by higher oxidative stress in the prostate and testes and a lower sperm quality. Sperm cells had reduced total numbers, increased abnormal morphology, decreased motility and a lower viability (137). As nicotine is a single-selected component of CS, the effects of whole cigarette smoke need to be addressed in experimental studies. This was investigated by a study of adolescent exposure to cigarette smoke, leading to behavioral changes in male and female mice that suggested a higher risk of drug abuse in these animals (138). However, the observations of these studies were only conducted in the F0 generation and the findings cannot be extended to the next generation.

8.2.2 Environmental exposures of fathers can alter disease risk in offspring

Epidemiological evidence exists that adolescent smoking of fathers increases risks of obesity in children (57). At present, murine studies focused on high-fat diet (HFD) and obesity models to investigate the underlying mechanisms of paternal factors on offspring's disease risks. Several studies successfully transmitted the obese phenotype onto the next generation, even by feeding the offspring with standard chow (54,55). Molecules that were highly implicated in the transmission of the paternal phenotype to the offspring were miRNAs in sperm cells (54,128). In this study, these latest observations suggest that the body weight alterations observed in male offspring from adolescent smoking fathers originate from miRNA dynamics, induced from cigarette smoke in germ cells during pubertal development.

Two epidemiological studies observed that smoking of fathers before the age of 15 increased the risk of asthma in children (24,58). Further experimental studies could utilize the murine preconceptional smoking model developed in this study to investigate the suggested increased asthma risk in offspring. The experimental approach by an additional asthma model could investigate potential mechanisms of father's pubertal smoking on the asthma phenotype in murine F1 progeny.

Of note, epidemiological data suggest an elevated asthma risk in children from fathers that were obese in early puberty (56). Hence, it is speculative if grandpaternal smoking could lead to obesity in sons and – if still present at puberty – the obese phenotype of sons could transmit to a higher asthma risk in grandchildren.

8.2.3 Sperm-borne miRNAs and paramutations in offspring

Evidence that sperm-borne sncRNAs can carry an ancestral epigenetic memory has been supported by a few studies in mice. The injection of total sperm-borne RNAs or a specific subtype of sncRNAs (miRNAs, tsRNAs) obtained from stressed males (52,53,139) or HFD models (54,127) into normal zygotes resulted in offspring exhibiting the paternal phenotype. The paramutations – mutations that do not follow Mendelian inheritance patterns – were transgenerationally transmitted as they were partially passed on to two proceeding generations (52). More studies confirmed miRNAs as key players of the inherited paternal phenotypes via microinjection of total sperm-borne sncRNAs (52,140),

a combination of miRNAs (53) or a single miRNA (129,130) into early zygotes. Of note, Grandjean and colleagues (2015) identified a specific, highly expressed miRNA (miR-19b) in the sperm of male mice on a HFD. Offspring obtained from zygote injections of miR-19b were obese and developed glucose intolerance (54). In this study, the expression of miR-340-5p was decreased in the sperm of pubertal smoking fathers. miR-340-5p has been described to be downregulated in sperm cells from males fed with a HFD (55). This is in congruence to the observations in this study, supporting the effect of miR-340-5p on the higher body weight in male offspring. In a study that investigated hypothermic stress on murine testis, miR-340-5p was found to be decreased (141), but Fullston and colleagues (2013) demonstrated that miRNA-340-5p was increased in the testes whereas decreased in the sperm cells (55). This suggests that in spermatogenesis, the miRNA content undergoes changes during sperm differentiation and does not imply that altered miRNA frequency in the testes is stable in mature spermatozoa. As suggested earlier in this study, miR-340-5p expression was upregulated in liver tissues from obese mice induced by a HFD, and insulin-like substrate-1 (IRS-1) was shown as its putative target (142). Furthermore, in hepatocarcinomas, miR-340-5p was found to be decreased (143), supporting the argument from other studies that identified miR-340-5p as a tumor suppressor (144–146). In white subcutaneous and visceral adipose tissue from HFD mice, increased expression of miR-340-5p was detected (147). Taken these observations together, miR-340-5p can lead to paramutations, affecting multiple obesity-related tissues. In this study, KEGG analysis associated the sperm-borne miR-340-5p with the Hippo signaling pathway, which is essential for organ size control in animals through the regulation of cell proliferation and apoptosis (reviewed in (148,149)). Further investigations are needed to examine if a negatively regulated miR-340-5p in spermatozoa of adolescent smoking mice could play a pivotal role in the phenotype that was observed in F1 males in this study.

Another miRNA regulated in the sperm of CS-exposed fathers was miR-204-5p. This miRNA is associated with adipogenesis through a putative target called Runx2 (150,151). As miRNA-204-5p was upregulated in the spermatozoa in this mouse model, it suggests that miR-204-5p could relate to a promotion of adipogenesis in the F1 progeny. Male offspring from adolescent smoking fathers were heavier in the first days of life, but to

specifically relate this observation to muscular mass, bone density and fat tissues needs to be addressed in future studies. Moreover, evidence exists that miRNA-204-5p in sperm cells could likely influence embryogenesis. A study by Saunders et al (2010) documented decreased Sirtuin1 (SIRT1) protein levels – a type III histone/protein deacetylase – in embryonic stem cells after injecting miRNA-204-5p (152).

In smokers, SIRT1 is downregulated by cigarette smoke, promoting inflammation and cellular senescence in the lungs. SIRT1 protects the lungs from oxidative stress (153) as well as in embryonic stem cells (152). A proposed mechanism about how SIRT1 inhibits oxidative stress is via forkhead box protein O3 (FOXO3) (153). In this study, it remains speculative if increased paternal miR-204-5p delivered from the sperm cell into the zygote could influence methylation and the quality of the blastocyst by affecting the SIRT1 pathway.

Moreover, FOXO3a is a putative target of miRNA-96-5p via an AhR/miR-96 axis explained by an increase in FOXO3a from a downregulated miR-96-5p in the lungs of CS-exposed mice (154), which correlates with a decreased expression of miR-96-5p in the spermatozoa of smoking fathers in this study. But to identify if FOXO3a is affected in early zygotes needs further investigation.

Of note, miR-204-5p has been associated with brain development (155,156) which raises the question if murine offspring from this study would develop behavioral abnormalities.

The mechanism by which sperm-borne sncRNAs influence gene translation in the early zygote remains unclear. Sperm-borne miRNAs have to interact with maternal mRNA to some extent, so as to alter embryonic development through cellular mechanisms which may include apoptosis, cell survival, differentiation and proliferation. Furthermore, it remains difficult to resemble the physiological conditions of an altered miRNA in a single sperm cell. Therefore the induction of molecular, cellular and phenotypic changes observed in recent studies remains challenging under physiological conditions in *in vitro* fertilization experiments using microinjection of miRNAs. Moreover, the exchange of sncRNAs in the epididymis during spermatozoal maturation could potentially influence the miRNA abundance that was altered in spermatozoa of preconceptionally CS-exposed fathers in this study. sncRNAs can be carried by membrane-bound microstructures called extracellular vesicles (EVs) (157). In the epididymis, epididymal epithelial cells produce

EVs (epididymosomes) that contain over 350 miRNAs and can influence the miRNA content in maturing sperm cells (158,159). Investigating this mechanism could help to understand how epigenetic characteristics can be transmitted from the paternal line to the offspring.

8.2.4 Limitations II

The model used in this study has several limitations. First, puberty in mice is difficult to precisely determine. In females, the onset of puberty can be visually identified by the vaginal opening but in males, the preputial separation is challenging to observe. In addition, the completion of puberty cannot be determined by phenotypically characteristics.

Second, although this study could generate a murine model to investigate environmental influences of fathers on offspring's health that reproduces correlations observed in human studies (57,58), possible limitations are a) that it is likely that the cigarette smoke exposure has been continued after completion of puberty and b) the non-smoking period while mating.

Third, NGS data of miRNA were not validated with qRT-PCR in sperm samples of mice.

Finally, it remains speculative how the changed expression of miRNAs in spermatozoa directly influence transcription, therefore may leading to functional changes in sperm cells.

8.2.5 Conclusion II

In conclusion, to the best of knowledge this is the first study to show evidence that smoking during puberty affects germ cells in both sexes, resulting in parent-of-origin-dependent phenotypes in the F1 generation. Spermatozoa contain ancestral memory that possibly influences paramutations in the zygote and therefore transmits paternal phenotypes and/or increases disease risks. In this study, altered miRNA expression in spermatozoa could be responsible for the observed increase in body weight of the male F1 progeny from preconceptional smoking fathers. However, this finding needs to be further explored. Nonetheless, this study indicates that – despite well-investigated risks of maternal smoking – paternal smoking bears health risks for future offspring. miRNAs offer putative targets in form of genes and pathways to understand the connection

between environmental paternal exposures and transmittable epigenetic changes to the progeny, connecting to metabolic and developmental alterations as well as increased susceptibility to allergy and asthma.

8.3 Future perspectives

Both murine models of prenatal and preconceptional smoking are in need of further investigations:

8.3.1 Prenatal mild maternal smoking

1. The suggested T_{IM} cells, identified in thymi of mildly *in utero* CS-exposed offspring, are in need of a detailed characterization. This can be utilized by flow cytometry, as these cells are described to express the surface markers CD44 and CD122 as well as the transcription factor *Eomes* (reviewed in (115,118)).
2. Furthermore, the decreased number of total thymocytes observed at PND56 from mildly smoking dams is of interest to identify a potential underlying effect on thymic involution.
3. The increased frequency of CD4SP thymic T cells could originate from an inadequate positive and/or negative selection process in the thymus.

8.3.2 Preconceptional adolescent smoking

1. The successful establishment of a murine model of preconceptional paternal smoking opens the opportunities to continue this study by investigating targets of selected miRNAs (miR-340-5p, miR-204-5p and miR-96-5p) on early zygotes by microinjections.
2. In this study, strong effects of adolescent maternal smoking were detected on a decreased body weight in offspring of both sexes during the first 3 days of life and the follow-up until PND21. The investigation of e.g. changed DNA-methylations and/or transcriptome of the oocytes or early blastocyst of preconceptionally smoking mothers could give insight into potential mechanisms. The investigation clearly is of great interest as girls start smoking equivalently early to boys, especially in developed and high-income countries (1,13)

8.3.3 Asthma models

In both parental exposure models, murine asthma models challenging the offspring with an allergen like HDM or ovalbumin (OVA) are necessary to investigate increased asthma risks from CS exposures of different parental smoking behaviors.

9 BIBLIOGRAPHY

1. World Health Organization (WHO). European tobacco use, trends report 2019. 2019
2. Man MA, Oancea C, Lesan A, Domokos B, Motoc N, Pop M. Smoking during pregnancy. In: *Tobacco, Smoking Control and Health Education*. European Respiratory Society 2017: 50: PA1267.
3. Crozier SR, Robinson SM, Borland SE, Godfrey KM, Cooper C, Inskip HM. Do women change their health behaviours in pregnancy? Findings from the Southampton Women's Survey. *Paediatr Perinat Epidemiol* 2009;**23**:446–453.
4. Butler NR, Goldstein H, Ross EM. Cigarette smoking in pregnancy: its influence on birth weight and perinatal mortality. *Br Med J* 1972;**2**:127–130.
5. Gilliland FD, Li YF, Peters JM. Effects of maternal smoking during pregnancy and environmental tobacco smoke on asthma and wheezing in children. *Am J Respir Crit Care Med* 2001;**163**:429–436.
6. Tsakiridis I, Mamopoulos A, Papazisis G, Petousis S, Liozidou A, Athanasiadis A et al. Prevalence of smoking during pregnancy and associated risk factors: A cross-sectional study in Northern Greece. *Eur J Public Health* 2018;**28**:321–325.
7. den Dekker HT, Voort AMMS der, de Jongste JC, Reiss IK, Hofman A, Jaddoe VW V et al. Tobacco Smoke Exposure, Airway Resistance, and Asthma in School-age Children: The Generation R Study. *Chest* 2015;**148**:607–617.
8. Svanes C, Omenaas E, Jarvis D, Chinn S, Gulsvik A, Burney P. Parental smoking in childhood and adult obstructive lung disease: results from the European Community Respiratory Health Survey. *Thorax* 2004;**59**:295–302.
9. Dietz PM, Homa D, England LJ, Burley K, Tong VT, Dube SR et al. Estimates of Nondisclosure of Cigarette Smoking Among Pregnant and Nonpregnant Women of Reproductive Age in the United States. *Am J Epidemiol* 2010;**173**:355–359.
10. Fischer ST, Lili LN, Li S, Tran VLT, Stewart KB, Schwartz CE et al. Low-level maternal exposure to nicotine associates with significant metabolic perturbations in second-trimester amniotic fluid. *Environ Int* 2017;**107**:227–234.
11. Polańska K, Hanke W, Laudański T, Kalinka J. Serum cotinine level as a biomarker of tobacco smoke exposure during pregnancy | Steżenie kotyniny w osoczu jako

- biomarker czynnej i biernej ekspozycji kobiet ciężarnych na dym tytoniowy. *Ginekol Pol* 2007;**78**:796–801.
12. Spector LG, Murphy SE, Wickham KM, Lindgren B, Joseph AM. Prenatal Tobacco Exposure and Cotinine in Newborn Dried Blood Spots. *Pediatrics* 2014;**133**:e1632–e1638.
 13. World Health Organization (WHO). WHO Global Report on Trends in Prevalence of Tobacco Smoking. 2018
 14. Miller LL, Pembrey M, Smith GD, Northstone K, Golding J. Is the growth of the fetus of a non-smoking mother influenced by the smoking of either grandmother while pregnant? *PLoS One* 2014;**9**:e86781.
 15. Li YF, Langholz B, Salam MT, Gilliland FD. Maternal and grandmaternal smoking patterns are associated with early childhood asthma. *Chest* 2005;**127**:1232–1241.
 16. Magnus MC, Haberg SE, Karlstad O, Nafstad P, London SJ, Nystad W. Grandmother's smoking when pregnant with the mother and asthma in the grandchild: the Norwegian Mother and Child Cohort Study. *Thorax* 2015;**70**:237–243.
 17. Lodge CJ, Bråbäck L, Lowe AJ, Dharmage SC, Olsson D, Forsberg B. Grandmaternal smoking increases asthma risk in grandchildren: a nationwide Swedish cohort. *Clin Exp Allergy* 2017;**48**:167–174.
 18. Miller LL, Henderson J, Northstone K, Pembrey M, Golding J. Do grandmaternal smoking patterns influence the etiology of childhood asthma? *Chest* 2014;**145**:1213–1218.
 19. Selroos O, Kupczyk M, Kuna P, Łacwik P, Bousquet J, Brennan D et al. National and regional asthma programmes in Europe. *Eur Respir Rev* 2015;**24**:474–483.
 20. Punnoose AR, Burke AE, Golub RM. ERS white book: Childhood asthma. *JAMA - J Am Med Assoc* 2012;**307**:421.
 21. Moheimani F. Flu jab: for asthmatics, avoiding the flu vaccine could be a fatal mistake. *Conversat.* 2019.<http://theconversation.com/flu-jab-for-asthmatics-avoiding-the-flu-vaccine-could-be-a-fatal-mistake-121347> (accessed 11 Dec2019).
 22. Stick SM, Burton PR, Gurrin L, Sly PD, LeSouef PN. Effects of maternal smoking during pregnancy and a family history of asthma on respiratory function in newborn infants. *Lancet* 1996;**348**:1060–1064.

23. Dai X, Dharmage SC, Lowe AJ, Allen KJ, Thomas PS, Perret J et al. Early smoke exposure is associated with asthma and lung function deficits in adolescents. *J Asthma* 2017;**54**:662–669.
24. Accordini S, Calciano L, Johannessen A, Portas L, Benediktsdóttir B, Bertelsen RJ et al. A three-generation study on the association of tobacco smoking with asthma. *Int J Epidemiol* 2018;**47**:1106–1117.
25. Ward C, Lewis S, Coleman T. Prevalence of maternal smoking and environmental tobacco smoke exposure during pregnancy and impact on birth weight: retrospective study using Millennium Cohort. *BMC Public Health* 2007;**7**:81.
26. Papoz L. Measures of maternal tobacco exposure and infant birth weight at term. *Am J Epidemiol* 2003;**157**:86–87.
27. Burke H, Leonardi-Bee J, Hashim A, Pine-Abata H, Chen Y, Cook DG et al. Prenatal and Passive Smoke Exposure and Incidence of Asthma and Wheeze: Systematic Review and Meta-analysis. *Pediatrics* 2012;**129**:735–744.
28. Ng SP, Zelikoff JT. Smoking during pregnancy: Subsequent effects on offspring immune competence and disease vulnerability in later life. *Reprod Toxicol* 2007;**23**:428–437.
29. Hammer B, Wagner C, Divac Rankov A, Reuter S, Bartel S, Hylkema MN et al. In utero exposure to cigarette smoke and effects across generations: A conference of animals on asthma. *Clin Exp Allergy* 2018;**48**:1378–1390.
30. Roeder T, Isermann K, Kallsen K, Uliczka K, Wagner C. A *Drosophila* asthma model - what the fly tells us about inflammatory diseases of the lung. *Adv Exp Med Biol* 2012;**710**:37–47.
31. Kallsen K, Zehethofer N, Abdelsadik A, Lindner B, Kabesch M, Heine H et al. ORMDL deregulation increases stress responses and modulates repair pathways in *Drosophila* airways. *J Allergy Clin Immunol* 2015;**136**:1105–1108.
32. Progatzy F, Cook HT, Lamb JR, Bugeon L, Dallman MJ. Mucosal inflammation at the respiratory interface: a zebrafish model. *Am J Physiol Lung Cell Mol Physiol* 2016;**310**:L551–L561.
33. Ellis LD, Soo EC, Achenbach JC, Morash MG, Soanes KH. Use of the zebrafish larvae as a model to study cigarette smoke condensate toxicity. *PLoS One* 2014;**9**:e115305.

34. Palpant NJ, Hofsteen P, Pabon L, Reinecke H, Murry CE. Cardiac development in zebrafish and human embryonic stem cells is inhibited by exposure to tobacco cigarettes and e-cigarettes. *PLoS One* 2015;**10**:e0126259.
35. Folkesson M, Sadowska N, Vikingsson S, Karlsson M, Carlhall CJ, Lanne T et al. Differences in cardiovascular toxicities associated with cigarette smoking and snuff use revealed using novel zebrafish models. *Biol Open* 2016;**5**:970–978.
36. Larcombe AN, Foong RE, Berry LJ, Zosky GR, Sly PD. In utero cigarette smoke exposure impairs somatic and lung growth in BALB/c mice. *Eur Respir J* 2011;**38**:932–938.
37. Vuolo M, Staff J. Parent and child cigarette use: a longitudinal, multigenerational study. *Pediatrics* 2013;**132**:e568–e577.
38. Drummond D, Baravalle-einaudi M, Lezmi G, Vibhushan S, Franco-Montoya M-L, Hadchouel A et al. Combined Effects of in Utero and Adolescent Tobacco Smoke Exposure in C57Bl/6J Mice. *Environ Health Perspect* 2017;**125**:392–399.
39. Blacquiere MJ, Timens W, Melgert BN, Geerlings M, Postma DS, Hylkema MN. Maternal smoking during pregnancy induces airway remodelling in mice offspring. *Eur Respir J* 2009;**33**:1133–1140.
40. Singh SP, Barrett EG, Kalra R, Razani-Boroujerdi S, Langley RJ, Kurup V et al. Prenatal cigarette smoke decreases lung cAMP and increases airway hyperresponsiveness. *Am J Respir Crit Care Med* 2003;**168**:342–347.
41. Eyring KR, Pedersen BS, Yang I V, Schwartz DA. In Utero Cigarette Smoke Affects Allergic Airway Disease But Does Not Alter the Lung Methylome. *PLoS One* 2015;**10**:e0144087.
42. Schröder PC, Casaca VI, Illi S, Schieck M, Michel S, Böck A et al. IL-33 polymorphisms are associated with increased risk of hay fever and reduced regulatory T cells in a birth cohort. *Pediatr Allergy Immunol* 2016;**27**:687–695.
43. Hartl D, Koller B, Mehlhorn AT, Reinhardt D, Nicolai T, Schendel DJ et al. Quantitative and functional impairment of pulmonary CD4+CD25hi regulatory T cells in pediatric asthma. *J Allergy Clin Immunol* 2007;**119**:1258–1266.
44. Walker C, Kaegi MK, Braun P, Blaser K. Activated T cells and eosinophilia in bronchoalveolar lavages from subjects with asthma correlated with disease severity. *J Allergy Clin Immunol* 1991;**88**:935–942.

45. Hinz D, Bauer M, Röder S, Olek S, Huehn J, Sack U et al. Cord blood Tregs with stable FOXP3 expression are influenced by prenatal environment and associated with atopic dermatitis at the age of one year. *Allergy Eur J Allergy Clin Immunol* 2012;**67**:380–389.
46. Herberth G, Bauer M, Gasch M, Hinz D, Röder S, Olek S et al. Maternal and cord blood miR-223 expression associates with prenatal tobacco smoke exposure and low regulatory T-cell numbers. *J Allergy Clin Immunol* 2014;**133**:543–550.e4.
47. Fleisch AF, Rifas-Shiman SL, Rokoff LB, Hivert MF, Mantzoros CS, Oken E. Associations of maternal prenatal smoking with umbilical cord blood hormones: the Project Viva cohort. *Metabolism* 2017;**72**:18–26.
48. Noakes PS, Holt PG, Prescott SL. Maternal smoking in pregnancy alters neonatal cytokine responses. *Allergy Eur J Allergy Clin Immunol* 2003;**58**:1053–1058.
49. Aycicek A, Ipek A. Maternal active or passive smoking causes oxidative stress in cord blood. *Eur J Pediatr* 2008;**167**:81–85.
50. Abbas AK, Lichtmann AH, Pillai S. *Cellular and Molecular Immunology*. 7th ed. ELSEVIER SAUNDERS 2012
51. Weerkamp F, Pike-Overzet K, Staal FJT. T-sing progenitors to commit. *Trends Immunol* 2006;**27**:125–131.
52. Gapp K, Jawaid A, Sarkies P, Bohacek J, Pelczar P, Prados J et al. Implication of sperm RNAs in transgenerational inheritance of the effects of early trauma in mice. *Nat Neurosci* 2014;**17**:667–669.
53. Rodgers AB, Morgan CP, Leu NA, Bale TL. Transgenerational epigenetic programming via sperm microRNA recapitulates effects of paternal stress. *Proc Natl Acad Sci* 2015;**112**:13699–13704.
54. Grandjean V, Fourné S, De Abreu DAF, Derieppe MA, Remy JJ, Rassoulzadegan M. RNA-mediated paternal heredity of diet-induced obesity and metabolic disorders. *Sci Rep* 2015;**5**:18193.
55. Fullston T, Teague EMCO, Palmer NO, Deblasio MJ, Mitchell M, Corbett M et al. Paternal obesity initiates metabolic disturbances in two generations of mice with incomplete penetrance to the F2 generation and alters the transcriptional profile of testis and sperm microRNA content. *FASEB J* 2013;**27**:4226–4243.
56. Johannessen A, Lønnebotn M, Calciano L, Benediktsdóttir B, Bertelsen RJ, Bråbäck L

- et al. Being overweight in childhood, puberty, or early adulthood: Changing asthma risk in the next generation? *J Allergy Clin Immunol* Published Online First: 2019. doi:10.1016/j.jaci.2019.08.030
57. Northstone K, Golding J, Davey Smith G, Miller LL, Pembrey M. Prepubertal start of father's smoking and increased body fat in his sons: further characterisation of paternal transgenerational responses. *Eur J Hum Genet* 2014;**22**:1382–1386.
58. Svanes C, Koplín J, Skulstad SM, Johannessen A, Bertelsen RJ, Benediktsdóttir B et al. Father's environment before conception and asthma risk in his children: A multi-generation analysis of the Respiratory Health In Northern Europe study. *Int J Epidemiol* 2017;**46**:235–245.
59. Dong H, Wang Y, Zou Z, Chen L, Shen C, Xu S et al. Abnormal Methylation of Imprinted Genes and Cigarette Smoking: Assessment of Their Association with the Risk of Male Infertility. *Reprod Sci* 2017;**24**:114–123.
60. Alkhaled Y, Laqqan M, Tierling S, Lo Porto C, Amor H, Hammadeh ME. Impact of cigarette-smoking on sperm DNA methylation and its effect on sperm parameters. *Andrologia* 2018;**50**:e12950.
61. Yu B, Qi Y, Liu D, Gao X, Chen H, Bai C et al. Cigarette smoking is associated with abnormal histone-to-protamine transition in human sperm. *Fertil Steril* 2014;**101**:51–57.el.
62. Marczylo EL, Amoako AA, Konje JC, Gant TW, Marczylo TH. Smoking induces differential miRNA expression in human spermatozoa: A potential transgenerational epigenetic concern? *Epigenetics* 2012;**7**:432–439.
63. Watanabe G, Terasawa E. In Vivo Release of Luteinizing Hormone Releasing Hormone Increases with Puberty in the Female Rhesus Monkey. *Endocrinology* 1989;**125**:92–99.
64. Sisk CL, Richardson HN, Chappell PE, Levine JE. In Vivo Gonadotropin-Releasing Hormone Secretion in Female Rats during Peripubertal Development and on Proestrus. *Endocrinology* 2001;**142**:2929–2936.
65. Harris GC, Levine JE. Pubertal Acceleration of Pulsatile Gonadotropin-Releasing Hormone Release in Male Rats as Revealed by Microdialysis. *Endocrinology* 2003;**144**:163–171.
66. Seminara SB, Messenger S, Chatzidaki EE, Thresher RR, Acierno JS, Shagoury JK et al.

- The *GPR54* Gene as a Regulator of Puberty. *N Engl J Med* 2003;**349**:1614–1627.
67. Rilling JK, Worthman CM, Campbell BC, Stallings JF, Mbizva M. Ratios of plasma and salivary testosterone throughout puberty: Production versus bioavailability. *Steroids* 1996;**61**:374–378.
68. Boswell HB. Normal Pubertal Physiology in Females. In: *Female Puberty*. Springer New York 2014: 7–30.
69. Ito T, Bai T, Tanaka T, Yoshida K, Ueyama T, Miyajima M et al. Estrogen-dependent proteolytic cleavage of semaphorin 4D and plexin-B1 enhances semaphorin 4D-induced apoptosis during postnatal vaginal remodeling in pubescent mice. *PLoS One* 2014;**9**:e97909.
70. Rodriguez I, Araki K, Khatib K, Martinou JC, Vassalli P. Mouse vaginal opening is an apoptosis-dependent process which can be prevented by the overexpression of Bcl2. *Dev Biol* 1997;**184**:115–121.
71. Nelson JF, Karelus K, Felicio LS, Johnson TE. Genetic Influences on the Timing of Puberty in Mice. *Biol Reprod* 1990;**42**:649–655.
72. Korenbrot CC, Huhtaniemi IT, Weiner RI. Preputial Separation as an External Sign of Pubertal Development in the Male Rat. *Biol Reprod* 1977;**17**:298–303.
73. Piekarski DJ, Johnson CM, Boivin JR, Thomas AW, Lin WC, Delevich K et al. Does puberty mark a transition in sensitive periods for plasticity in the associative neocortex? *Brain Res* 2017;**1654**:123–144.
74. Gilbert S. *Developmental Biology - Spermatogenesis*. 6th ed. Sunderland (MA): Sinauer Associates 2000<https://www.ncbi.nlm.nih.gov/books/NBK10095/> (accessed 4 Dec2019).
75. Lüllmann-Rauch RL-R. Männliche Geschlechtsorgane. In: *Histologie*. Stuttgart: Georg Thieme Verlag 2003: 399–416.
76. Chen Q, Yan W, Duan E. Epigenetic inheritance of acquired traits through sperm RNAs and sperm RNA modifications. *Nat Rev Genet* 2016;**17**:733–743.
77. Lee RC, Feinbaum RL, Ambros V. The *C. elegans* Heterochronic Gene *lin-4* Encodes Small RNAs with Antisense Complementarity to *lin-14*. *Cell* 1993;**75**:843–854.
78. Lee Y, Ahn C, Han J, Choi H, Kim J, Yim J et al. The nuclear RNase III Droscha initiates microRNA processing. 2003;**425**:415–419.
79. Zeng Y, Cullen BR. Sequence requirements for micro RNA processing and function

- in human cells. *RNA* 2003;**9**:112–123.
80. Yi R, Qin Y, Macara IG, Cullen BR. Exportin-5 mediates the nuclear export of pre-microRNAs and short hairpin RNAs. *Genes Dev* 2003;**17**:3011–3016.
 81. Lund E, Güttinger S, Calado A, Dahlberg JE, Kutay U. Nuclear Export of MicroRNA Precursors. *Science* 2004;**303**:95–98.
 82. Lund E, Dahlberg JE. Substrate selectivity of exportin 5 and Dicer in the biogenesis of microRNAs. *Cold Spring Harb Symp Quant Biol* 2006;**71**:59–66.
 83. Bartel DP. MicroRNAs: Genomics, Biogenesis, Mechanism, and Function. *Cell* 2004;**116**:281–297.
 84. Bartel DP. MicroRNAs: Target Recognition and Regulatory Functions. *Cell* 2009;**136**:215–233.
 85. Zempleni J, Aguilar-Lozano A, Sadri M, Sukreet S, Manca S, Wu D et al. Biological Activities of Extracellular Vesicles and Their Cargos from Bovine and Human Milk in Humans and Implications for Infants. *J Nutr* 2017;**147**:3–10.
 86. Reithmair M, Buschmann D, Märte M, Kirchner B, Hagl D, Kaufmann I et al. Cellular and extracellular miRNAs are blood-compartment-specific diagnostic targets in sepsis. *J Cell Mol Med* 2017;**21**:2403–2411.
 87. Dobin A, Davis CA, Schlesinger F, Drenkow J, Zaleski C, Jha S et al. STAR: ultrafast universal RNA-seq aligner. *Bioinformatics* 2013;**29**:15–21.
 88. Love MI, Huber W, Anders S. Moderated estimation of fold change and dispersion for RNA-seq data with DESeq2. *Genome Biol* 2014;**15**:550.
 89. Spornraft M, Kirchner B, Haase B, Benes V, Pfaffl MW, Riedmaier I. Optimization of extraction of circulating RNAs from plasma - Enabling small RNA sequencing. *PLoS One* 2014;**9**:e107259.
 90. Buschmann D, Kirchner B, Hermann S, Märte M, Wurmser C, Brandes F et al. Evaluation of serum extracellular vesicle isolation methods for profiling miRNAs by next-generation sequencing. *J Extracell Vesicles* 2018;**7**:1481321.
 91. Andrews S. FastQC: a quality control tool for high throughput sequence data. 2010.<https://www.bioinformatics.babraham.ac.uk/projects/fastqc/> (accessed 20 Jan2020)
 92. Kong Y. Btrim: A fast, lightweight adapter and quality trimming program for next-generation sequencing technologies. *Genomics* 2011;**98**:152–153.

93. Buschmann D, Haberberger A, Kirchner B, Spornraft M, Riedmaier I, Schelling G et al. Toward reliable biomarker signatures in the age of liquid biopsies - How to standardize the small RNA-Seq workflow. *Nucleic Acids Res* 2016;**44**:5995–6018.
94. Consortium TR. RNAcentral: an international database of ncRNA sequences. *Nucleic Acids Res* 2015;**43**:D123–D129.
95. Kozomara A, Griffiths-Jones S. MiRBase: Annotating high confidence microRNAs using deep sequencing data. *Nucleic Acids Res* 2014;**42**:68–73.
96. Langmead B, Trapnell C, Pop M, Salzberg SL. Ultrafast and memory-efficient alignment of short DNA sequences to the human genome. *Genome Biol* 2009;**10**:R25.
97. Vlachos IS, Zagganas K, Paraskevopoulou MD, Georgakilas G, Karagkouni D, Vergoulis T et al. DIANA-miRPath v3.0: Deciphering microRNA function with experimental support. *Nucleic Acids Res* 2015;**43**:W460–W466.
98. Kawajiri K. Chapter 15. CYP1A1. 1999;:IARC Scientific Publications No. 148; 159-169.
99. Seller MJ, Bnait KS. Effects of tobacco smoke inhalation on the developing mouse embryo and fetus. *Reprod Toxicol* 1995;**9**:449–459.
100. Esposito ER, Horn KH, Greene RM, Pisano MM. An animal model of cigarette smoke-induced in utero growth retardation. *Toxicology* 2008;**246**:193–202.
101. Dehmel S, Nathan P, Bartel S, El-Merhie N, Scherb H, Milger K et al. Intrauterine smoke exposure deregulates lung function, pulmonary transcriptomes, and in particular insulin-like growth factor (IGF)-1 in a sex-specific manner. *Sci Rep* 2018;**8**:7547.
102. Meyer KF, Krauss-Etschmann S, Kooistra W, Reinders-Luinge M, Timens W, Kobzik L et al. Prenatal exposure to tobacco smoke sex dependently influences methylation and mRNA levels of the Igf axis in lungs of mouse offspring. *Am J Physiol - Lung Cell Mol Physiol* 2017;**312**:L542–L555.
103. Diemert A, Hartwig I, Pagenkemper M, Mehnert R, Hansen G, Tolosa E et al. Fetal thymus size in human pregnancies reveals inverse association with regulatory T cell frequencies in cord blood. *J Reprod Immunol* 2016;**113**:76–82.
104. Zeyrek D, Ozturk E, Ozturk A, Cakmak A. Decreased thymus size in full-term newborn infants of smoking mothers. *Med Sci Monit* 2008;**14**:CR423–CR426.

105. Li L, Hsu H, William GE, Stockard CR, Ho K, Lott P et al. Cellular Mechanism of Thymic Involution. *Scand J Immunol* 2003;**57**:410–422.
106. Nohara K, Pan X, Tsukumo S, Hida A, Ito T, Nagai H et al. Constitutively Active Aryl Hydrocarbon Receptor Expressed Specifically in T-Lineage Cells Causes Thymus Involution and Suppresses the Immunization-Induced Increase in Splenocytes. *J Immunol* 2005;**153**:2778–2786.
107. Wheatley LM, Urso D, Tumas K, Maltzman J, Loh E, Levinson AI. Molecular evidence for the expression of nicotinic acetylcholine receptor alpha-chain in mouse thymus. *J Immunol* 1992;**148**:3105–3109.
108. Toyabe S, Imai T, Fukuda M, Kawamura T, Suzuki S, Uchiyama M et al. Identification of nicotinic acetylcholine receptors on lymphocytes in the periphery as well as thymus in mice. *Immunology* 1997;**92**:201–205.
109. Kuo YP, Lucero L, Michaels J, DeLuca D, Lukas RJ. Differential expression of nicotinic acetylcholine receptor subunits in fetal and neonatal mouse thymus. *J Neuroimmunol* 2002;**130**:140–154.
110. Middlebrook AJ, Martina C, Chang Y, Lukas RJ, DeLuca D. Effects of Nicotine Exposure on T Cell Development in Fetal Thymus Organ Culture: Arrest of T Cell Maturation. *J Immunol* 2002;**169**:2915–2924.
111. Chen T, Yan YE, Liu S, Liu HX, Yan HY, Hou LF et al. Increased Fetal Thymocytes Apoptosis Contributes to Prenatal Nicotine Exposure-induced Th1/Th2 Imbalance in Male Offspring Mice. *Sci Rep* 2016;**6**:39013.
112. Qu W, Zhao W hao, Wen X, Yan H yi, Liu H xiao, Hou L fang et al. Prenatal nicotine exposure induces thymic hypoplasia in mice offspring from neonatal to adulthood. *Toxicol Lett* 2019;**304**:30–38.
113. Singh SP, Razani-Boroujerdi S, Pena-Philippides JC, Langley RJ, Mishra NC, Sopori ML. Early postnatal exposure to cigarette smoke impairs the antigen-specific T-cell responses in the spleen. *Toxicol Lett* 2006;**167**:231–237.
114. Ng SP, Zelikoff JT. The Effects of Prenatal Exposure of Mice to Cigarette Smoke on Offspring Immune Parameters. *J Toxicol Environ Health* 2008;**71**:445–453.
115. White JT, Cross EW, Kedl RM. Antigen-inexperienced memory CD8+ T cells: Where they come from and why we need them. *Nat Rev Immunol* 2017;**17**:391–400.
116. Sharma A, Chen Q, Nguyen T, Yu Q, Sen JM. T cell factor-1 and β -catenin control

- the development of memory-like CD8 thymocytes. *J Immunol* 2012;**188**:3859–3868.
117. Jacomet F, Cayssials E, Basbous S, Levescot A, Piccirilli N, Desmier D et al. Evidence for eomesodermin-expressing innate-like CD8⁺ KIR/NKG2A⁺ T cells in human adults and cord blood samples. *Eur J Immunol* 2015;**45**:1926–1933.
118. Lee YJ, Jameson SC, Hogquist KA. Alternative memory in the CD8 T cell lineage. *Trends Immunol* 2011;**32**:50–56.
119. Intlekofer AM, Takemoto N, Wherry EJ, Longworth SA, Northrup JT, Palanivel VR et al. Effector and memory CD8⁺ T cell fate coupled by T-bet and eomesodermin. *Nat Immunol* 2005;**6**:1236–1244.
120. Carty SA, Koretzky GA, Jordan MS. Interleukin-4 regulates eomesodermin in CD8⁺ T cell development and differentiation. *PLoS One* 2014;**9**:e106659.
121. Istaces N, Splittgerber M, Lima Silva V, Nguyen M, Thomas S, Le A et al. EOMES interacts with RUNX3 and BRG1 to promote innate memory cell formation through epigenetic reprogramming. *Nat Commun* 2019;**10**:3306.
122. Shouval DS, Ouahed J, Biswas A, Goettel JA, Horwitz BH, Klein C et al. Interleukin 10 receptor signaling: Master regulator of intestinal mucosal homeostasis in mice and humans. In: *Advances in Immunology*. Academic Press Inc. 2014: 177–210.
123. Shukla M, Kumar P, Mishra V, Chaudhari BP, Munjal AK, Tripathi SS et al. Carryover of cigarette smoke effects on hematopoietic cytokines to F1 mouse litters. *Mol Immunol* 2011;**48**:1809–1817.
124. Balcombe JP, Barnard ND, Sandusky C. Laboratory Routines Cause Animal Stress. *J Am Assoc Lab Anim Sci* 2004;**43**:42–51(10).
125. Meek LR, Burda KM, Paster E. Effects of prenatal stress on development in mice: maturation and learning. *Physiol Behav* 2000;**71**:543–549.
126. Pincus-Knackstedt MK, Joachim RA, Blois SM, Douglas AJ, Orsal AS, Klapp BF et al. Prenatal Stress Enhances Susceptibility of Murine Adult Offspring toward Airway Inflammation. *J Immunol* 2006;**177**:8484–8492.
127. Chen Q, Yan M, Cao Z, Li X, Zhang Y, Shi J et al. Sperm tsRNAs contribute to intergenerational inheritance of an acquired metabolic disorder. *Science* 2016;**351**:397–400.
128. Fullston T, Ohlsson-Teague EMC, Print CG, Sandeman LY, Lane M. Sperm microRNA

- content is altered in a mouse model of male obesity, but the same suite of microRNAs are not altered in offspring's sperm. *PLoS One* 2016;**11**:e0166076.
129. Grandjean V, Gounon P, Wagner N, Martin L, Wagner KD, Bernex F et al. The miR-124-Sox9 paramutation: RNA-mediated epigenetic control of embryonic and adult growth. *Development* 2009;**136**:3647–3655.
 130. Wagner KD, Wagner N, Ghanbarian H, Grandjean V, Gounon P, Cuzin F et al. RNA Induction and Inheritance of Epigenetic Cardiac Hypertrophy in the Mouse. *Dev Cell* 2008;**14**:962–969.
 131. Talhout R, Schulz T, Florek E, Van Benthem J, Wester P, Opperhuizen A. Hazardous Compounds in Tobacco Smoke. *Int J Environ Res Public Health* 2011;**8**:613–628.
 132. Zbikowski SM, Swan GE, McClure JB. Cigarette smoking and nicotine dependence. *Med Clin North Am* 2004;**88**:1453–1465.
 133. Yuan M, Cross SJ, Loughlin SE, Leslie FM. Nicotine and the adolescent brain. *J Physiol* 2015;**593**:3397–3412.
 134. Kelley BM, Rowan JD. Long-term, low-level adolescent nicotine exposure produces dose-dependent changes in cocaine sensitivity and reward in adult mice. *Int J Dev Neurosci* 2004;**22**:339–348.
 135. Klein LC, Stine MM, Vandenberg DJ, Whetzel CA, Kamens HM. Sex differences in voluntary oral nicotine consumption by adolescent mice: A dose-response experiment. *Pharmacol Biochem Behav* 2004;**78**:13–25.
 136. Adriani W, Granstrem O, Macri S, Izykenova G, Dambinova S, Laviola G. Behavioral and neurochemical vulnerability during adolescence in mice: Studies with nicotine. *Neuropsychopharmacology* 2004;**29**:869–878.
 137. Budin SB, Kho JH, Lee JH, Ramalingam A, Jubaidi FF, Latif ES et al. Low-dose nicotine exposure induced the oxidative damage of reproductive organs and altered the sperm characteristics of adolescent male rats. *Malaysian J Med Sci* 2017;**24**:50–57.
 138. Abreu-Villaça Y, Filgueiras CC, Correa-Santos M, Cavina CC, Naiff VF, Krahe TE et al. Tobacco smoke containing high or low levels of nicotine during adolescence: effects on novelty-seeking and anxiety-like behaviors in mice. *Psychopharmacology* 2015;**232**:1693–1703.
 139. Rodgers AB, Morgan CP, Bronson SL, Revello S, Bale TL. Paternal stress exposure alters sperm MicroRNA content and reprograms offspring HPA stress axis

- regulation. *J Neurosci* 2013;**33**:9003–9012.
140. Rassoulzadegan M, Grandjean V, Gounon P, Vincent S, Gillot I, Cuzin F. RNA-mediated non-mendelian inheritance of an epigenetic change in the mouse. *Nature* 2006;**441**:469–474.
141. Rao M, Zeng Z, Tang L, Cheng G, Xia W, Zhu C. Next-generation sequencing-based microRNA profiling of mice testis subjected to transient heat stress. *Oncotarget* 2017;**8**:111672–111682.
142. Yang WM, Min KH, Lee W. MicroRNA expression analysis in the liver of high fat diet-induced obese mice. *Data Br* 2016;**9**:1155–1159.
143. Tessitore A, Ciccirelli G, Del Vecchio F, Gaggiano A, Verzella D, Fischietti M et al. MicroRNA expression analysis in high fat diet-induced NAFLD-NASH-HCC progression: study on C57BL/6J mice. *BMC Cancer* 2016;**16**:3.
144. Wu ZS, Wu Q, Wang CQ, Wang XN, Huang J, Zhao JJ et al. MiR-340 inhibition of breast cancer cell migration and invasion through targeting of oncoprotein c-Met. *Cancer* 2011;**117**:2842–2852.
145. Fernandez S, Risolino M, Mandia N, Talotta F, Soini Y, Incoronato M et al. MiR-340 inhibits tumor cell proliferation and induces apoptosis by targeting multiple negative regulators of p27 in non-small cell lung cancer. *Oncogene* 2015;**34**:3240–3250.
146. Poenitzsch Strong AM, Setaluri V, Spiegelman VS. MicroRNA-340 as a modulator of RAS-RAF-MAPK signaling in melanoma. *Arch Biochem Biophys* 2014;**563**:118–124.
147. Wijayatunga NN, Pahlavani M, Kalupahana NS, Kottapalli KR, Gunaratne PH, Coarfa C et al. An integrative transcriptomic approach to identify depot differences in genes and microRNAs in adipose tissues from high fat fed mice. *Oncotarget* 2018;**9**:9246–9261.
148. Yu FX, Zhao B, Guan KL. Hippo Pathway in Organ Size Control, Tissue Homeostasis, and Cancer. *Cell* 2015;**163**:811–828.
149. Halder G, Johnson RL. Hippo signaling: Growth control and beyond. *Development* 2011;**138**:9–22.
150. Chartoumpakis D V., Zaravinos A, Ziros PG, Iskrenova RP, Psyrogiannis AI, Kyriazopoulou VE et al. Differential expression of microRNAs in adipose tissue after long-term high-fat diet-induced obesity in mice. *PLoS One* 2012;**7**:e34872.

151. Enomoto H, Furuichi T, Zanma A, Yamana K, Yoshida C, Sumitani S et al. Runx2 deficiency in chondrocytes causes adipogenic changes in vitro. *J Cell Sci* 2004;**117**:417–425.
152. Saunders LR, Sharma AD, Tawney J, Nakagawa M, Okita K, Yamanaka S et al. miRNAs regulate SIRT1 expression during mouse embryonic stem cell differentiation and in adult mouse tissues. *Aging* 2010;**2**:415–431.
153. Yao H, Sundar IK, Ahmad T, Lerner C, Gerloff J, Friedman AE et al. SIRT1 protects against cigarette smoke-induced lung oxidative stress via a FOXO3-dependent mechanism. *Am J Physiol - Lung Cell Mol Physiol* 2014;**306**:816–828.
154. Rogers S, De Souza AR, Zago M, Lu M, Guerrina N, Gomez A et al. Aryl hydrocarbon receptor (AhR)-dependent regulation of pulmonary miRNA by chronic cigarette smoke exposure. *Sci Rep* 2017;**7**:40539.
155. Venø MT, Venø ST, Rehberg K, van Asperen J V., Clausen BH, Holm IE et al. Cortical morphogenesis during embryonic development is regulated by miR-34c and miR-204. *Front Mol Neurosci* 2017;**10**:31.
156. McAdams RM, McPherson RJ, Beyer RP, Bammler TK, Farin FM, Juul SE. Dose-dependent effects of morphine exposure on mRNA and microRNA (miR) expression in hippocampus of stressed neonatal mice. *PLoS One* 2015;**10**:e0123047.
157. Zomer A, Vendrig T, Hopmans ES, van Eijndhoven M, Middeldorp JM, Pegtel DM. Exosomes: fit to deliver small RNA. *Commun Integr Biol* 2010;**3**:447–450.
158. Reilly JN, McLaughlin EA, Stanger SJ, Anderson AL, Hutcheon K, Church K et al. Characterisation of mouse epididymosomes reveals a complex profile of microRNAs and a potential mechanism for modification of the sperm epigenome. *Sci Rep* 2016;**6**:31794.
159. Nixon B, Stanger SJ, Mihalas BP, Reilly JN, Anderson AL, Tyagi S et al. The MicroRNA Signature of Mouse Spermatozoa Is Substantially Modified During Epididymal Maturation. *Biol Reprod* 2015;**93**:91, 1–20.

10 EIDESSTATTLICHE VERSICHERUNG

Hiermit erkläre ich, Barbara Hammer, an Eides statt, dass ich die hier vorliegende Dissertation mit dem Thema

Parental smoking behavior – cellular and molecular consequences for murine offspring

selbstständig verfasst, die Arbeit unter der Einhaltung der Regeln guter wissenschaftlicher Praxis der Deutschen Forschungsgemeinschaft entstanden ist, ich mich außer der angegebenen keiner weiteren Hilfsmittel bedient und alle Erkenntnisse, die aus dem Schrifttum ganz oder annähernd übernommen sind, als solche kenntlich gemacht und nach ihrer Herkunft und Bezeichnung der Fundstelle einzeln nachgewiesen habe.

Ich erkläre des Weiteren, dass die hier vorgelegte Dissertation nicht in gleicher oder ähnlicher Form bei einer anderen Stelle zur Erlangung eines akademischen Grades eingereicht und kein akademischer Grad entzogen wurde.

Ort, Datum

Unterschrift

11 APPENDIX

11.1 Supplemental results

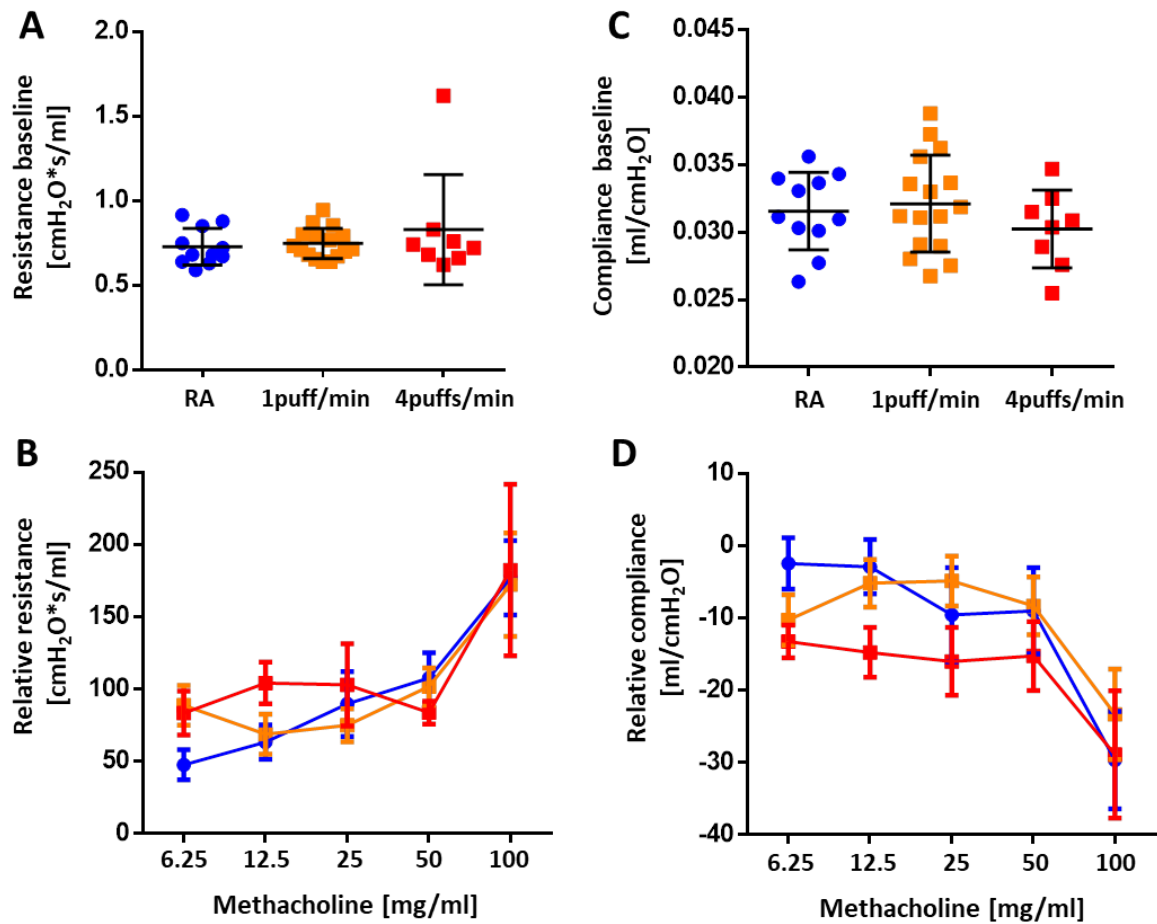


Figure S1 Invasive lung function measurements in adult virgin females. A, Baseline resistance. B, Baseline compliance. C, Relative resistance (MCh: 6.25, 12.5, 25, 50 and 100 mg/ml). D, Relative compliance (MCh: 6.25, 12.5, 25, 50 and 100 mg/ml). A-D, RA ● (n= 11), 1 puff/min ■ (n= 16), 4 puffs/min ■ (n= 8). A-B, 1way ANOVA, mean ± SD; each data point represents and individual animal. C-D, 2way ANOVA, mean ± SEM. A, Dunn's multiple comparison test. B-D, Tukey's multiple comparison test. Room air (RA), methacholine (MCh). * p<0.05, ** p<0.01, *** p<0.001, **** p<0.0001.

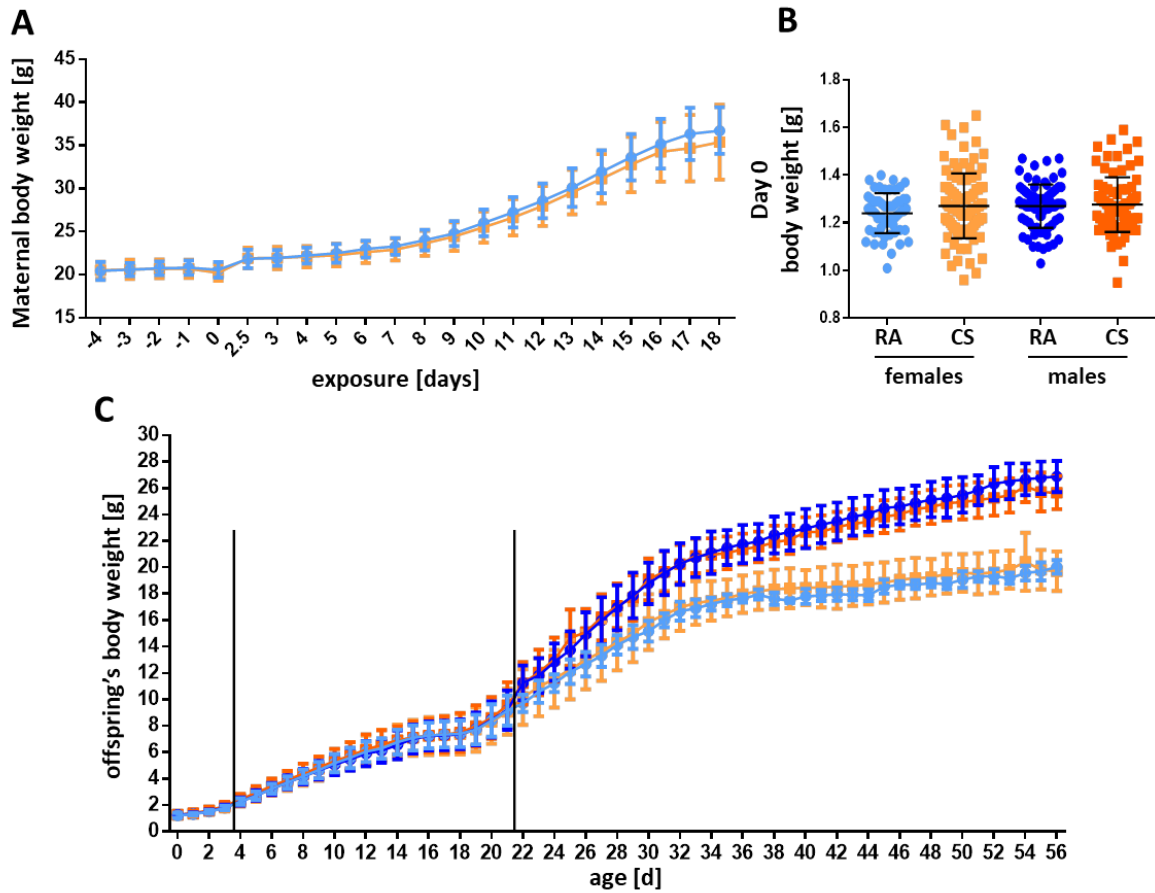


Figure S2 Body weight development in dams and offspring following mild maternal smoking. A, Maternal body weight of RA ● (n= 20) or CS ■ (n= 29) exposed mice. Day 0 of exposure refers to the mating. B, Body weight at day of birth (day 0) of female (RA ● n= 59, CS ■ n= 99) and male (RA ● n= 82, CS ■ n= 58) offspring. C, Body weight development of female and male offspring (PND3: RA female n= 60, CS female n= 103, RA male n= 85, CS male n= 89; PND21: RA female n= 45, CS female n= 84, RA male n= 69, CS male n= 71; PND56: RA female n= 5, CS female n= 21, RA male n= 13, CS male n= 18). The black lines highlight the analysis time points at PND3 and PND21. A,C, Data are expressed as mean ± SD compared by 2way ANOVA. B, Each data point represents an individual animal. Data are expressed as mean ± SD compared by 1way ANOVA. A, Sidak's multiple comparison test. B-C, Tukey's multiple comparison test. Room air (RA), cigarette smoke (CS), postnatal day (PND), day (d). * p<0.05, ** p<0.01, *** p<0.001, **** p<0.0001.

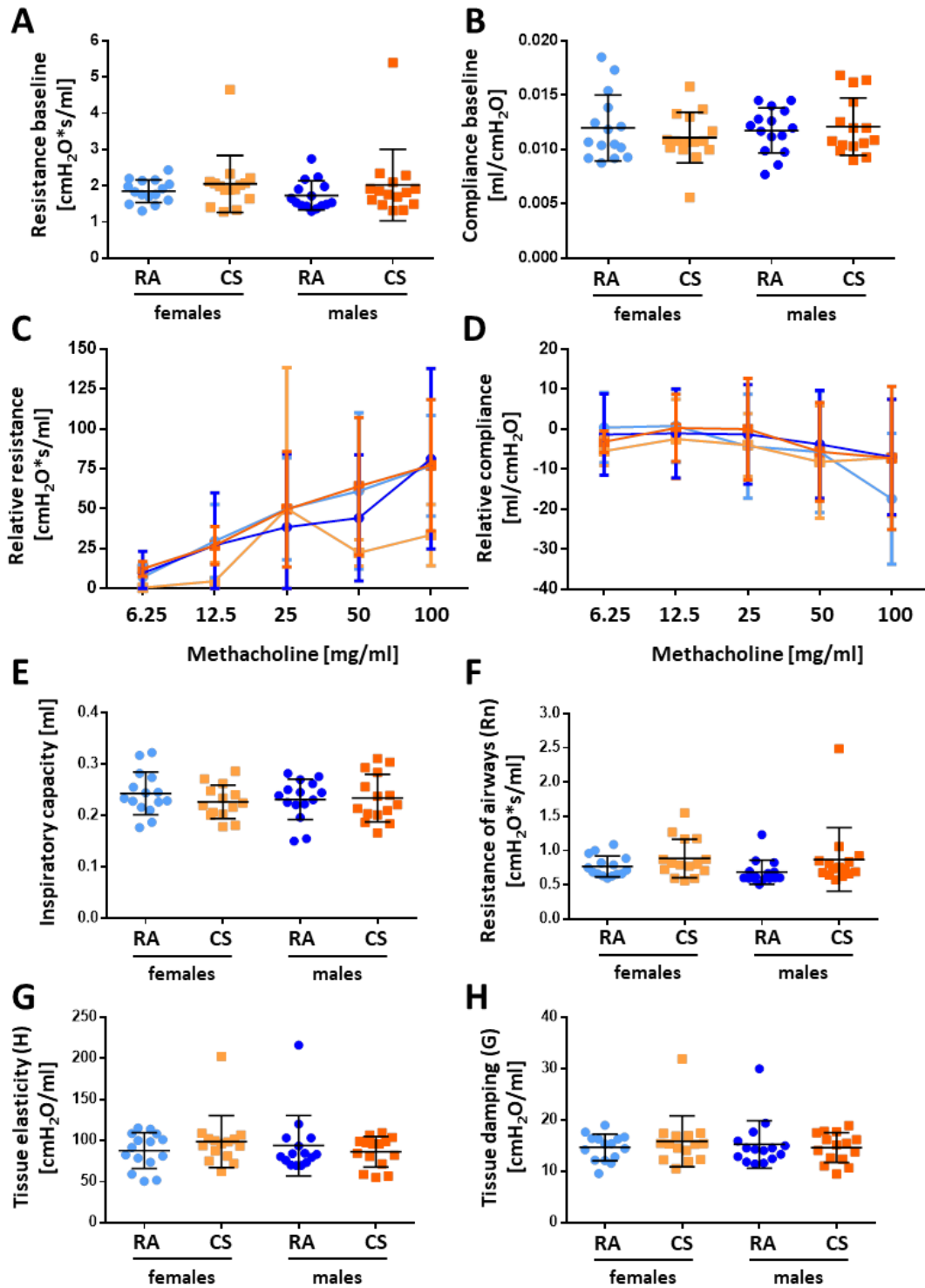


Figure S3 Lung function parameters measured in offspring at PND21. A, Baseline resistance and B, baseline compliance in female (RA \bullet $n=15$, CS \blacksquare $n=14-15$) and male (RA \bullet $n=15$, CS \blacksquare $n=15$) offspring. C, Relative resistance and D, relative compliance in female (RA \bullet $n=9$, CS \blacksquare $n=4$) and male (RA \bullet $n=9$, CS \blacksquare $n=6$) offspring at different MCh concentrations (6.25, 12.5, 25, 50 and 100 mg/ml). E, Inspiratory capacity. F, Resistance of small airways (R_n). G, Tissue elasticity (H). H, Tissue damping (G). A-H, Data are expressed as mean \pm SD. A-B, E-H, Each data point represents an individual animal. A, F-H, Kruskal-Wallis test. B,E, 1way ANOVA. C-D, 2way ANOVA. B-D,E, Tukey's multiple comparison test. A,F-H, Dunn's multiple comparison test. Room air (RA), cigarette smoke (CS), postnatal day (PND), methacholine (MCh). * $p<0.05$, ** $p<0.01$, *** $p<0.001$, **** $p<0.0001$.

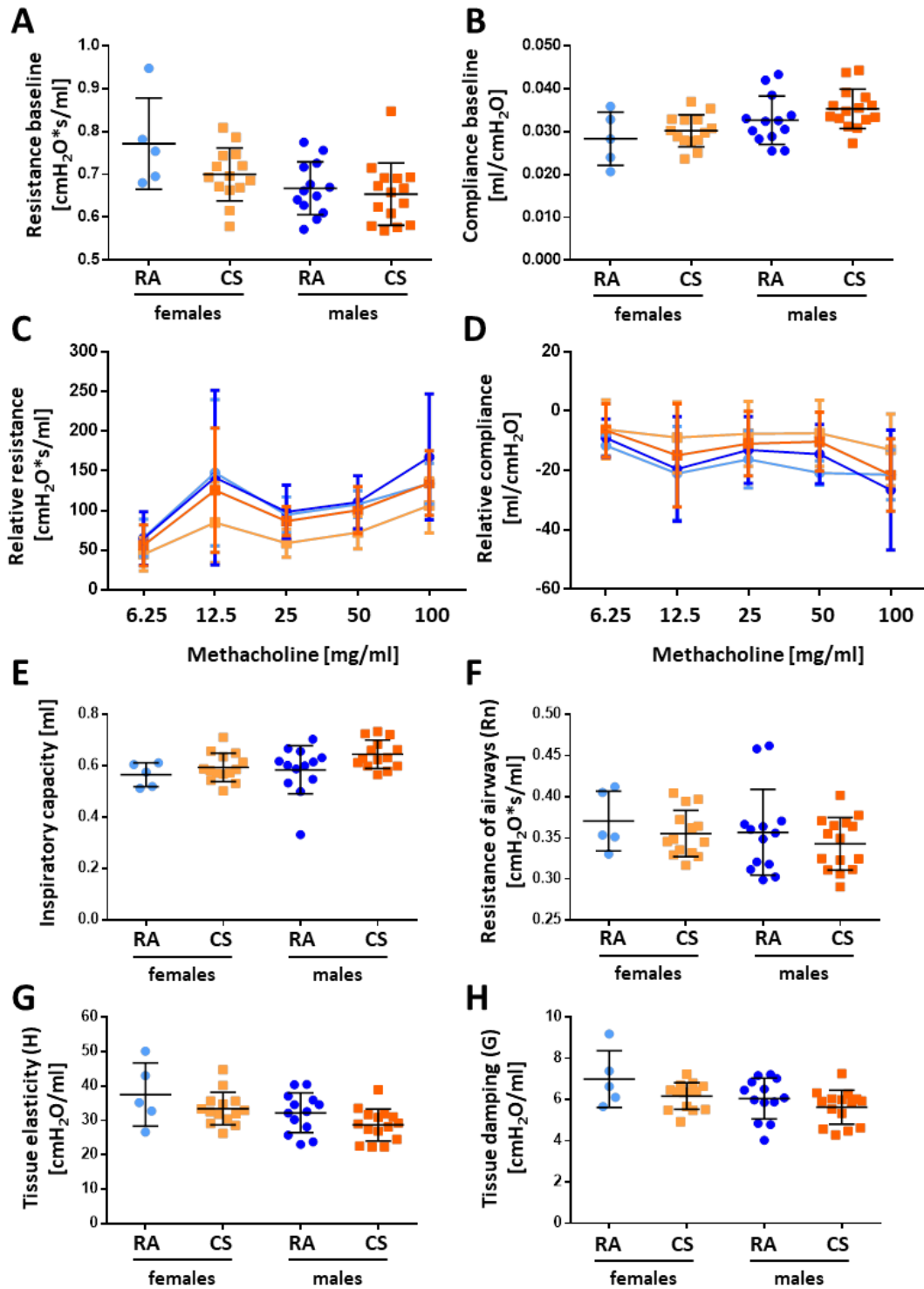


Figure S4 Lung function parameters measured in offspring at PND56. A, Baseline resistance and B, baseline compliance in female (RA \bullet $n=5$, CS \blacksquare $n=14$) and male (RA \bullet $n=13$, CS \blacksquare $n=14-15$) offspring. C, Relative resistance and D, relative compliance at different MCh concentrations (6.25, 12.5, 25, 50 and 100 mg/ml). E, Inspiratory capacity. F, Resistance of small airways (R_n). G, Tissue elasticity (H). H, Tissue damping (G). A-H, Data are expressed as mean \pm SD. A-B, E-H, Each data point represents an individual animal. A-B, E-H, Kruskal-Wallis test. C-D, 2way ANOVA. A-B, E-H, Dunn's multiple comparison test. C-D, Tukey's multiple comparison test. Room air (RA), cigarette smoke (CS), postnatal day (PND), methacholine (MCh). * $p<0.05$, ** $p<0.01$, *** $p<0.001$, **** $p<0.0001$.

APPENDIX

Day of analysis	Parameter	RA		CS		p-value
		female	male	female	male	
PND3	body weight (end)	1.76	1.79	1.78	1.77	♀: 0.66 (t test)
		±0.146 g	±0.146 g	±0.188 g	±0.245 g	♂: 0.79 (t test)
	Lung weight	0.045 ±	0.044 ±	0.04 ±	0.041 ±	♀: 0.12 (t test)
		0.0074 g	0.0077 g	0.0072 g	0.0076 g	♂: 0.32 (t test)
	Lung/BW ratio	0.026	0.025	0.023	0.023	♀: 0.11 (t test)
		±0.004	±0.004	±0.005	±0.003	♂: 0.29 (t test)
	Lung total cell count	7.31E+05	7.72E+05	6.74E+05	7.01E+05	♀: 0.73 (t test)
		±3.51E+05	±5.43E+05	±3.10E+05	±1.98E+05	♂: 0.73 (t test)
	Spleen weight	0.003 ±	0.004 ±	0.003 ±	0.003 ±	♀: 0.87 (t test)
		0.0005 g	0.0006 g	0.0008 g	0.0009 g	♂: 0.47 (t test)
Spleen/BW ratio	0.002	0.002	0.002	0.002	♀: 0.51 (t test)	
	±0.0002	±0.0002	±0.0003	±0.0004	♂: 0.39 (t test)	
Spleen total cell count	6.10E+05	8.74E+05	5.73E+05	4.50E+05	♀: 0.71 (t test)	
	±2.12E+05	±2.62E+05	±2.02E+05	±2.74E+05	♂: 0.004 (t test)	
Thymus total cell count	4.28E+06	4.08E+06	2.81E+06	3.21E+06	♀: 0.053 (MWU)	
	±2.17E+06	±2.83E+06	±1.61E+06	±2.16E+06	♂: 0.40 (t test)	
PND21	body weight (end)	10.21	9.97	9.56	9.57	♀: 0.14 (t test)
		±0.719 g	±1.136 g	±1.454 g	±1.719 g	♂: 0.48 (t test)
	Lung weight	0.203	0.188	0.180	0.176	♀: 0.009 (t test)
		±0.0184 g	±0.0186 g	±0.0237 g	±0.0279 g	♂: 0.17 (t test)
	Lung/BW ratio	0.020	0.019	0.019	0.019	♀: 0.28 (t test)
		±0.001	±0.001	±0.002	±0.002	♂: 0.66 (MWU)
	Lung total cell count	3.32E+06	2.72E+06	2.38E+06	2.93E+06	♀: 0.052 (t test)
		±1.44E+06	±1.53E+06	±9.37E+05	±1.57E+06	♂: 0.80 (MWU)
Spleen weight	0.097	0.091	0.077	0.077	♀: 0.013 (t test)	
	±0.0125 g	±0.0191 g	±0.0250 g	±0.0285 g	♂: 0.12 (t test)	
Spleen/BW ratio	0.009	0.009	0.008	0.008	♀: 0.058 (t test)	
	±0.0014	±0.0017	±0.0023	±0.0023	♂: 0.13 (t test)	
Spleen total cell count	3.23E+07	2.99E+07	3.04E+07	2.79E+07	♀: 0.77 (t test)	
	±1.55E+07	±1.48E+07	±1.82E+07	±1.63E+07	♂: 0.65 (MWU)	
Thymus total cell count	1.02E+08	7.99E+07	9.24E+07	8.69E+07	♀: 0.69 (t test)	
	±7.25E+07	±3.96E+07	±5.07E+07	±5.85E+07	♂: 0.99 (MWU)	

PND56	body weight (end)	19.73 ±0.488 g	27.22 ±1.204 g	20.48 ±1.035 g	26.27 ±1.421 g	♀: 0.14 (MWU) ♂: 0.08 (t test)
	Lung weight	0.297 ±0.0166 g	0.343 ±0.0273 g	0.279 ±0.0497 g	0.330 ±0.0327 g	♀: 0.35 (MWU) ♂: 0.31 (t test)
	Lung/BW ratio	0,015 ±0,0009	0,012 ±0,0010	0,014 ±0,0022	0,013 ±0,0016	♀: 0.12 (MWU) ♂: 0.27 (t test)
	Lung total cell count	4.51E+06 ±2.00E+06	3.42E+06 ±8.84E+05	4.72E+06 ±1.65E+06	5.62E+06 ±1.91E+06	♀: 0.72 (MWU) ♂: 0.0011 (t test)
	Spleen weight	0.078 ±0.0072 g	0.087 ±0.0102 g	0.083 ±0.0072 g	0.083 ±0.0094 g	♀: 0.37 (MWU) ♂: 33 (t test)
	Spleen/BW ratio	0.004 ±0.0004	0.003 ±0.0004	0.004 ±0.0003	0.003 ±0.0004	♀: 0.71 (MWU) ♂: 0.40 (t test)
	Spleen total cell count	3.19E+07 ±1.92E+07	4.78E+07 ±1.94E+07	4.32E+07 ±1.68E+07	3.74E+07 ±2.31E+07	♀: 0.30 (MWU) ♂: 0.23 (t test)
	Thymus total cell count	7.76E+07 ±2.26E+07	3.14E+07 ±7.96E+06	4.14E+07 ±2.49E+07	2.07E+07 ±7.52E+06	♀: 0.008 (MWU) ♂: 0.002 (t test)

Table S1 Characterization of offspring at PND3, PND21 and PND56. Data are expressed as mean ± SD; unpaired t test (t test) or Mann Whitney test (MWU) were chosen after testing for normal distribution. Room air (RA), cigarette smoke (CS), postnatal day (PND), body weight (BW). * p<0.05, ** p<0.01, *** p<0.001, **** p<0.0001.

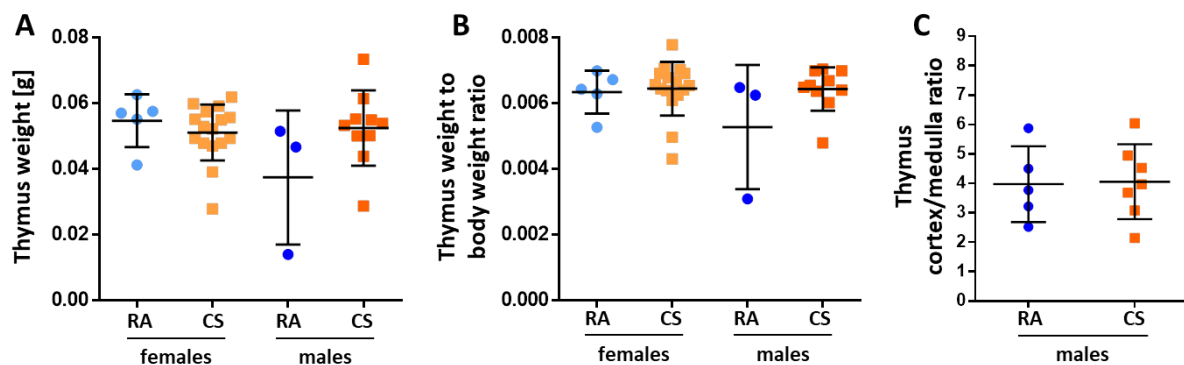


Figure S5 Thymus weight and cortex/medulla ratio at PND21 after *in utero* exposure. A, Thymus total weight. B, Thymus weight to body weight ratio in female (RA ● n= 5, CS ■ n= 16) and male (RA ● n= 3, CS ■ n= 10) offspring. C, The ratio of cortical and medullary area of male offspring (RA ● n= 5, CS ■ n= 7). A-C, Each data point represents an individual animal; data are expressed as mean ± SD compared by Kruskal-Wallis test with Dunn's multiple comparison test. Room air (RA), cigarette smoke (CS), postnatal day (PND). * p<0.05, ** p<0.01, *** p<0.001, **** p<0.0001.

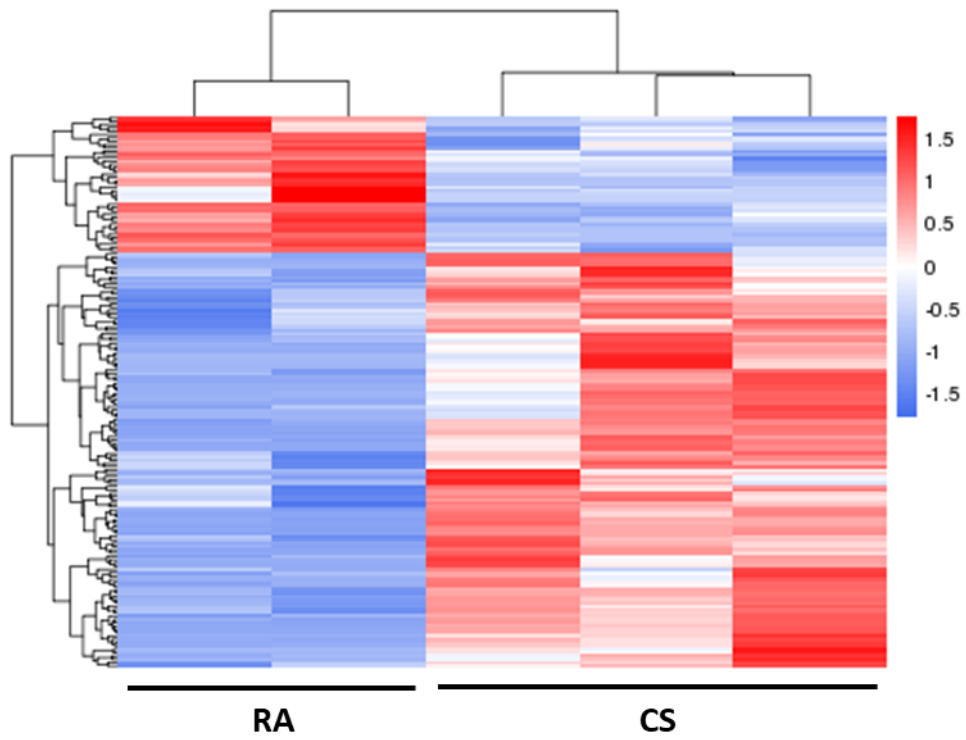


Figure S6 Heatmap of differentially regulated genes in CD8SP thymocytes after *in utero* exposure to RA and CS. Increased fold change (red), decreased fold change (blue). Each column represents an individual animal (females only). Room air (RA), cigarette smoke (CS).

11.2 Abbreviations

AAAAA	poly-adenine tail
AC	adluminal compartment
Adipoq	adiponectin
AGO	Argonaute
AGO2	Argonaute 2
AhR	aryl hydrocarbon receptor
AHR	airway hyperresponsiveness
ANOVA	Analysis of variance
BALF	bronchoalveolar lavage fluid
BC	basal compartment
BLAST	basic local alignment search tool
bp	base pair
BSA	bovine serum albumin
CD	cluster of differentiation
CI	confidence interval
cDNA	complementary DNA
cm	centimeter
COPD	chronic obstructive pulmonary disease
CS	cigarette smoke
Ct	threshold cycle
cTECs	cortical thymic epithelial cells
CTLA4	cytotoxic T-lymphocyte-associated Protein 4
CTLs	cytotoxic T cells
Cyp1a1	cytochrome P450 family 1 subfamily A member 1
d	day
DAPI	4',6-diamidino-2-phenylindole
DGE	Differential gene expression
DN	double-negative
DNA	deoxyribonucleic acid
DP	double-positive
ED	embryonic day
EDTA	ethylenediaminetetraacetic acid

ELISA	enzyme-linked immuno sorbent assay
ENA	European Nucleotide Archive
Eomes	eomesodermin
eSpt	early spermatids
EtOH	ethanol
EVs	extracellular vesicles
F1	filial generation 1
FACS	Fluorescence activated cell sorting
FC	fold change
FDR	false discovery rate
FOXO3	forkhead box protein O3
Foxp1	forkhead box protein P1
Foxp3	forkhead box protein P3
FSC	forward scatter
g	gram
GO	gene ontology
h	hour
HDM	house dust mite
HPRT	hypoxanthine guanine phosphoribosyltransferase
i.p.	intraperitoneal
IgG	immunoglobulin G
IGF-1	insulin-like growth factor 1
Il	interleukin
Il10rb	interleukin 10 receptor beta
IL4ra	interleukin 4 receptor alpha
Insr	insulin receptor
IPA	Ingenuity pathway analysis
IQR	interquartile range
IRS-1	insulin-like substrate-1
IVC	individually ventilated cages
kb	kilobase pair
KEGG	Kyoto Encyclopedia of Genes and Genomes
kg	kilogram
Ki67	Antigen KI-67 or MKI67

Lepr	leptin receptor
lfcSE	log ₂ -fold change standard error
LOCI	Laboratory for Optical and Computational Instrumentation
ISpt	late spermatids
MCh	methacholine
mg	milligram
MHC	major histocompatibility complex
μl	microliter
μm	micrometer
miR	microRNA
miRNA	microRNA
miRNA*	passenger strand
ml	milliliter
mm	millimeter
MMAD	Aerodynamic diameter
mmu	mus musculus
mRNA	messenger RNA
mTECs	medullary thymic epithelial cells
MWU	Mann-Whitney U test
My	myofibroblasts
n	number of animals
NaCl	sodium chloride
NFκB	nuclear factor 'kappa-light-chain-enhancer' of activated B-cells
ng	nanogram
NGS	next-generation sequencing
nm	nanometer
n.s.	not significant
nt	nucleotide
OVA	ovalbumin
padj	adjusted p-value
PBS	phosphate buffered saline
Pik3cg / PI3K	phosphatidylinositol-4,5-bisphosphate 3-kinase
piRNA	piwi-interacting RNA

pmol	picomol
PND	postnatal day
Pparg	peroxisome proliferator-activated receptor gamma
pre-miRNA	precursor miRNA
pri-miRNA	primary miRNA
qRT-PCR	quantitative real-time polymerase chain reaction
R	residual bodies
RA	room air
RISC	RNA-induced silencing complex
RNA	ribonucleic acid
rRNA	ribosomal RNA
rpm	rounds per minute
RT	room temperature
Runx2	runt-related transcription factor 2
Runx3	runt-related transcription factor 3
SD	standard deviation
sec	seconds
SEM	standard error of the mean
Seq	sequencing
SIRT1	Sirtuin1
sncRNA	small non-coding RNA
snoRNA	small nuclear RNA
SP	single-positive
SpC I	primary spermatocytes
SpC II	secondary spermatocytes
SpG_A	type A spermatogonia
SpG_B	type B spermatogonia
SpG_i	intermediate spermatogonia
SSC	sideward scatter
STAR	Spliced Transcripts Alignment to a Reference
STAT3	signal transducer and activator of transcription 3
t test	unpaired student's t test
TBE	Tris-borate-EDTA

Tbp TATA binding protein

TCR T cell receptor

T_{IM} 'innate memory' CD8 T cells

TPM total particulate matter

tRFs tRNA-derived RNA fragments

tsRNA transfer-RNA-derived small RNA

UTR untranslated region

UV ultraviolet

V volt

WT wild type

5'-cap 5-prime cap

11.3 List of figures

Figure 1 The prevalence of tobacco smoking in boys and girls in Europe and worldwide	2
Figure 2 Simplified illustration of the pathophysiology of asthma	3
Figure 3 Comparison of the 4 different respiratory systems of human, mouse, fruit fly and zebrafish	5
Figure 4 Stages of thymic T cell development.....	8
Figure 5 Murine development.....	9
Figure 6 Schema of the germinal epithelium in testis.. ..	11
Figure 7 Spatiotemporal distribution of sncRNAs	12
Figure 8 Simplified schema of miRNA biogenesis.....	13
Figure 9 Schema of exposure to RA or CS for dose finding experiments.	26
Figure 10 Schematic protocol of prenatal CS exposure (1 puff/min).....	27
Figure 11 Schema of preconceptional RA or CS exposure of mice and experimental setup	27
Figure 12 Gating strategies for flow cytometry	31
Figure 13 Validation of CS exposure in virgin females.....	41
Figure 14 Inflammatory cells in BALF of virgin females.....	42
Figure 15 Total cell counts of lungs and whole spleen of prenatally exposed offspring to RA or CS at PND3, 21 and 56	45
Figure 16 T cell proportions in lungs and spleen in offspring after intrauterine exposure to RA or CS	46
Figure 17 Thymocytes after <i>in utero</i> CS exposure in offspring	47
Figure 18 Regulated genes of network 4 in CD8SP thymic T cells (PND21) after <i>in utero</i> CS exposure normalized with RA-exposed offspring	50
Figure 19 Validation of single genes of interest detected in CD8SP thymocytes	51
Figure 20 CS exposure during adolescence decreases weight gain in future fathers and mothers	52
Figure 21 Analysis of inflammatory cells in BALF of lungs from RA- and CS-exposed fathers and mothers	53
Figure 22 Total count and morphology of spermatozoa in RA- and CS-exposed fathers....	54
Figure 23 Analysis of spermatogonia in murine fathers	54

Figure 24 Influence of paternal and maternal preconceptional CS exposure on the body weight of F1 offspring until PND3.....	55
Figure 25 Influence of paternal and maternal preconceptional CS exposure on the body weight of F1 offspring until PND21.....	58
Figure 26 Heatmap of miRNAs regulated in spermatozoa from adolescent CS-exposed mice.....	61
Figure 27 Regulation of selected genes in the liver of offspring at PND21 from RA and CS-exposed fathers	63
Figure S1 Invasive lung function measurements in adult virgin females	92
Figure S2 Body weight development in dams and offspring following mild maternal smoking	93
Figure S3 Lung function parameters measured in offspring at PND21	94
Figure S4 Lung function parameters measured in offspring at PND56	95
Figure S5 Thymus weight and cortex/medulla ratio at PND21 after <i>in utero</i> exposure	97
Figure S6 Heatmap of differentially regulated genes in CD8SP thymocytes after <i>in utero</i> exposure to RA and CS	98

11.4 List of tables

Table 1 Mouse strain used for animal experiments	16
Table 2 Chemicals and reagents	17
Table 3 Buffers and solutions	19
Table 4 Monoclonal and polyclonal antibodies used for flow cytometry (FC) and immunohistochemistry (IHC)	19
Table 5 Genes and primer sequences for qRT-PCR	20
Table 6 Commercial kits.	20
Table 7 Equipment and devices	23
Table 8 Software and websites.....	24
Table 9 Consumables	25
Table 10 Light cycler protocol for qRT-PCR.....	33
Table 11 Pregnancy outcome and CS exposure characteristics of dams.....	43
Table 12 Cononical pathways suggested by IPA®	48
Table 13 Top Diseases and Functions suggested by IPA®	49
Table 14 Multilevel mixed analysis of body weight development (all offspring) until PND21 after paternal and maternal adolescent smoking	56
Table 15 Multilevel mixed analysis of body weight development (male offspring) until PND21 after paternal and maternal adolescent smoking	57
Table 16 Multilevel mixed analysis of body weight development (female offspring) until PND21 after paternal and maternal adolescent smoking	57
Table 17 13 miRNAs were upregulated in spermatozoa from preconceptionally CS-exposed fathers	59
Table 18 32 miRNAs were downregulated in spermatozoa from preconceptionally CS-exposed fathers	60
Table S1 Characterization of PND3, PND21 and PND56 offspring.....	97

11.5 Curriculum vitae

Name: Barbara Hammer

Date of birth: 24.07.1989 in Tulln an der Donau

Nationality: Austrian

Academic education

Jan. 2016 –

Mar. 2020 **PhD Thesis**

Parental smoking behavior – cellular and molecular consequences for murine offspring

Early Life Origins of Chronic Lung Diseases, Research Center Borstel, Leibniz Lung Center, Member of the German Lung Society (DZL), Borstel, Germany

Apr. 2013 –

Jan. 2016 **Master of Science (Biology)**

Acute and chronic allergy models and their effect on behavior and immune signaling in the hippocampus

Institute of Molecular Regenerative Medicine, Paracelsus Medical University Salzburg, Austria

Division of Allergy and Immunology, University of Salzburg, Austria

Major subjects: Genetics/Molecular biology, Immunology

Oct. 2009 –

Apr. 2013 **Bachelor of Science (Biology)**

Major subjects: Genetics/Molecular biology, Immunology

University of Salzburg, Austria

Jun. 2009

General qualification for university entrance (Matura)

Höhere Lehranstalt für Wirtschaftliche Berufe (HLW), Tulln an der Donau, Austria

Vocational education

2008 cook and waitress

Höhere Lehranstalt für Wirtschaftliche Berufe (HLW), Tulln an der Donau, Austria

2008 bartender

Höhere Lehranstalt für Wirtschaftliche Berufe (HLW), Tulln an der Donau, Austria

Wirtschaftsförderungsinstitut Österreich (WIFI), Austria

Publications

2018 **Hammer B**, Wagner C, Divac Rankov A, et al. In utero exposure to cigarette smoke and effects across generations: a conference of animals on asthma. *Clin Exp Allergy*. 2018;**48**:1378-1390.

Awards and prizes

2018 Poster Award

Smoking in adolescence alters the body weight of the next generation in a sex-specific manner

2nd International Symposium on Allergy meets Infection, Luebeck, Germany

2019 Poster Prize

Mild maternal smoking regulates gene expression in CD8 SP Thymic T cells in prenatally exposed murine offspring

Poster Discussion Session

European Academy of Allergy and Clinical Immunology (EAACI) Congress 2019, Lisbon, Portugal

Certificates

2017 Federation for Laboratory Animal Science Associations Category B (FELASA B)

University Medical Center Hamburg-Eppendorf, Hamburg, Germany

Christian-Albrechts-Universitaet zu Kiel, Kiel, Germany

2019 LSRII – Level 1, Fluorescence Cytometry

Research Center Borstel, Borstel, Germany

11.6 Acknowledgments

This PhD thesis would not have been possible without all the colleagues and collaborators working together with me on the projects.

Foremost, I want to thank Prof. Dr. Susanne Krauss-Etschmann for the opportunity to work on two very interesting mouse models during my PhD and the possibility to attend several national and international conferences. It was always a pleasure traveling to new places and representing the Research Center Borstel and our research group in the best way possible. I thank Susanne for her advice, her guidance and the many fruitful discussions.

I have to give a big and heartfelt *Thank You!* to Sebastian Reuter, who taught me all I needed to know about mouse experiments and their execution. I am grateful for the foundation he laid out for me in form of the animal proposals he had written for the two projects.

No less, I have to thank Martin Wolff and Janin Braun, whose help in the lab was fundamental.

It is the least for me to thank the above-mentioned colleagues and all other present and former members of our research group *Early Origins in Chronic Lung Diseases* for their great teamwork, which was always of high value in our group.

Thank you, Susanne Krauss-Etschmann, Sebastian Reuter, Martin Wolff, Janin Braun, Gregor Jatzlauk, Joni Valeska Lund, Draginja Kovacevic, Sabine Bartel, Gabriele Huß, Arne Krüger, Michelle Wörbel, Natalia El-Merhie, Masha Spauszus, Eistine Boateng and Huan Ma.

Next, I want to thank the collaborators that supported this PhD thesis with their expertise in next-generation sequencing and biostatistics. This would not have been possible without the work of mRNA NGS from Daniela Indenbirken and Michael Spohn from the Heinrich-Pette-Institute, and miRNA NGS from Dominik Buschmann from the Technical University of Munich.

I have to give a great *Thank you!* to two biostatisticians: Faisal Rezwan and Latha Kadalayil – and to John Holloway from the University of Southampton – for their important work, help and lively discussions. Faisal was a detrimental part with his KEGG and GO analyses

of the miRNA sequencing data and Latha Kadalayil with her multilevel mixed models for longitudinal body weigh data. I am very grateful I had the opportunity to work with such highly skilled collaborators.

The members of the Fluzyt core facility Jochen Behrends, Thomas Scholzen and Martina Hein I want to thank for their support and maintenance of the flow cytometers LSRII and Ariallu. A special *Thank You* to Martina, who performed the sorting of thymocytes with me.

Furthermore, I want to thank Zane Orinska and Philipp Hagemann for always being available for questions and support of flow cytometry, gating strategies and sharing their mouse expertise.

Natalia and Eistine, I am thanking you both for your skillful scientific writing and your great support for the paper manuscripts.

I want to thank Holger Heine for his supervision and input at discussions at all sorts of meetings and conferences. Furthermore, this brings me to Cecilie Svanes and Machteld Hylkema, who were a pleasure to work with and discuss about epidemiological data, the projects of my PhD thesis and cigarette smoke mouse models.

I want to acknowledge other research groups of the Research Center Borstel and all their members for their advice and the permission to use equipment of their lab: Innate Immunity (Heine), Asthma Exacerbation & Regulation (Wegmann), Experimental Pneumology (Fehrenbach), Infection Immunology (Hölscher), Microbial Interface Biology (Reiling) and the Pathology (Perner).

Sevgi Sarcan, I want to thank you for the great artwork of Figure 3.

At the end, I want to give a very special *Thank You* to Martin Wolff, who was not just always available to help in the lab, but who also shared his knowledge and support generously throughout my PhD. Thank you for your great camaraderie as a colleague and a friend!

Last but not least, I want to thank my family for their unconditional love, support and that you always believed in me!